RCA REVIEW

a technical journal

RADIO AND ELECTRONICS
RESEARCH · ENGINEERING

VOLUME XIV   **DECEMBER 1953**   **NO. 4**

PRINTED IN U.S.A.

RCA REVIEW

a technical journal

RADIO AND ELECTRONICS
RESEARCH • ENGINEERING

Volume XIV	December, 1953	Number 4

CONTENTS

RCA REVIEW

BOARD OF EDITORS

REPUBLICATION AND TRANSLATION

A CAPACITIVE-TUNED ULTRA-HIGH-FREQUENCY TELEVISION TUNER*

By

E. M. HINSDALE, JR. AND IRWIN D. BAUMEL

Industry Service Laboratory, RCA Laboratories Division,
New York, N. Y.

Summary—This paper describes a capacitive-tuned circuit and its application to an ultra-high-frequency (UHF) television tuner covering the 470-890 megacycle range. Essentially this tuned circuit consists of a closed metal box housing a variable air balanced split-stator capacitor commonly known as a butterfly capacitor, which spans opposite faces. The inductance of the tuned circuit contributed by the inside walls of the box is extremely small, making necessary a relatively large capacitor to cover the ultra-high-frequency television tuning range. The Q of this capacitive-tuned box is between 1000 and 1500 over the band. A fundamental frequency oscillator using this type circuit exhibits unusual frequency stability because of the high capacity shunting the oscillator tube.

A tuner using two of these tuned circuits for preselection, one tuned circuit for the oscillator, and a 1N82 crystal diode as the mixer provides a relatively high degree of performance. The circuit Q's attainable with this type of tuned box permit low insertion loss and high spurious signal rejection. Noise figures on the order of 13 decibels have been obtained, and spurious responses are more than 38 decibels below signal level.

The one to five minute oscillator warm-up drift is less than 150 kilocycles at any frequency in the tuning range.

THE TUNED CIRCUIT

A PRACTICAL tuned circuit for covering the 470-890 megacycle UHF television band should be readily tunable, with sufficiently high Q, over the entire frequency range. The selection of a tuned circuit will be influenced by such factors as ease of construction, advantages of rotary motion as opposed to longitudinal motion in tuning, and the desirability of eliminating sliding contacts.

A conventional capacitor–coil tuned circuit appears to offer some of the desirable electrical and mechanical characteristics, but has certain limitations. Extending the frequency range of such a circuit to the UHF region is difficult because the physical size of the elements becomes impractically small.

The tuned circuit herein described and shown in Figure 1 consists of a relatively large lumped variable capacitance and a small inductance. The variable capacitance is a balanced split-stator or butterfly

---

* Decimal Classification: R583✕R310.

capacitor housed in a metal box. The box itself constitutes the inductance.

In describing its principle of operation, an analogy to a lower-frequency circuit is helpful. The inductance may be conceived of as a C-shaped loop of wire across the stator plates of the capacitor. By rotation of the loop about the capacitor, a closed surface is generated. Electrically, the closed surface consists of a large number of parallel loops which together reduce the single-loop inductance to a value usable in the UHF range.

There are a number of possibilities for the form and dimensions of the generated surface. Among these, several cylindrical and rec-
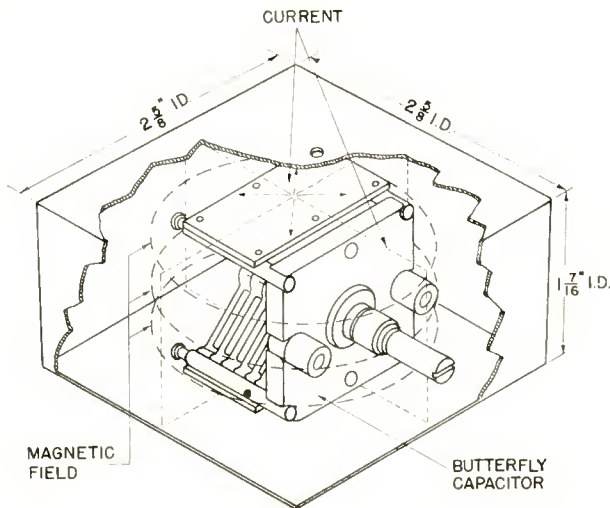
Fig. 1—Basic tuned circuit.

tangular parallelepiped forms were investigated. The dimensions were governed by the physical size of the capacitor and the required value of inductance. In each case, the closed surface (or enclosure) was constructed of copper or silver-plated copper, and the capacitor chosen was one that was commercially available and of the proper value to tune the UHF range.

Three different experimental box-type configurations, one larger, one smaller, and one identical to that shown in Figure 1, were studied to determine which would provide the most desirable characteristics. Of these, the design in Figure 1 was chosen on the basis of maximum Q consistent with convenient physical size. A cylindrical enclosure of equivalent inductance, and using the same size capacitor yielded sub-

stantially the same performance. Since results were the same, the box type rather than the cylindrical construction was preferred because of its mechanical advantages.

During the experimental work, both single-stator and butterfly capacitors were used. A single-stator capacitor in the tuned circuit requires circulating currents to flow through its rotor shaft and wiping contacts. However, current need not flow through the rotor shaft of a butterfly capacitor operating in split-stator fashion. Considerably higher Q's were measured in the latter case, apparently because of the absence of contact resistance.

The capacitance range of the butterfly capacitor used is 3-15 micro-microfarads. At maximum capacitance, the tuned circuit resonates at 450 megacycles, and the effective inductance is calculated to be 0.008 microhenry. With the capacitance at minimum, the circuit resonates at 1200 megacycles and the inductance computes to be 0.006 micro-henry. The apparent change in inductance is due to the inductance of the capacitor plates. This change is of no particular consequence since adequate range appears to be no problem. However, its effect is in the direction of increasing the range.

An electromagnetic field surrounds the capacitor within the box. Its distribution is dependent upon the magnitude and density of the circulating currents on the inside surface. Consider first the magnitude of current flow. If the inside surface consisted of a large number of parallel current paths, all of which were common at the center of the box, then the currents would flow outward from the capacitor, along these paths, down the sides, and back again to the capacitor. The paths carrying the most current would be the shortest or those of least impedance, and within a symmetrical box would cross each of the four rectangular sides at their centers.

Consider next the current density, and assume, for the moment, that current flows equally in all directions from the center. The density on the inside surface is then inversely proportional to the distance from the capacitor. This means that the current density is greater at the center of each side of the box than at the corners. However, it was shown in the previous paragraph that current does not flow equally in all directions, but favors the shortest paths. The combined effect is to increase further the current density at the center of each side, and decrease the density in the corners.

A magnetic field is produced with a strength that is proportional to the current density, and in a direction that is at right angles to the current flow (Figure 1). This implies that the magnetic field within the box is strong at the mid point of the sides, and weak in the corners,

This information is useful in locating and orienting coupling loops which are described in a later section.

As previously explained, a butterfly capacitor is mounted in the center of a copper enclosure. It is of utmost importance that a good electrical contact be made between these two primary parts. Poor contact has resulted in severely decreased circuit Q. The measured unloaded Q of properly constructed units varied between 1000 and 1500 throughout the UHF television band. In the developmental model, a small amount of copper oxide between the capacitor and its contact surface caused a 50 per cent decrease in Q. Two possible methods that might avoid this difficulty are soldering the capacitor directly to each surface, or silver plating the box. In the tuning units described in this paper, the box was silver plated and the capacitor was fastened to the box by screws. Mounting plates were soldered to the two stator sections of the capacitor, and then each mounting plate was drilled and tapped to accommodate six 2-56 screws. This method was used so that the experimental unit might be readily assembled and disassembled.
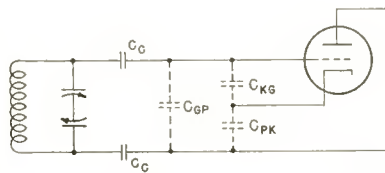
Fig. 2—Basic oscillator circuit.

THE OSCILLATOR

As the next step in the development of the tuner, an oscillator based on the tuned circuit just described was designed. Its basic requirements were maximum frequency stability, minimum variation of output with frequency, and a tuning range of 510-930 megacycles for use with a 40-megacycle intermediate frequency (i-f).

The most convenient type of oscillator for operating in the UHF range appears to be the ultraudion, or modified Colpitts. In this type of circuit the interelectrode tube capacitances serve to provide the necessary feedback to maintain oscillation (Figure 2). In addition, however, they act as partial frequency-determining elements. Variations of these tube capacitances caused by change in temperature and voltage will affect the frequency stability. The degree to which frequency stability is affected will depend upon oscillator design and circuit parameter values.

In constructing the oscillator, it was found necessary to mount the

tube socket for the 6AF4 UHF triode on the last two stator plates of the butterfly-type capacitor (Figures 3 and 4). Lead inductances are reduced to a minimum and the tube is brought closer to the center of the box and thereby nearest the highest impedance point in the tuned circuit.

The coupling capacitors between the tuned circuit and the tube each consist of a stator plate, four 0.005-inch layers of polytetrafluoroethylene, and a brass tube-socket mounting plate. In adjusting the size of the capacitors, it was found desirable to keep them equal so that electrical symmetry might be maintained between the tube and either side of the box. An approximate value of 4 micromicrofarads for each was required as a compromise between low- and high-frequency oscillator operation.

Two silver–mica button radio-frequency (r-f) bypass capacitors, soldered into holes of the proper size in the box wall, allow connecting leads to be brought into the enclosure. Chokes, oriented so that they will be perpendicular to the magnetic field within the box, as illustrated in Figure 4, are connected between these capacitors and the tube socket terminals.

The choke sizes were arrived at by a trial-and-error process. Uniformity of plate current with frequency was the criterion, and the objective was to minimize or eliminate current dips indicating spurious resonances. As indicated by the curves in Figure 5, the plate current variation over the tuning range is within ±20 per cent of the mean value. By orienting the chokes perpendicular to the magnetic field (and, where possible, to one another), interaction and absorption of power is reduced.

Figure 2 shows a schematic diagram of the basic frequency-determining elements in the oscillator. The effective capacitance consists of the 3-15 micromicrofarad butterfly capacitor shunted by the series combination of blocking and interelectrode capacitances. Because the tube capacitances are tapped down on the tuned circuit, and their values are small compared to the main tuning capacitor, small variations in interelectrode capacitance will have a minimum effect upon tuned frequency.

At 930 megacycles, the effective tube capacitance is approximately half the total circuit capacitance. This means that there is an improvement of frequency stability by a factor of about two over the case where the tube is the only contributor of capacitance. As the tuning capacitance is increased, the stability is further improved until, at the low end of the band, a factor of approximately five is attained.

Several stability measurements were considered of interest. The
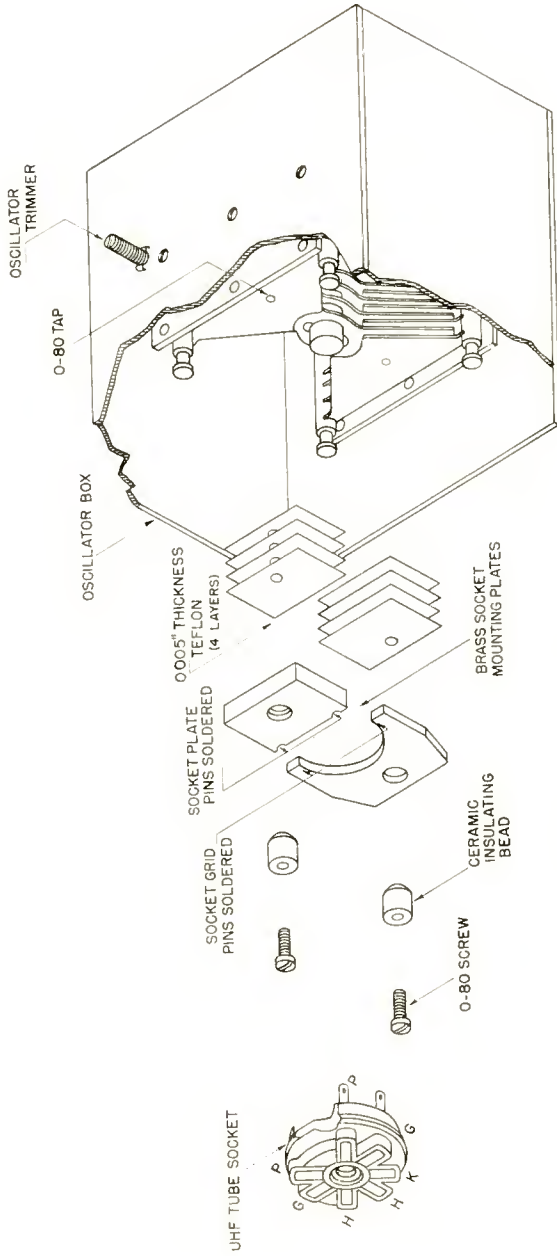
Fig. 3—Construction of oscillator tube mounting.

OSCILLATOR TRIMMER

0-80 TAP

OSCILLATOR BOX

0.005" THICKNESS TEFLON (4 LAYERS)

SOCKET PLATE PINS SOLDERED

BRASS SOCKET MOUNTING PLATES

SOCKET GRID PINS SOLDERED

CERAMIC INSULATING BEAD

0-80 SCREW

UHF TUBE SOCKET
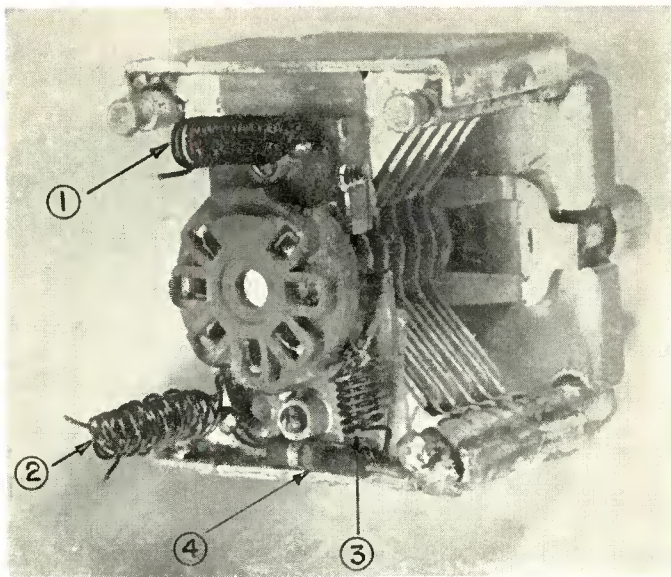
Fig. 4—Oscillator tube mount.

1. Plate choke, 15 turns ⅛″ D., ½″ L., No. 29 enamel.
2. Heater choke, 15 turns twisted pair, wound. ⅛″ D., ½″ L., No. 28 enamel.
3. Cathode choke, 8 turns ⅛″ D., 3/16″ L., No. 29 enamel.
4. 10,000-ohm grid resistor.
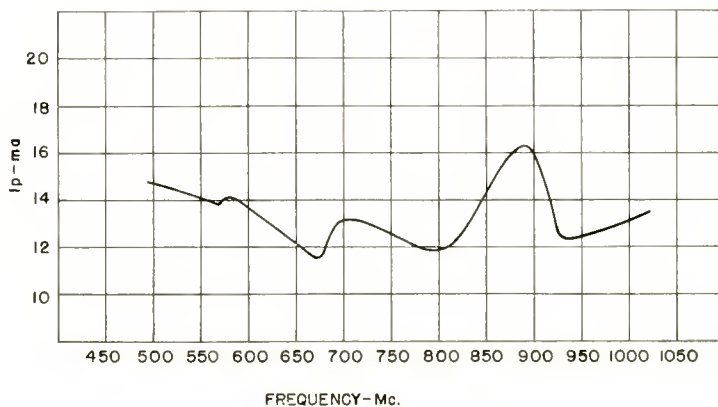
Fig. 5—Oscillator plate current versus frequency.

plate and heater voltages were varied 10 per cent above and below their normal operating values, and warm-up drift was recorded from zero to five minutes. Results of these measurements are given in Figures 6, 7 and 8. Figure 8 shows that most of the warm-up drift occurs during the first minute after oscillation starts for constant ambient temperature. The three curves of Figure 8 also show the oscillator drift for three representative tubes.

The curves in Figure 9 were obtained by simulating a temperature rise that would be expected within a television receiver. With the
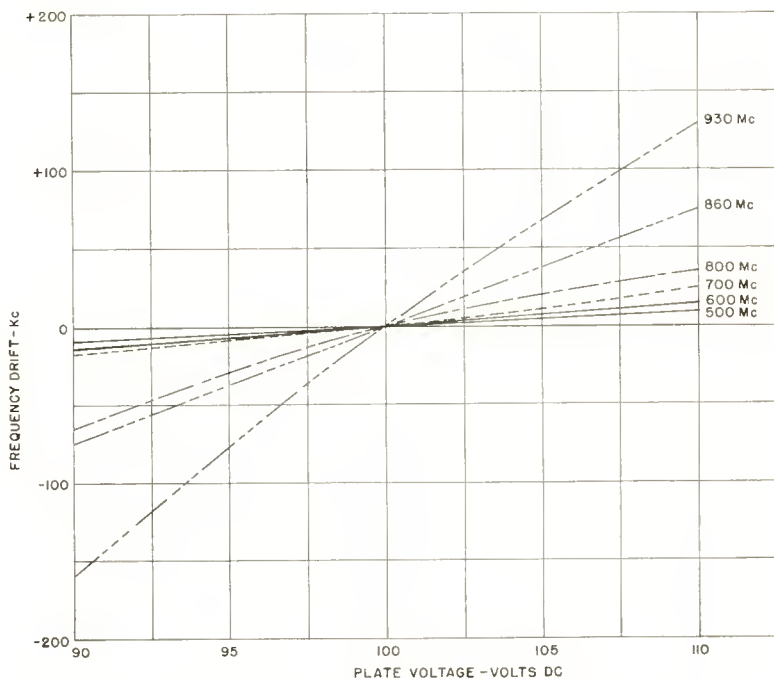
Fig. 6—Oscillator frequency drift versus plate voltage.

oscillator enclosed in a cardboard box, the air temperature inside was slowly raised about 21° C. Curve *a* shows oscillator drift without, and curve *b* with, the trimmer capacitor.

THE UHF TUNER

The UHF tuner which was developed is one of several possible configurations using the tuned circuit and oscillator just described. Basically the circuit is a common type, with a passive double-tuned

preselector, an oscillator, a crystal mixer, and a driven-grounded-grid i-f amplifier (Figure 16).

As shown in Figures 10 and 11, two tuning elements are placed in line as the preselector, the oscillator is located above the output preselector unit, and the i-f amplifier subchassis is mounted on one side.

The preselector tuning capacitor shafts are rigidly coupled together by a ½-inch diameter polystyrene plastic dowel fastened with set screws. A pulley and dial-cord system then couples the oscillator to the preselector shaft.
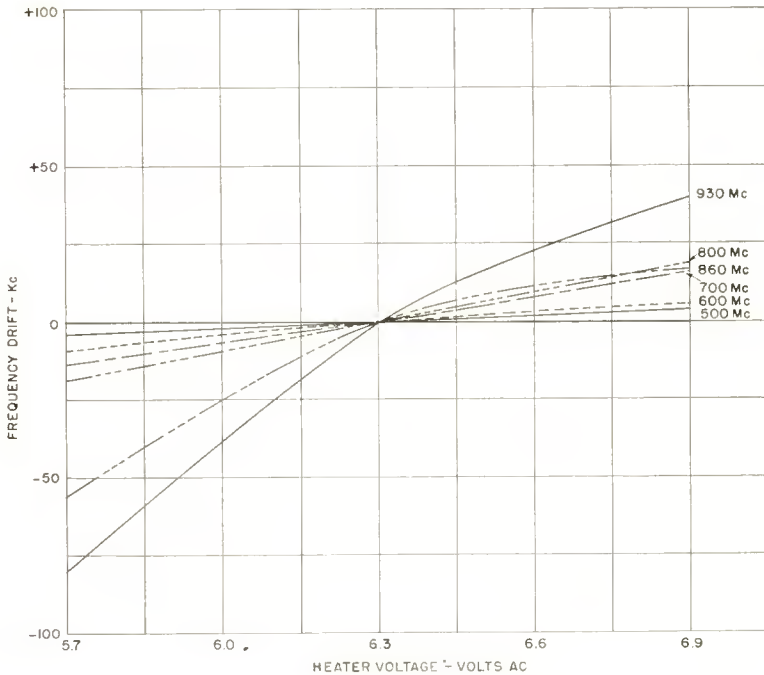
Fig. 7—Oscillator frequency drift versus heater voltage.

A crystal holder consisting of a phosphor-bronze tube and a polystyrene liner is mounted on the i-f amplifier side of the tuner (Figure 12). To make the crystal easily accessible, the tube end is fluted and a feed-through capacitor is clipped into it. Rigid support provided by the polystyrene liner permits the crystal to be almost completely within the box, minimizing the capacitance across the crystal.

The two tuned preselector circuits couple the antenna signal to the crystal mixer and act as a selective frequency filter. The effectiveness of signal transfer depends upon the ratio of the tuned circuit unloaded

to loaded Q. At 470 megacycles, the r-f bandwidth is 8.5 megacycles. As the tuned frequency is increased to 890 megacycles, the bandwidth broadens to 13 megacycles, and the individual loaded tuned circuit Q's remain below 100. Since the unloaded Q, determined by inherent circuit loss, ranges from 1000 to 1500, the calculated insertion loss is less than ½ decibel per tuned circuit at all operating frequencies.
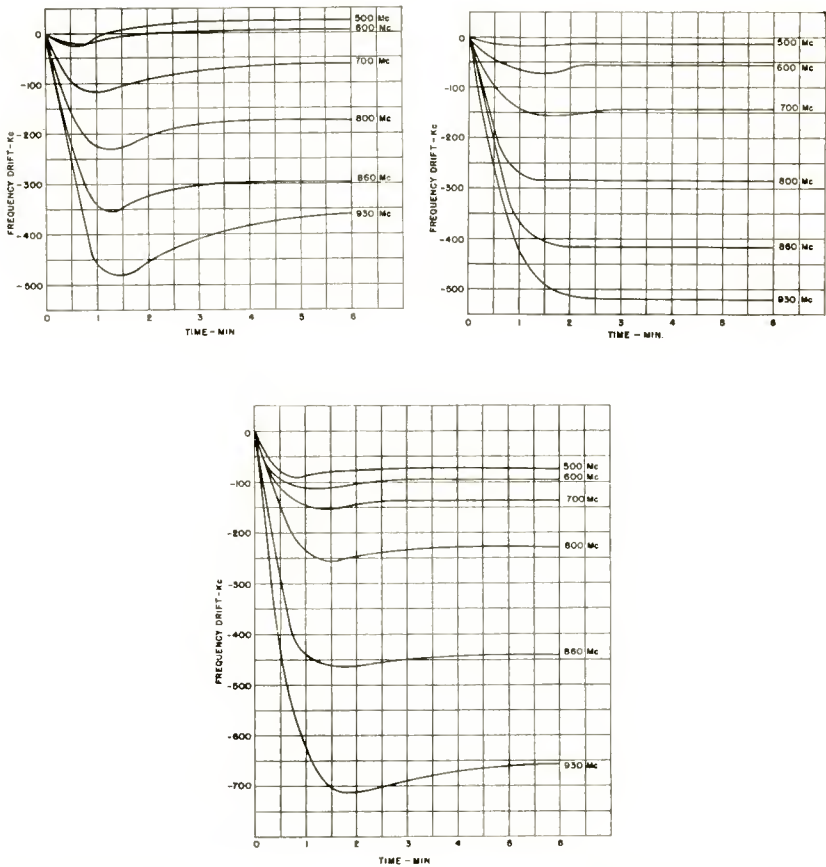
Fig. 8—Oscillator warm-up frequency drift from 0-5 minutes for three representative tubes.

In a system of this type, once the means of frequency selection and oscillator signal generation have been decided upon, the electrical design resolves itself into a series of coupling problems. The signal must be coupled into the preselector box, next to the mixer box, then into the crystal where it is mixed with an injected oscillator signal, and finally, from the crystal to the i-f amplifier.
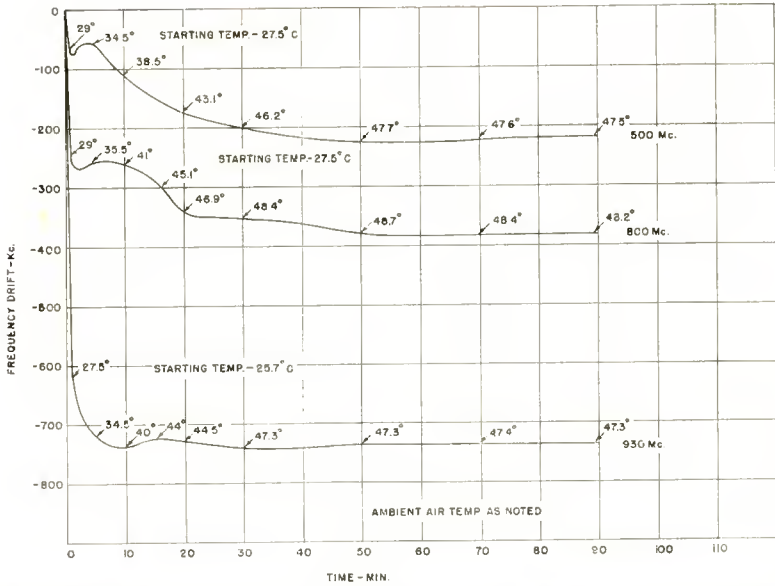
Fig. 9a—Oscillator frequency drift 0-90 minutes with about 21°C ambient air temperature rise without trimmer capacitor.
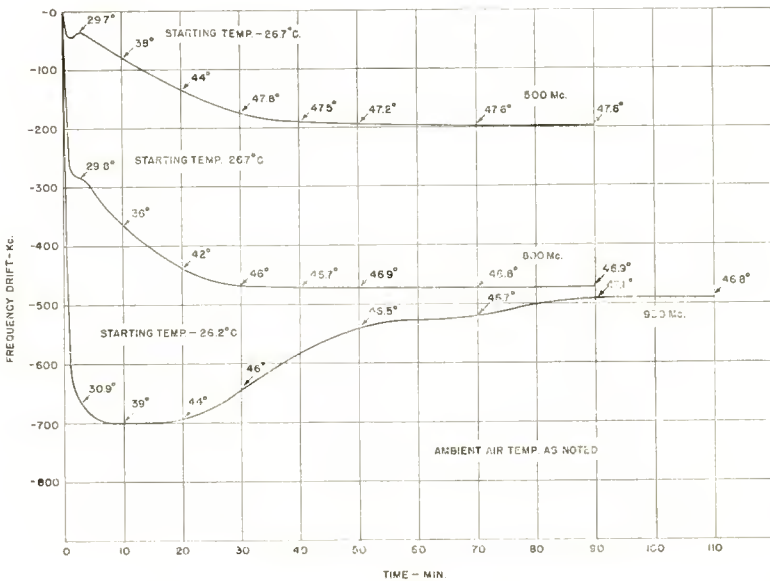
Fig. 9b—Oscillator frequency drift 0-90 minutes with about 21°C ambient air temperature rise with trimmer capacitor.
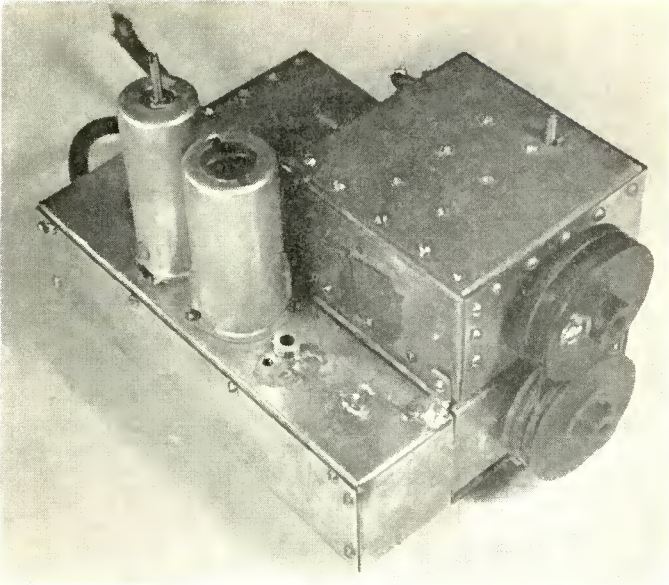
Fig. 10—Developmental UHF tuner.
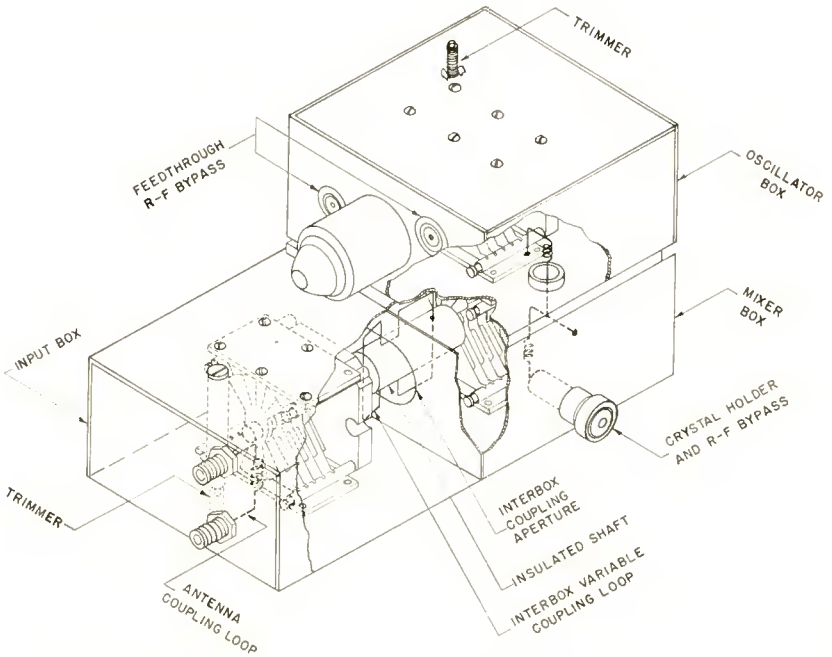
Fig. 11—Isometric view of tuner showing coupling systems.

R-f coupling in any of the boxes may be accomplished by the use of a loop, an aperature or a combination of both. When a loop of fixed size is used, maximum coupling is obtained when it is positioned as close as possible to the tuning capacitor, and when the plane of the loop is perpendicular to the magnetic field within the box. Coupling may be varied by changing loop size, distance from the center, and the angle with respect to the magnetic field.

Aperture coupling implies that a common opening between two boxes provides a mutual reactance, the amount of which is determined by aperture dimensions.
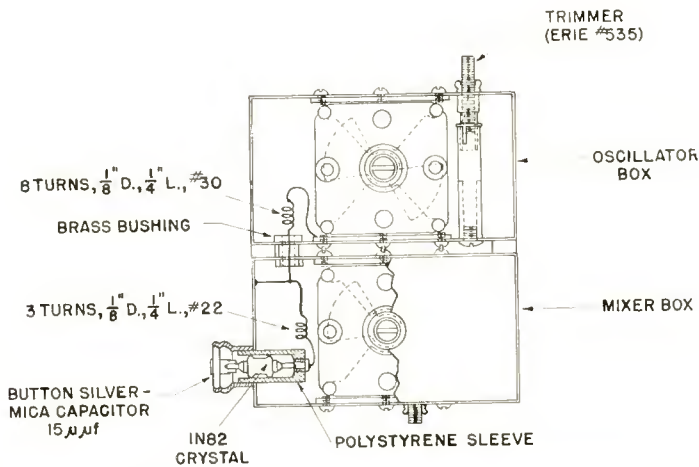
Fig. 12—Details of oscillator injection and mixer coupling.

With this background information, the various coupling problems will be discussed in the order that they were encountered in developmental work. In a system of coupled tuned circuits, it is first necessary to consider output loading.

The crystal, a 1N82 UHF silicon diode, serves as the preselector load and as the nonlinear device needed for frequency conversion. Its i-f impedance is on the order of 500 ohms. For experimental purposes, a single-tuned circuit, with the oscillator mounted above it as shown in Figure 12, was assembled specifically to study mixing and output loading.

Although the crystal input and output frequencies are different, there is a definite relationship between the load presented to the crystal

at i-f[1] and the load presented by the crystal to the preselector at r-f. The amount of interaction is a function of conversion loss. As an expedient, a very-low-Q i-f circuit having a tuned impedance of approximately 500 ohms was used as the i-f load. Then, over the r-f pass band, the i-f load remained substantially constant. This permitted proper adjustment of the crystal r-f coupling and associated oscillator injection circuits with minimum i-f reaction.

Crystal conversion loss, noise temperature, and internal impedances are functions of crystal current, but it was found that over a range of 0.5 to 3 milliamperes the changes in operating characteristics were not large. The tuner noise figure, which is a general measure of system merit, changes less than 1 decibel as the crystal current is varied between the above limits. Below 0.5 milliampere the conversion efficiency decreases rapidly, and above 3 milliamperes the crystal noise temperature becomes excessive.

Two requirements, then, are that the crystal current be relatively constant, and that the crystal present the proper load impedance to the preselector. Figures 11 and 12 show the mixing and injection system configuration used in the single-tuned experimental model and also in the complete tuner.

As shown in Figure 12, the oscillator injection loop is tapped into the output coupling loop at a low impedance point. Leakage reactance in series with the oscillator loop tends to reduce the crystal current change as the tuned frequency is increased.

For adjustment of the output coupling loop, the crystal i-f load was made 470 ohms and the r-f response was observed by placing a sensitive oscilloscope across a 47-ohm resistor in the crystal current return path. A sweep generator, lightly coupled into the experimental mixer box, provided the input signal.

Coupling to the crystal is a function of the loop area (Figure 12) and distance from the center of the box. Three turns of leakage reactance are included in the loop to reduce loading with increasing tuned frequency. This is necessary because the operating Q of the tuned circuit varies inversely with frequency when coupled to a constant load. Unless the loading is variable, the bandwidths will change by approximately 3.5:1 as the circuit is tuned from 470 to 890 megacycles. In the present tuner, the arrangement is such that bandwidth remains within 1.5:1 over the UHF range.

Since only the output preselector box, loaded by the crystal, was used for experimental study of the crystal coupling problem, the loop

---

[1] E. W. Herold, "Frequency Mixing in Diodes," *Proc. I.R.E.*, Vol. 31, pp. 575-582, October, 1943.

size and number of turns of leakage inductance were adjusted to pro-
vide a single-tuned 3-decibel response varying from 6 megacycles at
the low end of the band to 9 megacycles at the high end. When this
tuned circuit was slightly overcoupled to the tuner input circuit, which
had approximately the same operating Q (due to antenna loading) as
the mixer tuned circuit at all frequencies, the bandwidth increased by
a factor of about 1.4. Since the Q's change with tuned frequency, the
mutual reactance between the two circuits must increase as the oper-
ating Q's decrease, in order to maintain the same r-f response shape.

As shown in Figure 11, the interbox coupling consists of a fixed
aperture and a variable loop. The loop is rigidly mounted on the
polystyrene plastic shaft, and is rotated through 90 degrees as the
capacitors are tuned through the UHF range. It is perpendicular to
the magnetic field in each box when tuned to 470 megacycles and
parallel at 890 megacycles. The coupling therefore increases with
decreasing frequency. Combining variable loop and aperture coupling
results in a fairly uniform response throughout the band.

The aperture size was adjusted to provide the required interbox
coupling at the high end of the band, and the loop was adjusted for
the necessary additional coupling at the low end.

The tuner provides a 300-ohm balanced input. Coupling is obtained
by a floating loop of No. 18 wire with three turns of leakage reactance
in the center. This provides loading by the antenna on the first box
similar to that of the crystal on the second box. Adjustments of loop
size and position were made using a panoramic voltage-standing-wave
ratio indicating device.[2] Figures 13 and 14 show the curve of balance-
to-unbalance ratio, and voltage-standing-wave ratio versus frequency.
Since the point-by-point voltage-standing-wave ratio over the r-f pass-
band will vary slightly, the tabulated values are the averaged voltage-
standing-wave ratios between 3-decibel points at each tuned frequency.

The i-f amplifier stage is a low-noise, driven-grounded-grid type,[3]
making use of the 6BQ7. At 40 megacycles the input impedance is on
the order of 20,000 ohms. To match the 500-ohm crystal to the amplifier
would require an impedance transformation of 40 to 1. However, to
obtain minimum noise figure, an impedance match is not desirable. It
can be shown[4] that a mismatch of approximately three to one is the
best compromise between optimum signal power transfer (the matched
case), and a minimum amplifier noise figure (a 10:1 mismatch).

---

[2] John A. Bauer, "Special Applications of UHF Wide Band Sweep
Generators," *RCA Review*, Vol. VIII, pp. 564-575, September, 1947.

[3] R. M. Cohen, "Use of New Low-Noise Twin Triode in Television
Tuners," *RCA Review*, Vol. 12, pp. 3-25, March, 1951.

[4] Van Voorhis, *Microwave Receivers*, Vol. 23, M.I.T. Series, p. 87.
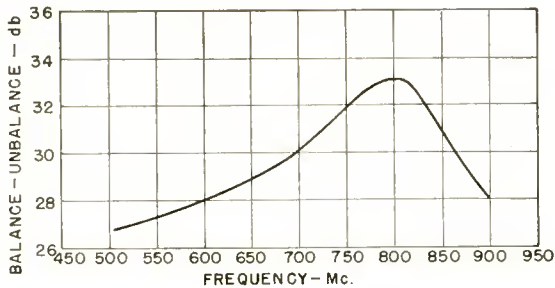
Fig. 13—Balance to unbalance rejection ratio versus frequency.

As mentioned earlier, the interaction between the crystal input and output circuits make it desirable to have the i-f load resistive and constant. For test purposes, a resistively damped i-f circuit was placed across the output to provide a 3-decibel i-f bandwidth of 18 megacycles. This was considered adequate for r-f adjustment because the r-f bandwidth never exceeded 18 megacycles. If the loading is reduced so that the i-f response is narrower than the r-f response, the phase change of the voltage across the i-f circuit is reflected back into the r-f section as reactive rather than resistive loading. The effect is most pronounced when the i-f voltage is changing phase most rapidly, i.e., on each side of the i-f response. When the swept r-f response is observed across a 47-ohm resistor in the crystal-current return path, it appears distorted in comparison to the response that was recorded using a low-Q i-f bandwidth. It is this portion, showing i-f resistive loading, that is of importance. The remaining unused r-f response is merely to allow for tracking tolerance.

To meet the requirements for a coupling system between the crystal

Fig. 14—Input voltage-standing-wave ratio versus frequency.

and i-f amplifier, a capacitance divider and double-tuned transformer are used (Figure 16). The transformer was adjusted so that the i-f response was slightly overcoupled and had about a 6.5-megacycle bandwidth at the 3-decibel points. Additional resistive damping was not required.

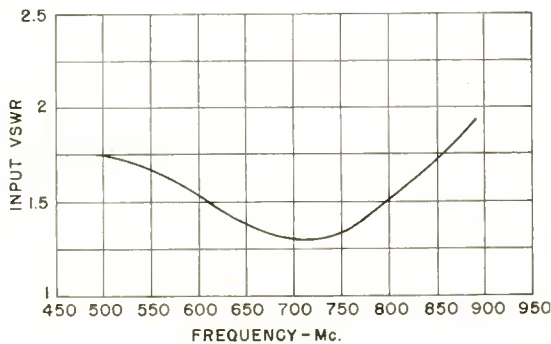For r-f alignment, the low-Q test conditions were restored by shunting the transformer primary with a 470-ohm resistor, and removing the amplifier tube from its socket to detune the secondary. Trimming was done by means of 0.7-3.0 micromicrofarad capacitors mounted in each of the three boxes. As shown in Figure 12, the capacitor was press fitted into the fluted end of a brass tube. The threaded slugs protrude from the top of the oscillator box, and from the bottom of the two preselector boxes. In each case, the trimmers have the greatest

M = INTERBOX COUPLING; COMBINATION OF FIXED APERTURE AND VARIABLE LOOP
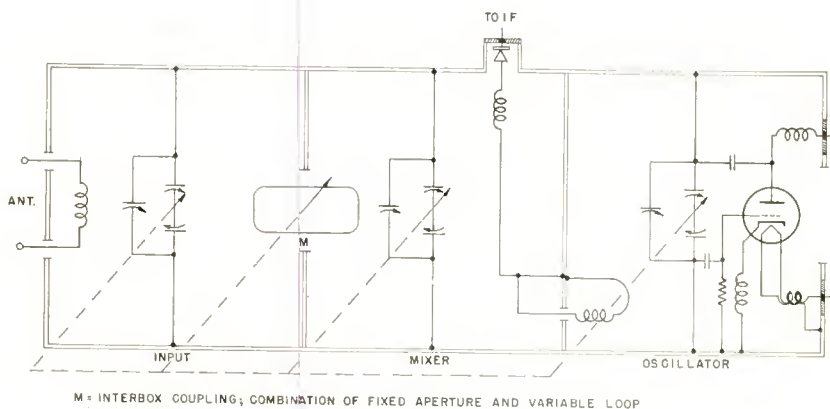
Fig. 15—Schematic of the UHF tuner.

effect when mounted closest to the tuning capacitors. As the distance from the center of the box is increased, a greater capacitance change is required to produce the same frequency variation. In addition to mounting the oscillator trimmer close to the tuning capacitor, it is also mounted at the farthest convenient distance from the tube socket (Figure 11).

To aid alignment at the low end or middle of the band, one rotor plate on each of the tuning capacitors was slotted. The resulting tabs were then bent as necessary.

After the tuner was aligned, measurements were made to determine its performance. Table I shows the r-f and i-f responses, crystal current, and noise figure at representative frequencies within the tuning range. The two-point noise-diode method was employed for all noise figure measurements.
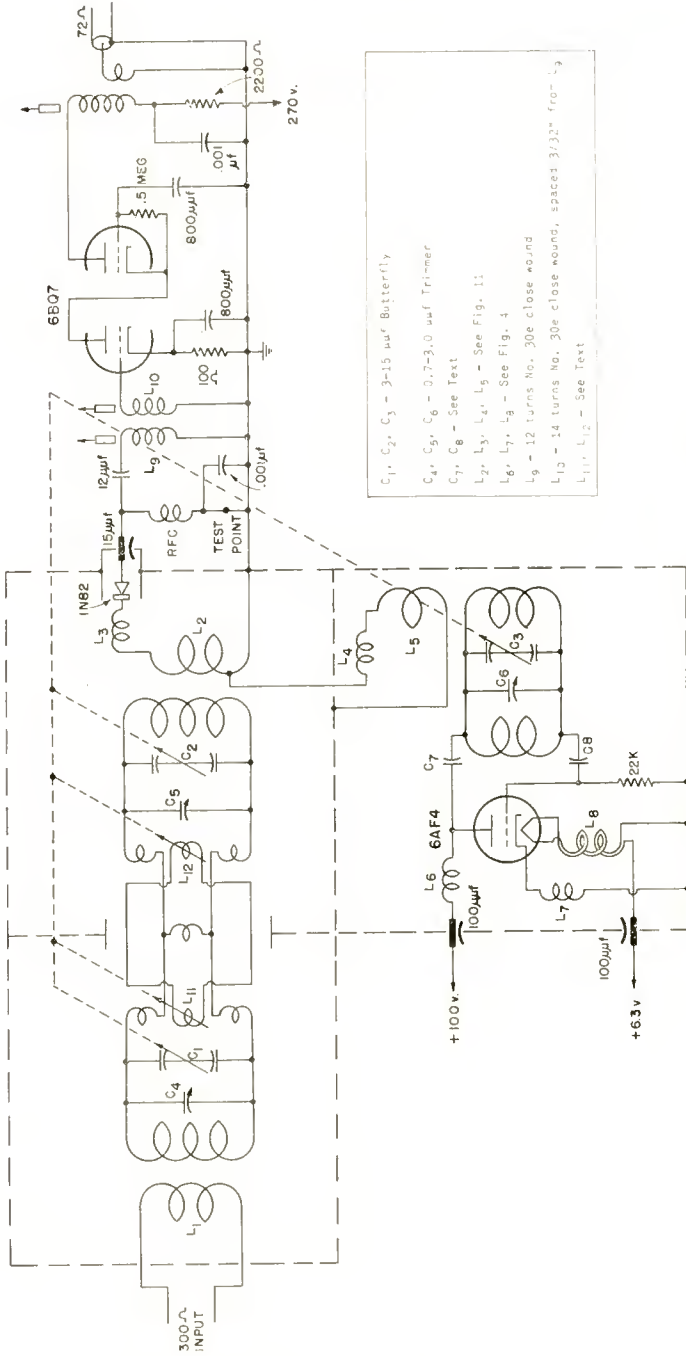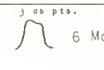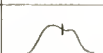
Fig. 16—Equivalent circuit of the UHF tuner.

C_1, C_2, C_3 — 3-15 $\mu\mu f$ Butterfly

C_4, C_5, C_6 — 0.7-3.0 $\mu\mu f$ Trimmer

C_7, C_8 — See Text

L_2, L_3, L_4, L_5 — See Fig. 11

L_6, L_7, L_9 — See Fig. 4

L_9 — 12 turns No. 30e close wound

L_{10} — 14 turns No. 30e close wound, spaces 3/32" from L_9

L_{11}, L_{12} — See Text

Since the tuner noise figure is largely dependent upon the crystal, it was found desirable to investigate this characteristic with a number of crystals. Noise figure measurements were made at 470, 700, and 890 megacycles for a random sample group of 20 crystals. Average

Table I

R-F and I-F Response, Crystal Current and Noise Figure vs Frequency With Tuner Aligned					
Freq. (Mc)	R-F Resp.*	BW 3 db pts.	IF resp.	Xtl. Cur. ma	N_f-db
470	43.5 Mc Below Osc.	8 Mc	3 db pts. 6 Mc	1.35	12.1
500		8.5	6 Mc	1.6	12.0
550		11	6 Mc	1.65	10.6
600		11.5	7 Mc	1.75	10.7
650		12	7 Mc	1.6	10.5
700		13	7 Mc	1.25	11.3
750		13	7 Mc	1.2	11.9
800		12	7 Mc	1.0	12.6
850		13	7 Mc	1.0	12.5
890		12	7 Mc	0.9	13.0
*RF response observed with 470 ohms i-f load as described in text.					

noise figures of 13.5, 11.5, and 13.8 decibels were obtained at these respective frequencies. The variation in noise figure between crystals was within ±1.5 decibels of the average at each of the test points.

Crystal current variation with frequency was also found to be dependent upon the crystal. Therefore, maximum and minimum crystal currents within the tuning range were measured for the 20 crystals. All currents were well within the limit of 0.5-3 milliamperes with an average maximum-to-minimum ratio of 1.9 to 1.

Spurious responses are given in Table II. Within the UHF television range the only responses less than 80 decibels below the desired signal were the image and one-half intermediate frequencies.

Oscillator radiation measurements indicated that the major source of leakage was the phosphor bronze dial cord which was excited by energy coupled from the oscillator capacitor shaft.
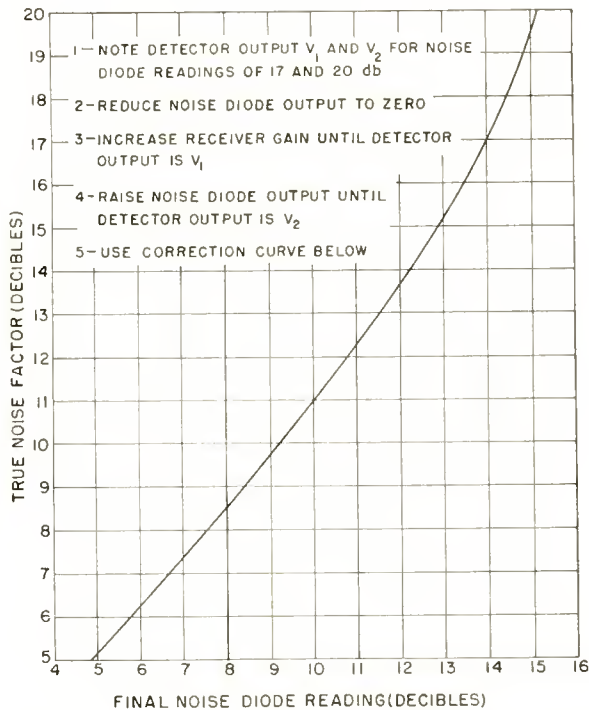
Fig. 17—Two-point noise-diode correction curve uncorrected for transit time.

APPENDIX

The two-point noise diode method was used to eliminate the necessity of determining detector linearity. This method consists basically of calibrating the detector at two alternating-current output levels using a noise diode, and then using these same detector levels for making the actual measurement (see Figure 4). Because the calibration is dependent upon the receiver noise factor, an appreciable correction factor is required when the receiver noise figure is of the same order of magnitude as the noise-diode levels used for calibrating.

As can be seen in Figure 17, if the noise-diode output levels used

Table II — Spurious Response Rejection Within UHF Range

Frequency	Image Rejection (decibels)	½ I-F Rejection (decibels)
500	49.5	84.4
550	49.3	82.0
600	46.1	79.0
650	45.2	76.0
700	45.2	76.0
750	43.0	78.0
800	42.2	75.0
850	37.0	70.5
890	38.3	68.0

for calibration were 20 and 17 decibels, and the noise figure indicated by use of these calibration points was 15 decibels, the true value would be 19.4 decibels, a difference of 4.4 decibels. For convenience, a suitable procedure is outlined in Figure 17. V_1 and V_2 are the detector levels read on the output indicating device. They result from the application of two voltages from the noise diode which differ by 3 decibels.

DEVELOPMENT OF A NEW PREMIUM TWIN TRIODE*

By

H. E. STUMMAN AND J. W. RITCEY

Tube Department, RCA Victor Division,
Harrison, N. J.

Summary—The development of a miniature twin triode, designated as the 6101, is described. This tube is a premium version of the 6J6. Factors involved in the choice of the common-cathode 6J6 structure, and design modifications such as increased mount rigidity are discussed. The use of more extensive controls on manufacturing processes is evaluated. Performance data accumulated throughout one and one-half years of production of the 6101 are compared with data for its prototype.

INTRODUCTION

MODERN military aircraft require the use of complex electronic equipment in which reliability is an important factor. The possibility of failure of such equipment is magnified by the increased number of electron tubes used, as well as by the close tolerances on tube characteristics required by the intricate circuits. To reduce the probability of equipment failure, it is necessary, among other things, to use tubes designed to provide increased reliability in specific circuits. It is also desirable that these "premium" tubes be capable of replacing conventional receiving-type tubes in existing sockets. The 6101, an improved and premium version of the medium-mu twin triode type 6J6, was developed for this purpose. Requirements for the premium type included the maintenance of tight characteristic limits throughout life, durability under conditions of shock and vibration, and a low percentage of inoperative tubes within 500 hours of operation. The only limitation placed on the construction of the 6101 was that it should be interchangeable electrically and mechanically with the 6J6.

MECHANICAL CONSTRUCTION

At the very outset of this project, it was necessary to decide whether this tube should use the single-cathode, split-grid construction that characterizes the 6J6, or a more conventional dual-unit construction having separate heaters and cathodes. Both types of construction are shown in Figure 1.

---

* Decimal Classification: R331.

Although the dual-unit construction may have slightly superior mechanical stability, the split-grid structure reduces the number of heater and cathode welds, simplifies the basing arrangement and assembly, and eliminates an extra cathode and heater in which failures can occur. The use of a single cathode also eliminates the problem of unbalanced activation which is inherent in the dual-unit structure. The most important factor in the decision to use the split-grid structure was the background of successful production experience on this design which meant that production of a tube of superior quality could begin almost immediately.
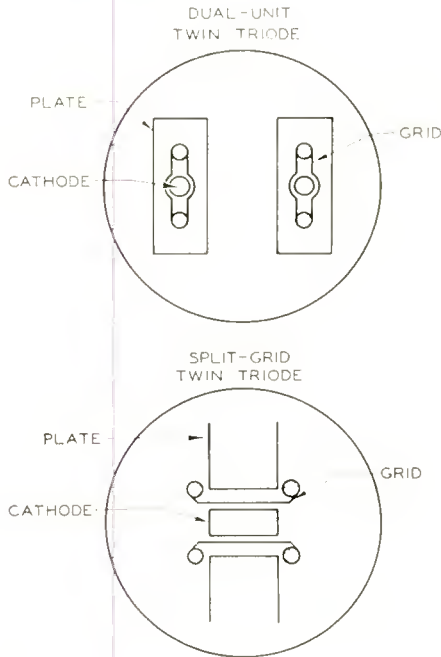
Fig. 1—Cross-sectional views illustrating dual-unit and split-grid twin-triode constructions.

The commercial 6J6 has several premium features which provided a firm foundation for the development of the 6101. These features follow:

1. A clip is welded to the cathode and clamped to the top mica to anchor the cathode firmly, as shown in Figure 1.
2. Tungsten-base heater wire is used to provide long life under conditions of frequent heater cycling.
3. A "normal" cathode material having 0.01 to 0.05 per cent

activating agent is used. Before a new cathode melt is approved for use in either the 6J6 or the 6101, both conduction and cutoff life tests are performed and results are analyzed for evidence of cathode deterioration.

During the development of the 6101, the following additional modifications were made on the mount structure, as shown in Figure 2.

1. An additional mica is used at both the top and bottom of the mount to hold the parts more firmly.
2. The cathode hole in the mica has been redesigned to provide a tighter fit.
3. The narrow edges of the cathode are embossed to hold the cathode rigidly in the mica.
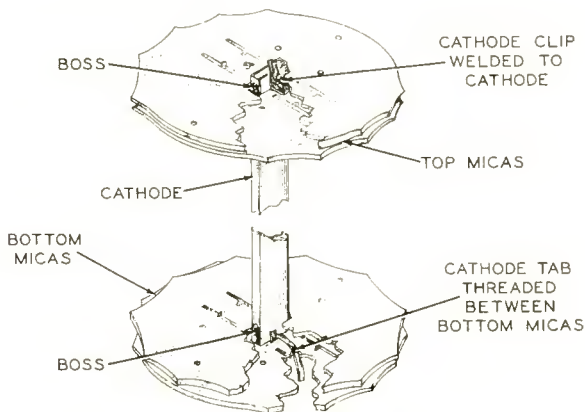
NOTE: BOTTOM VIEW OF STRUCTURE ROTATED 180° WITH RESPECT TO UPPER VIEW

Fig. 2—Mount structure of type 6101.

4. The cathode tab is threaded between the bottom micas to minimize cathode shift.
5. Chrome-copper grid side rods are used to improve heat-dissipation capabilities and thereby reduce the tendency for grid emission to develop.
6. Additional coating material is placed on the heater to reduce the possibility of heater-cathode shorts.

QUALITY-CONTROL PROCEDURES

In addition to the improvements made in the design of the tube, extensive quality-control procedures have been incorporated in the mounting operation. Sample mounts from each operator are inspected

hourly by quality-control inspectors for critical defects. Any operator faults detected at this inspection are corrected immediately. At this stage of the process, emphasis is placed on corrective action rather than lot acceptance. The hourly inspection of mounts is then supplemented by lot-acceptance tests in which items such as quality of welds, damage to parts, and the presence of foreign particles are inspected to an acceptable quality level of 2.5 per cent. This inspection is important because such items cannot always be detected by electrical or mechanical tests on the finished tube. It is primarily because of the quality-control procedures used at the mounting operation that the 6101 can meet an acceptable quality level (AQL) of 0.25 per cent for shorts and continuity on finished tubes. Records show that less than 0.1 per cent of 6101 tubes failed for shorts or continuity after the 48-hour stabilization period.

Controls have also been placed on the sealing-and-exhaust operation. Tubes are checked hourly for fusing of the heater, condition of the cathode coating, and other sealing and exhaust difficulties. A test for glass quality, in which the base of each tube is placed on a cone and immersed first in boiling water and then in water at room temperature, is performed on a sample taken hourly from each position of the sealing-and-exhaust machine. In addition, a quality-acceptance glass test is made after a two-week holding period. The process average for glass-test failures on the 6101 since the beginning of production is 1.3 per cent, which is considerably lower than the average for conventional receiving-type tubes.

Critical parts are also subjected to stringent process controls and quality acceptance procedures. Every possible precaution is taken to keep dirt and lint out of the tubes. Parts are washed, fired, and inspected for particles and lint, and cages and mounts are blown with compressed air. Exhaust ducts and collecting bags are used to collect the foreign particles removed from the tubes. Mount blowing is effective on the 6101 because of its open-type structure. Parts and mounts are also kept well covered between operations in special lint-free containers.

The grid-to-cathode spacing of each 6101 is adjusted by means of a comparative capacitance adjustment to center the major characteristics of the tube. Sample tubes from each adjustment bridge are checked for major characteristics on an hourly basis.

In addition to the required finishing tests, all tubes are microscopically inspected for particles, quality of welds, and general good workmanship. A high-resistance shorts test, as well as the standard shorts-and-continuity test, is made on every tube.

Test Specification

The 6101 test specification is summarized in Figure 3; the 6J6 specification is also shown for comparison. The limits for each test are shown graphically at the right side of the figure. In almost every case the 6101 limits are stricter than those of its prototype. The allowable noise output in the 2.5-g vibration test is reduced from 150 millivolts for the 6J6 to 50 millivolts for the 6101. The minimum allowable insulation resistance is tightened by a factor of ten from 10 to 100 megohms. The plate current of a 6J6 can vary 39 per cent on either side of the bogie value, but only 28-per-cent deviation is allowed for the 6101. Transconductance and amplification-factor limits are also stricter for the 6101. In addition, the 6101 specification includes a cutoff test which controls the characteristics of the tube in the cutoff
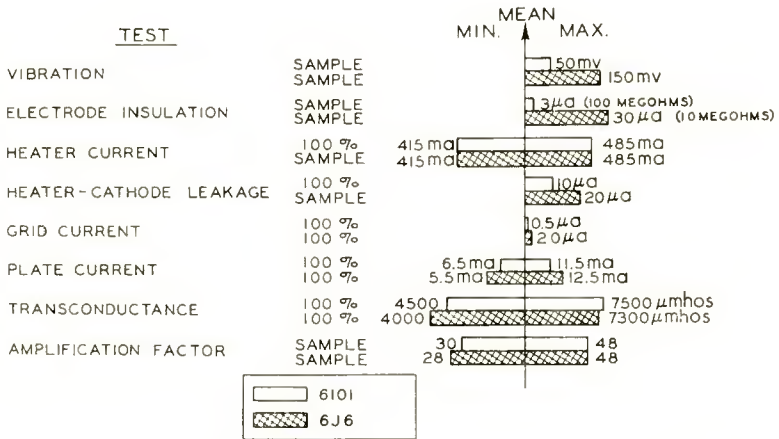
Fig. 3—Summary of test specifications for types 6101 and 6J6.

region more accurately, a "slump"-transconductance test which measures cathode activation on each tube, and a very strict 500-hour life test. In the 500-hour life test for 6J6 tubes, a minimum of 80 per cent of the total possible life hours in the sample must be completed successfully. End-point limits are specified for two characteristics of the 6J6 for this life test. For the 6101, endpoints are specified for eleven characteristics and the life-test sample must have 90 per cent average life at the end of 500 hours.

Plate Current Balance

In the equipment for which the 6101 was designed, there are some sockets in which close balance between the plate-current values of the

two triode units of each tube is required. As a result of the effort to meet this balance requirement, a separate tube, the 6099, was developed concurrently with the 6101. Type 6099 is identical to the 6101, but it has the additional requirement of plate-current balance.

The plate-current balance test for type 6099 was performed by adjustment of the bias on the grid of triode unit No. 1 for one milli-ampere of plate current, and measurement of the plate current of unit No. 2 at the same bias voltage. A limit of 250 microamperes was placed on the plate-current difference between units. In addition, it was proposed that this difference in current should not change more than 100 microamperes throughout life. The required initial balance be-
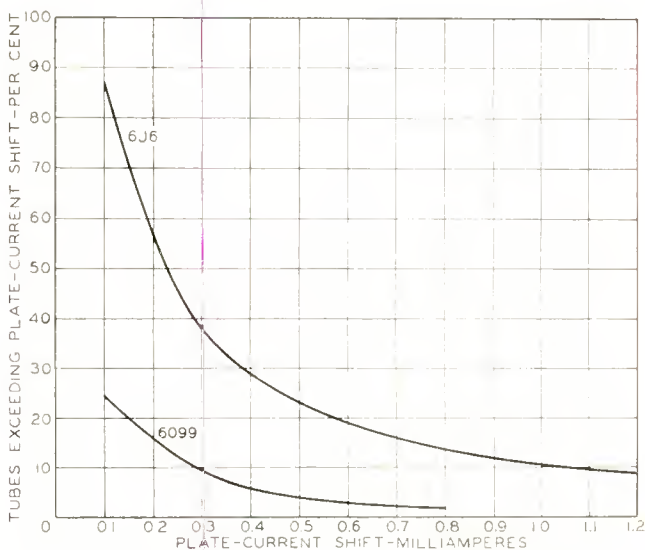
Fig. 4—Results of plate-current balance-stability tests for types 6099 and 6J6.

tween units can be achieved, but at the expense of throwing out a large percentage of the product. The additional requirement of balance throughout life, however, can not be attained with the split-grid structure even at great expense.

Because balance stability is affected primarily by movement of the tube elements, some improvement can be made by strengthening the tube structure. The structural modifications described earlier have resulted in a considerable improvement in the plate-current balance of this tube structure, as shown by the results of a test in which 6099's and 6J6's were tapped three times in each of four directions with a peak acceleration of approximately 50g. The curves of Figure 4 show

that for any specific value of allowable shift a far greater percentage of 6099's than of 6J6's were satisfactory.

The problems encountered in the development of type 6099 exemplify the difficulties encountered when conventional receiving-type tubes are used in circuits requiring control of characteristics other than those specified by the tube manufacturer. The 6J6, having a cathode that is common to both units, was never intended to be used in a circuit requiring plate-current balance between units. Although the 6099 shows considerable improvement over the 6J6, its basic design is unsuited for use in a circuit requiring this balance. This type is not recommended, therefore, for new equipment designs.
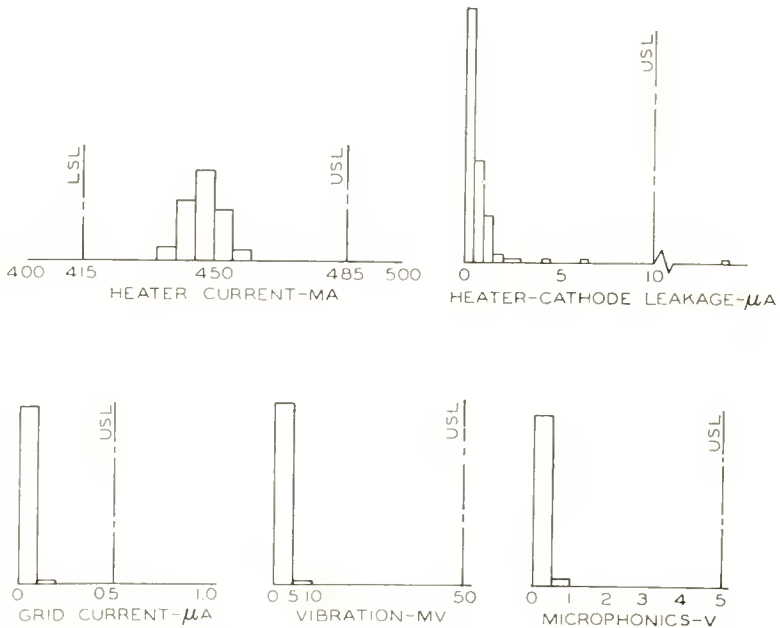
Fig. 5—Distribution curves for five characteristics of type 6101.

TUBE CHARACTERISTICS

Strengthening the 6101 tube structure and maintaining close controls on processing have resulted in a product which exceeds the original requirements in many respects. In Figure 5, distribution curves are shown for heater current, heater–cathode leakage, grid current, vibration, and microphonics. Each of these characteristics is well within the required limits. In the case of plate current, transconductance, and cutoff plate current, the limits are so strict that

careful process control is required to assure proper centering of these characteristics. After production tests, however, tubes meet a one-per cent acceptable quality level for nine characteristics combined, including plate current, transconductance, and cutoff plate current.

Shock and fatigue-vibration tests are not included in the 6101 specifications, but the Air Force has expressed an interest in these tests. Sample 6101 tubes tested under the 6J6W shock conditions of 20 blows at an impact acceleration of 500 g, showed an average trans-conductance shift of only 2.3 per cent, with the maximum at 8.0 per cent. Under 6J6W fatigue conditions, in which the tubes were vibrated at 2.5 g for 96 hours, the average transconductance change was only 4.8 per cent. The increase in heater-cathode leakage and vibrational output was negligible in both tests.

LIFE TESTS

The 90 per cent average-life requirement that must be met by the 500-hour life-test sample from each lot of 6101 tubes is very severe because of the limits specified for eleven different characteristics during the test. Tubes are considered unsatisfactory if they become inoper-ative or if they fail because of change outside of limits in plate current, transconductance, cutoff plate current, insulation resistance, grid cur-rent, or any of several other characteristics.

In Figure 6, the variation of plate current and transconductance throughout life is illustrated. The solid line on each graph is the average of the sample, and the dotted lines are measures of the sample dispersion. The average transconductance shift is only six per cent during life, and the plate-current variation is even less. The fact that the dispersions of the sample are practically constant throughout life shows that the product has good uniformity.

A breakdown of tube failures within 500 hours is shown in Figure 7. The failures, which are given in terms of per cent of tubes life-tested, were classified in relative order of importance and are arranged in this manner on the chart. The most serious type, inoperatives, is at the top of the list and the less important failures are placed in descending order below it. Tubes which failed for more than one cause were included in the higher category. If, for example, a tube failed for both grid current and plate current, it was classed as a grid-current failure. Of the 1076 tubes life-tested, only two, or 0.2 per cent, became inoperative. Heater current, vibration, amplification factor, and noise and microphonics were satisfactory in every tube. 0.1 per cent of the tubes tested failed for transconductance, and 0.2 per cent for the "slump" test. Plate-current and heater-cathode leakage failures each
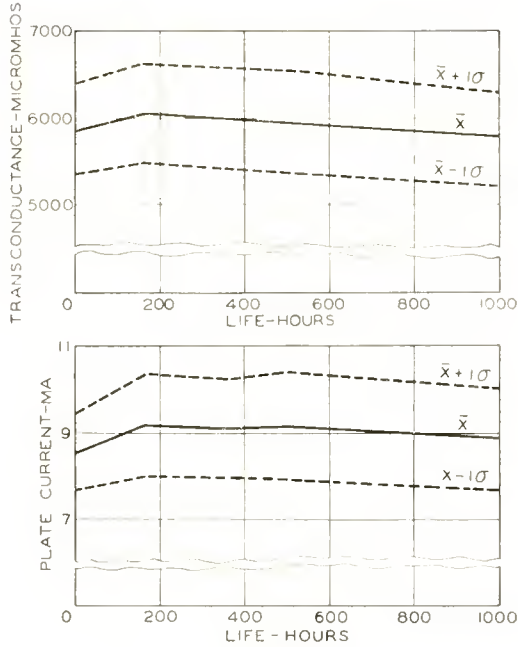
Fig. 6—Operating range of transconductance and plate current
of type 6101 on life.

accounted for 0.2 per cent of the tubes. Excessive tube handling due
to frequent testing on life was a contributing factor to the 1.4 per cent
which failed the cutoff tests. Because of the very tight cutoff limits
imposed during life, any slight change in the activation level can com-
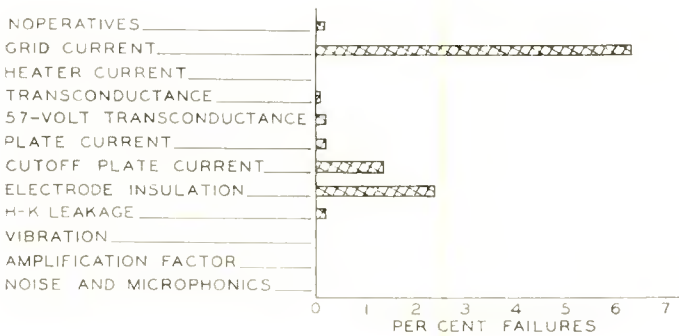
Fig. 7—Analysis of failures in group of 1076 type 6101 tubes
on 500-hour life test.

bine with a small mechanical shift in the tube elements to cause a cutoff failure.

The most serious life problem is obviously the elimination of grid-current and electrode-insulation failures. As mentioned previously, "normal" cathode material is used in the 6101. The use of this material, together with a relatively high cathode temperature, causes conducting material, usually barium, to be given off by the cathode and to settle on the micas. Leakages develop in this manner, showing up as both grid-current and electrode-insulation failures. The conducting material also settles on the grid wires and sometimes causes grid emission. The use of "passive" or electrolytically pure cathode material, although it tends to eliminate these failures, makes it difficult to obtain sufficient emission. Plated grid wire is also helpful, but it changes the contact potential and, consequently, the basic characteristics of the tube. The situation has been improved somewhat by the use of cathode clips and additional micas, which tend to lower the cathode temperature.

Conclusion

Perhaps the best way to summarize the capabilities of the 6101 is to outline the acceptance requirements proposed for standardization. The requirements follow:

1. Fatigue-vibration and shock tests, under 6J6W conditions but with a 6.5 per cent acceptable quality level and much more severe endpoints than those of the 6J6.
2. Shorts-and-continuity testing, to an acceptable quality level of 0.25 per cent.
3. Strict controls on all critical characteristics.
4. 2.5-g vibration testing, to a limit six times as severe as that used on the 6J6.
5. A 2000-cycle heater-cycling test.
6. A test for inoperatives, together with grid-current and low-transconductance failures, at 100 hours of life, to an acceptable quality level of 0.4 per cent.
7. A 500-hour life test, with strict controls on the amount of variation in all important characteristics as well as the absolute values.

Acknowledgment

VIEWING STORAGE TUBE WITH HALFTONE DISPLAY*†

By

M. Knoll**, P. Rudnick‡, and H. Hook**

Summary—A cathode-ray storage tube of the transmission control type is described which gives a bright visual display of a stored picture. The signals are written on the insulating surface of a storage grid by one focussed cathode-ray beam, and made visible by another (spray) beam of electrons passing through this storage grid and being accelerated before striking a fluorescent screen. Erasing is accomplished by pulsing the storage grid or the spray-beam cathode. The target assembly consists of two fine-mesh screens, parallel and close spaced to each other and to the fluorescent screen. The screen which is nearest to the phosphor surface is coated on one side with a layer of insulating material to serve as the storage surface; its holes act as tiny electron lenses, focussing the transmitted electrons to small separate beams. Writing speeds of three million spots per second and viewing durations up to the order of 10 minutes for halftone pictures (and of the order of many hours for black and white pictures or oscillograms) have been obtained using a pulse restoring method. The tube has possible application to radar, facsimile transmission, telemetering, and transient oscilloscopy.

Introduction

IN many applications of cathode-ray tubes, such as radar, facsimile transmission, oscilloscopy, and telemetering, there exists the need for a device which will provide a visual display, for an extended period of time, of bright patterns, oscillographs, or pictures which have been written in a fraction of a second. One attempt to fulfill this need was the development of long-persistence phosphors which permit the observation of a written picture up to several minutes, but only in a darkened room.[1] Another attempt was the dark-trace storage tube.[2]

---

[1] See, for example, H. W. Leverenz, *Introduction to the Luminescence of Solids*, John Wiley and Sons, New York, N. Y., 1949.

[2] See, for example, A. H. Rosenthal, "A System of Large Screen Television Reception Based on Certain Electron Phenomena in Crystals," *Proc. I.R.E.*, Vol. 28, p. 203, May, 1940; H. Kurzke and J. Rottgardt, "Über die Entfärbung von Alkalihalogenidkristalliten," *Ann. d. Phys.*, Vol. 39,

This tube employs the discoloration of a potassium chloride screen under electron bombardment, and has a relatively long viewing duration. However, the contrast is too poor, the erasing time too long, and the life of the screen too short for many applications.

One solution is the combination of a signal converter storage tube such as the Graphechon[3] with a conventional viewing cathode-ray tube. Such combinations are especially valuable where a stored picture has to be transmitted to *several* display points at the same time, since only *one* signal converter storage tube is needed. However, for systems where only one display per receiver is necessary, a direct-view or projection cathode-ray tube with storage is obviously preferable since less equipment is required.

DIRECT-VIEW STORAGE TUBES

Three types of direct-view storage tubes have been developed and described in the literature. These depend on the modulation of the viewing beam in several ways, and are known as the emission control type, the bistable landing velocity control type, and the transmission control type. In the first group, the viewing beam originates at a large cathode as a result of photoemission, thermal emission, or secondary emission (Figure 1). The cathode current is locally controlled by insulated elements on the cathode surface which are charged by a scanning writing beam, and imaged on the luminescent screen. Erasing is accomplished by switching the cathode voltage of the writing beam and scanning. To date, this type of viewing tube has been developed only with a photoelectric cathode,[4] which restricts its brightness considerably. The development of a thermionic cathode for such a tube seems to be difficult because of the considerable heating power and the low resistivity of the controlling elements at higher temperatures.

In the second group, a phosphor-covered target is employed with a collector grid parallel to it. The phosphor surface potential can be shifted by a separate erasing and writing beam to values above or below the first crossover of the secondary emission curve (Figure 2). As a result, the arriving viewing beam electrons will shift the surface potential either to the potential of their cathode, or to collector poten-

p. 619, 1941, and Vol. 41, p. 584, 1942; F. Seitz, O. Stern, I. Estermann, R. I. Maurer, S. Lasof, and G. I. Kirkland, "Theory of Dark Trace Tubes," National Defense Research Council (NDRC) Report 14-131, April, 1943, 14-172, September 1943, 14-257, April 1944, 14-265, May 1944; also "Darkening and Bleaching of KCl," NDRC 14-177, September 1943, and 14-205, November 1943.

[3] L. Pensak, "The Graphechon—A Picture Storage Tube," *RCA Review*, Vol. X, p. 59, March, 1949.

[4] Built by G. Krawinkel. See T. F. Adams, "The Krawinkel Image Storing Cathode Ray Tube," Fiat Final Report 1021, P.B. 78273, April, 1947.
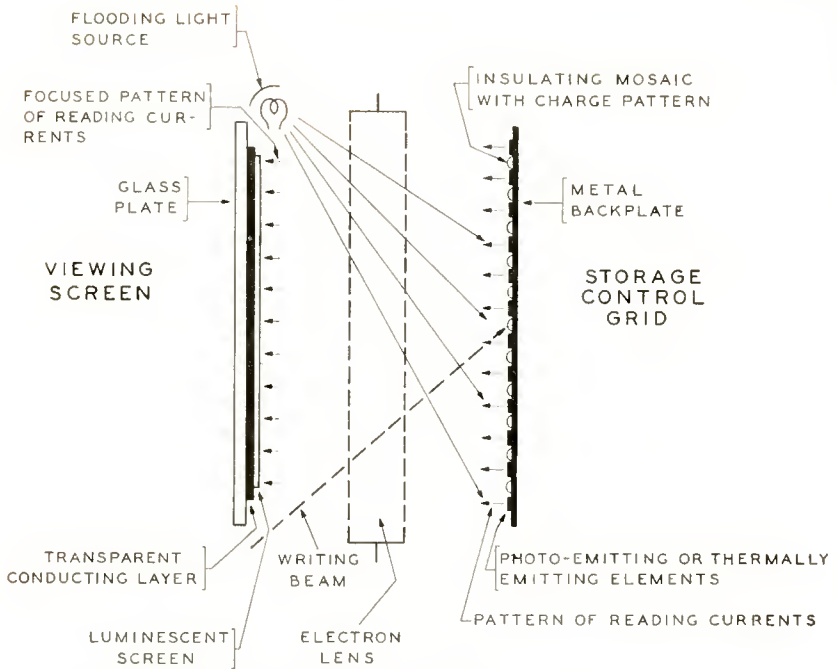
Fig. 1—Principle of emission control in viewing storage tubes.

tial. Thus, "black on white" or "white on black" writing patterns can be obtained at the luminescent screen. This type of tube[5] has a thermionic cathode, but it has a restricted brightness, partially due to limited final electron speed because of secondary emission requirements,
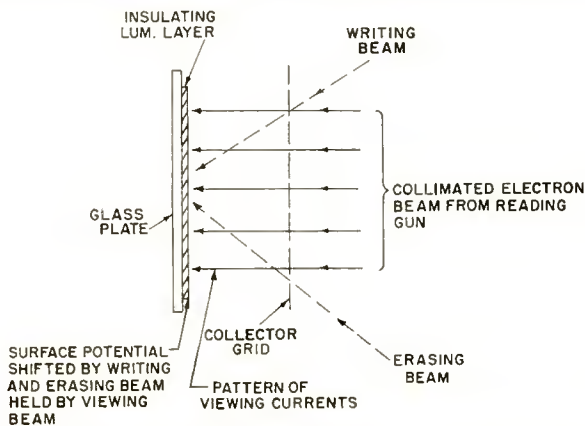
Fig. 2—Principle of bistable landing control in viewing storage tubes.

[5] A. V. Haeff, "A Memory Tube," *Electronics*, Vol. 20, p. 80, September, 1947.

and to the low allowable potential gradient between black and white areas of the pattern.

For the third method (transmission control, Figure 3) the storage target is constructed of a sheet of metal mesh coated with insulating material on one side. A writing beam can produce a pattern of charges on the insulating elements, and thereby locally control the transmission of a flooding viewing beam through the storage target. This beam is

STORAGE
CONTROL
GRID

VIEWING   — METALLIC GRID
SCREEN   [INSULATING LAYER OR MOSAIC
              [WITH CHARGE PATTERN

GLASS   COLLIMATED ELECTRON
PLATE   BEAM FROM READING
                                   GUN.

                                  WRITING BEAM

                          COLLECTOR GRID
                     PATTERN OF READING CURRENTS
              LUMINESCENT LAYER
          TRANSPARENT CONDUCTING LAYER
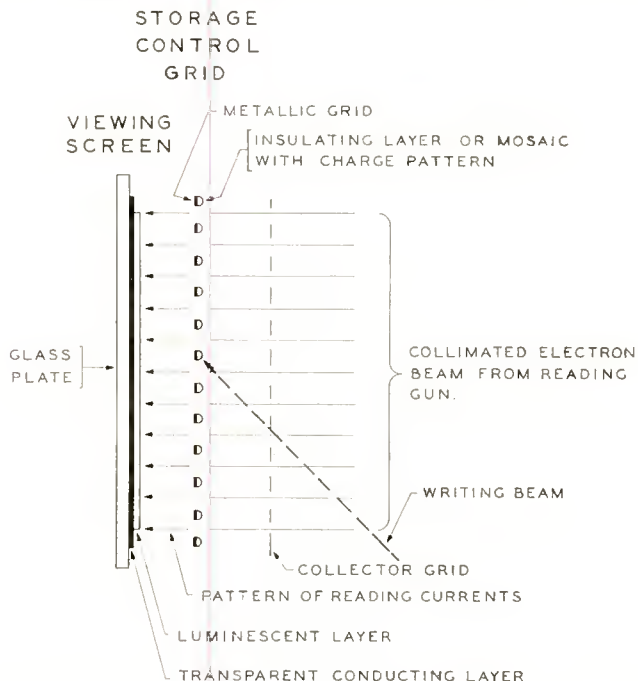
Fig. 3—Principle of transmission control in viewing storage tubes.

then accelerated toward a luminescent screen.[6] Writing of the potential pattern on the controlling storage grid may be accomplished as equilibrium writing, nonequilibrium writing, or bistable writing (with the viewing beam used as a holding beam), whereby not only secondary emission, but also bombardment-induced conductivity of the storage layer may shift its surface potential. Erasing is also performed by

---

[6] Concerning the basic properties of such transmission control storage tubes, and their simplification by the use of electron lens raster image amplifiers, see M. Knoll, "Electron Lens Raster Systems," and about their design, see M. Knoll and P. Rudnick, "Electron Lens Raster Viewing Storage Tubes," in Reports of the National Bureau of Standards Symposium on Electron Physics, November 5-7, 1951. Also: S. T. Smith and H. E. Brown, "Direct Viewing Memory Tube," *Proc. I.R.E.*, Vol. 41, p. 1167, September, 1953.

secondary emission or bombardment induced conductivity, using either
the writing beam, the viewing beam, or a special erasing beam.[7]

<div align="center">TRANSMISSION CONTROL STORAGE TUBE</div>

Figure 4 shows a direct-view storage tube of the transmission
control type* which is capable of simultaneous[8] writing and viewing.
It employs a writing gun and a flooding viewing gun. The storage grid
has the collector grid mounted on one side and a luminescent screen on
the opposite side. All three elements are close spaced and parallel.
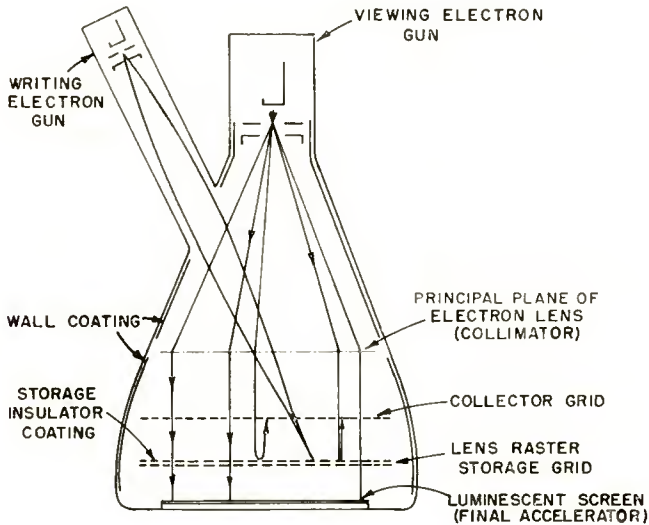
Fig. 4—Direct view storage tube, two-gun type.

The storage grid consists of a fine-mesh (100-500 per linear inch)
metal screen, covered on the gun side with an insulating layer such as
vitreous silica or magnesium fluoride a few microns thick. Input sig-
nals are applied to the control grid of the writing gun while the writing
beam, in scanning, builds up a potential pattern on the storage surface

---

[7] For a description of the different methods of writing, viewing and
erasing mentioned above, see M. Knoll and B. Kazan, *Storage Tubes and
Their Basic Principles*, John Wiley and Sons, New York, N. Y., 1952, p. 79.

* Developed at RCA Laboratories Division, Princeton, N. J., under a
Signal Corps contract.

[8] A transmission control type signal converter storage tube with non-
simultaneous writing and reading, which may be used as a viewing storage
tube also but has to be operated with time sharing writing and reading
circuits, was described by R. C. Hergenrother and B. C. Gardner, "The
Recording Storage Tube," *Proc. I.R.E.*, Vol. 38, p. 745, Fig. 10, July, 1950.
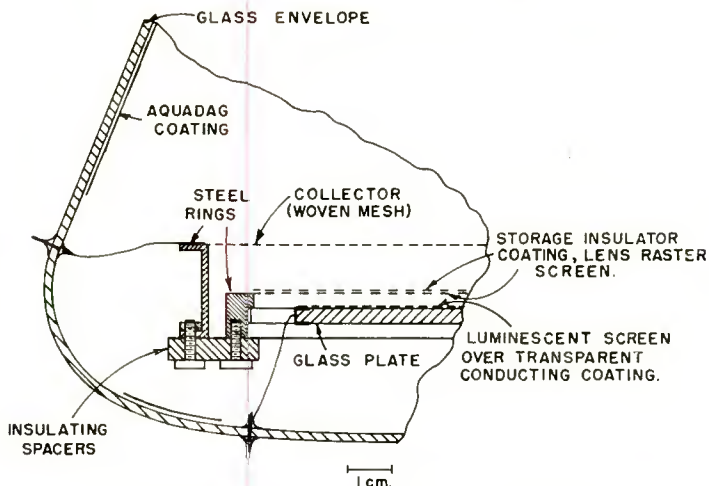
Fig. 5—Viewing storage system using electron lens raster.

due to secondary emission and, in addition, bombardment-induced conductivity. This pattern controls the local transmission of the collimated viewing-beam electrons, which are then accelerated to about 5000 volts in the space between storage grid and anode (luminescent screen). Figure 5 shows the mounting of the target assembly, Figure 6 the exploded view of its elements, and Figure 7 a view of the envelope.

Since focussing requirements do not limit the total current of the flooding viewing beam, such a tube offers, in addition to storage, the
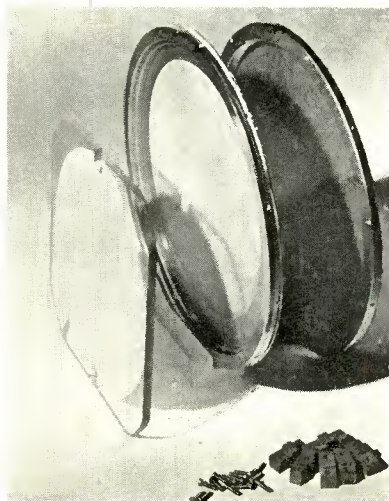
Fig. 6—Viewing storage tube target assembly.
Left to right: luminescent screen, storage grid, and collector grid.

advantage of high brightness for low anode voltages. As a result, a luminance of 500 foot-lamberts has been obtained from a stored 10×10 centimeter picture with only 5000 volts anode voltage. In systems with low frame repetition rates, picture perception is enhanced and flicker effects are reduced, since the viewing beam does not scan the luminescent screen.
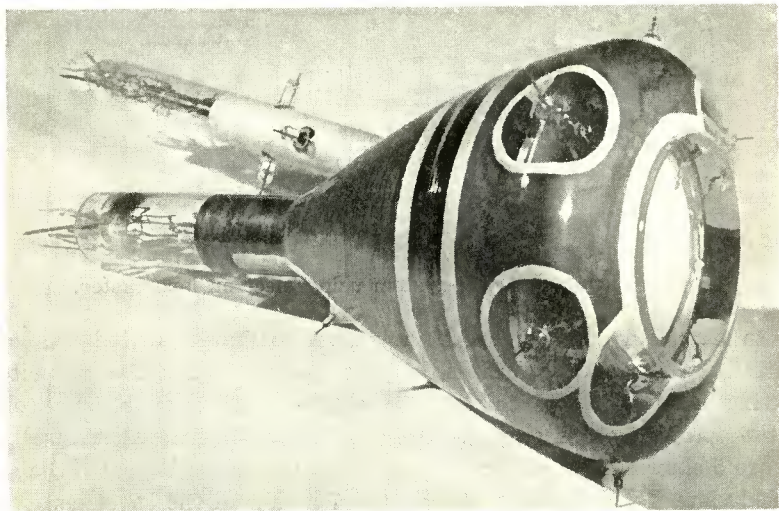
Fig. 7—Direct view storage tube, two-gun type.

OPERATION, RESOLUTION, AND VIEWING DURATION

The viewing beam is collimated and directed toward the storage grid. If, then, in one mode of operation the backplate potential (with respect to viewing cathode) is kept between zero and the first cross-over potential of the secondary emission curve, the viewing beam maintains the storage layer surface at viewing beam cathode potential. Due to the high field strength between viewing screen and storage grid, a large portion of the viewing current will pass through this grid if its surface and metal support (backplate) are both kept near viewing cathode potential. However, by pulsing the backplate a few (10-30) volts positive, the storage surface as a whole can be shifted to a negative potential which will cut off the viewing beam. During writing, a more positive charge pattern may be established at the storage surface by the writing beam, e.g., by using a secondary-emission factor greater than unity and nonequilibrium writing, charging the surface toward collector potential. This positive pattern modulates the viewing current so that a bright positive (white on black) image appears on the

luminescent screen. By a somewhat different process, a negative (black on white) image may also be achieved. Erasing may be accomplished in a fraction of a second by pulsing the storage grid surface positive (approximately $+15$ volts) or by negative pulsing of the viewing cathode so that landing viewing electrons charge the surface to the instantaneous viewing cathode potential during the pulse.

The resolution of the picture may theoretically* be as small as the storage grid hole spacing because of the fact that each of the holes may act as a tiny electron lens, focussing the transmitted electrons to

Immediately.

After 3 minutes.

After 6 minutes.

After 14 minutes.

Fig. 8—Quality of a stored white-on-black picture. The white circle is due to the ion landing effect; pressure is 4×10^{-8} millimeter of mercury.

small separated beams. Such a condition is dependent on a proper choice of the geometry of the target electrodes and their potentials.[6]

At present, 170 mesh per inch storage screens have resolved 100 lines per inch in the stored picture. However, the spot size of the writing beam may be the limitation of resolution in this case.

Figure 8 shows a white-on-black picture displayed on the tube. It was written in approximately 0.1 second. Because all parts of the

---

* This assumes that the focus diameter of the writing beam is sufficiently small.

controlling potential pattern at the storage layer surface are more negative than the viewing cathode, viewing electrons do not land at the storage layer. However, positive ions excited by the viewing beam in the residual gas do land at the storage layer, and thus limit the viewing duration by causing the appearance of the circular white background seen in Figure 8. It was found that, in the absence of target leakage, the viewing duration is inversely proportional to the pressure in the tube.

Fig. 9—Quality of a stored halftone picture. Viewing duration is from one to ten seconds, depending on the residual gas pressure.

HALFTONES

Fundamentally, transmission control type storage tubes are capable of producing halftones but only if variations in secondary emission and amplification factor over the storage grid are kept small,[9] and the erasing action of positive ions limited.[10] Figure 9 shows the quality of stored halftone pictures (which may be written in 1/30 second) obtained with the direct-view storage tube. Here the nonuniformity of the background plays a more important role than in black and white

[9] M. Knoll, "Background Patterns in Storing Image Amplifier Systems due to Variations in Amplification Factor and Secondary Emission," National Conference on Electron Tube Techniques, October 15, 1953, New York, N. Y.

[10] R. P. Stone, "Some Problems in the Design of a Direct View Storage Tube," National Conference on Electron Tube Techniques, October 15, 1953, New York, N. Y.

pictures, where the "black" areas of the storage surface can be charged to a much higher negative potential than the cutoff potential of the viewing current characteristic. The viewing durations obtained in a vacuum of 10^{-7} millimeter of mercury were of the order of 10 seconds without using the restoring operation mentioned below.

The effect of ion landing may be avoided by pulsing the backplate slightly more positive than the first crossover potential V_{cr1}. During the pulse, viewing electrons will land with velocities $> V_{cr1}$ at storage surface areas corresponding to bright picture areas, and viewing electrons will land with velocities $< V_{cr1}$ at storage surface areas corresponding to dark picture areas. Thus, a restoring action is performed, whereby the more negative storage layer potentials are driven more negative, and the less negative storage layer potentials are driven less negative (or positive) during the pulse. If the pulses are too short, the restoring action is insufficient. If the pulses are too long, the surface tends to go to collector potential which may cause layer breakdown and creeping of electrical charges across the surface.

With this pulse restoring method, using pulses of approximately 1 microsecond at a repetition rate of 15,000 per second, viewing durations as long as 27 hours have been observed for black and white pictures, and 15 minutes for halftone pictures.

Considering the fact that high brightness at low viewing voltage, simultaneous writing and viewing, and the storage of halftones can be achieved by adding only a few elements to the conventional cathode ray tube, it seems that the transmission-type storage tube is at present the most promising of the viewing storage tubes.

ACKNOWLEDGMENT

FILTER-HELIX TRAVELING-WAVE TUBE*

PART I. THE FILTER HELIX, A NEW CIRCUIT ELEMENT FOR TRAVELING-WAVE AMPLIFIERS AND OSCILLATORS

By

W. J. DODDS AND R. W. PETER

Research Department, RCA Laboratories Division,
Princeton, N. J.

Summary—This paper introduces a new delay-line circuit for traveling-wave amplifiers and oscillators: the filter helix. A filter helix consists essentially of a helical transmission line with periodic inhomogeneities which cause local power reflection. It is, therefore, basically a special type of a one-dimensional lattice, and exhibits all its characteristic features. It has frequency pass and stop bands and it is dispersive, i.e., its phase velocity changes with frequency in the pass bands. The particular characteristics and advantages of the filter helix as delay-line circuit in low-voltage traveling-wave tubes are discussed.

In this paper, the filter helix is treated as a passive circuit element. Various possible constructions of filter helices are discussed and classified into three types. The frequency pass and stop bands, the phase velocity of different propagation modes, and the impedance are related to various filter-helix parameters. These studies are based upon a simplified model of the actual filter helix.

In later papers, it is planned to treat the behavior of filter helices in the presence of an electron beam and their particular advantages as interaction circuits for medium power and low-noise traveling-wave tubes. Remarkable results have been obtained in some experimental filter-helix tubes: 22 per cent efficiency in an 800-volt 5-watt power tube operated at 2000 megacycles, and less than 8 decibels noise factor in a 500-volt low-noise tube operated at 3000 megacycles.

Part of the work covered in these papers was done under a Signal Corps contract and has been reported earlier.[1]

INTRODUCTION

IN many applications for microwave amplifiers, e.g., radio relays, radar receivers, etc., the frequency band to be amplified is relatively small, usually less than 1 per cent. A helix-type traveling-wave tube, however, is inherently a broadband amplifier. Like any other amplifier it can be characterized by its "gain × bandwidth" product. One of the two factors can always be increased at the cost of the other, since, in general, the product stays constant over a considerable range of operating conditions. From this viewpoint it is readily seen that a

---

* Decimal Classification: R339.2.
[1] Fourth Quarterly Report (February-April 1952), Contract No. DA36-039-sc-5548.

broadband traveling-wave tube which is required to amplify only a small frequency band is not operating at the optimum gain which it is capable of producing over the given band.

The gain of a traveling-wave tube can be increased either by reducing the stored energy per unit length of interaction circuit which is necessary to produce a certain field in the interaction region, or by reducing the group velocity on the circuit. To reduce the group or energy velocity along the circuit, its dispersion, i.e., the change of phase velocity with frequency, has to be increased. Since a traveling-wave tube amplifies only if beam and phase velocity are nearly equal, increased dispersion means reduced amplification bandwidth.

These relations have been pointed out by Pierce.[2, 3] Concerning the stored energy, his comparative study shows that at beam voltages below 1000 volts, the helix has the smallest stored energy for a given interacting field strength. Other structures, e.g., disc-loaded waveguides and coaxial lines,[4-5] are superior at larger beam voltages. In this study, only the low-voltage tube application where the helix is the preferred circuit is considered.

To increase the gain of a helix tube and reduce the amplification bandwidth, either the "natural" dispersion of the helix may be used, as did Robinson,[6] or "artificial" dispersion may be introduced which leads directly to the concept of the filter helix. This original aim of controllably increasing the dispersion in a helix is achieved in closest approximation in what is later defined as the type-B filter helix.

Later constructional developments have revealed other advantages of the filter helix. For example, the large possible physical size permits large currents with low circuit losses which is particularly desirable at ultra-high frequencies.

THREE TYPES OF FILTER HELICES

The filter-helix consists of a helical conductor with periodic inhomogeneities. These inhomogeneities can be external or internal with respect to the helix or in the same surface as the helical conductor

[2] J. R. Pierce, "Circuits for Traveling-Wave Tubes," *Proc. I.R.E.*, Vol. 37, p. 510, May, 1949.

[3] J. R. Pierce, *Traveling-Wave Tubes*, D. Van Nostrand Co., Inc., New York, N. Y., 1950.

[4] L. M. Field, "Some Slow-Wave Structures for Traveling-Wave Tubes," *Proc. I.R.E.*, Vol. 37, pp. 34-40, January, 1949.

[5] G. C. Dewey, P. Parzan, T. J. Marchese, "Periodic-Waveguide Traveling-Wave Amplifier for Medium Powers," *Proc. I.R.E.*, Vol. 39, p. 153, February, 1951.

[6] F. N. H. Robinson, "Traveling-Wave Tubes with Dispersive Helices," *Wireless Eng.*, Vol. 28, p. 110, April, 1951.

(more accurately between the two cylindrical surfaces enveloping it). According to these structural differences, filter helices may be classified as three types:

Type A—Filter helices with periodic structure external to helical con-
        ductor,

Type B—filter helices with periodic structure coplanar with the helical
        conductor,

Type C—filter helices with periodic structure contained within the
        cylinder defined by the helical conductor.

Several practical filter helices of the three types are shown schematically in Figure 1, and photographs of their actual construction in Figures 2 to 7.

Figure 2 shows the type-A structure used in the first filter-helix traveling-wave tube built. This is represented by the schematic of Figure 1a. The beam flows through the center of the helix which is held in position by ceramic rods and is close spaced with respect to the surrounding periodic disc structure. The disadvantage of this construction is that the spacing between helix and discs has to be kept very small to obtain sufficient coupling in a low-voltage circuit. The required tolerances on the disc dimensions then become impractically narrow.

Figure 3 shows three different versions of the type-A filter helix of Figure 1b. Short tabs are welded to the helix wire in a periodic array. The helix could be supported on such tabs within a glass or nonpropagating metal envelope (i.e., a waveguide below cutoff).

In the examples for type-B filter helices, the periodic inhomogeneity consists in the case of Figure 4 of a change of pitch which represents a change in impedance, and in the filter helix of Figure 5 of a short circuit between adjacent turns. These two possibilities correspond to those of Figures 1c and 1d. Instead of a direct connection between adjacent turns, adjustable capacitive shunting could be used to control the circuit impedance and propagation constant independently.

Figures 6 and 7 represent filter helices of type C. Equally spaced concentric rings are suspended inside the helix by welded tabs. The great advantage of these circuits is their larger physical size which results in large power-carrying capacity, lower circuit loss and greater rigidity—qualities which are especially desired in power tubes.

TYPE-B FILTER HELIX

Every filter helix, being basically a one-dimensional periodic struc-

ture, produces a traveling field configuration which can be resolved in an infinite number of space-harmonic modes $E_n(r)$ each moving with a different propagation constant
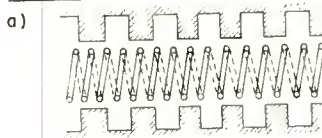
$$\beta_n = \frac{\theta + 2\pi n}{l_0} \qquad n = \cdots -2, -1, 0, 1, 2, \cdots \qquad (1)$$

where l_0 is the axial physical length of one filter unit and θ its electrical phase angle for the fundamental mode. The total field, therefore, can be expressed as

$$E(r, z, t) = \sum_n E_n(r)\, e^{-j\beta_n z}\, e^{j\omega t}. \qquad (2)$$

FILTER HELIXES

TYPE A

a)

b)

TYPE B
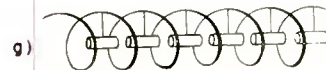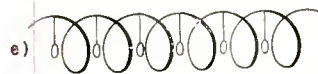
c)

d)

TYPE C

e)

f)

g)

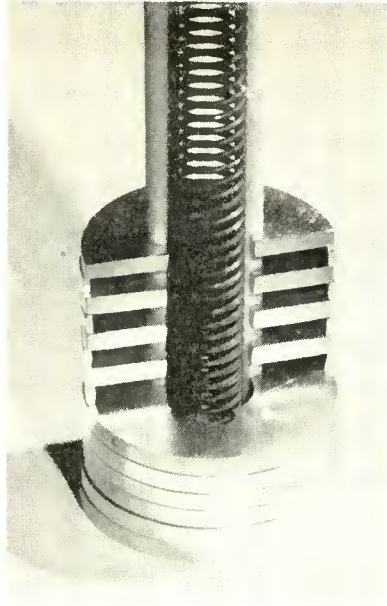Fig. 1—Classification of filter-helix types.

Fig. 2—Type-A filter helix, showing periodic loading by changes in diameter of outer conductor. This corresponds to Figure 1a.

This field is built up by energy W_x stored in the periodic lumped reactances, and by energy W_h stored in the helical line. The contribution of energies W_x and W_h to the field of the interacting mode may vary depending upon the location of the interacting electron beam within the field of the filter helix.

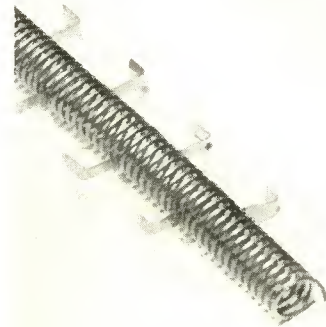It is readily seen that in the case of the type-A filter helices, beam

Fig. 3—Type-A filter helix, showing periodic loading by addition of local reactances which consist of short tabs. This filter helix corresponds to **Figure 1b.**

Fig. 4—Type-B filter helix with periodic changes in helix impedance by changes in pitch. This corresponds to the variable-pitch filter helix of Figure 1c.

interaction is predominantly with the helix energy W_h, whereas in the case of type-C circuits, interaction is mainly with the lumped-reactance energy W_x. In the type-B filter helices, essentially all the energy is stored on the helix. For this case, the lumped-reactance energy, W_x, i.e., the energy stored in the shorting strips in Figure 1d, is negligible in comparison with the helix energy, W_h. Therefore, essentially all the stored energy contributes to the beam-interaction field.

The gain of a traveling-wave tube may be characterized by the gain factor[3]

$$C = \left(\frac{K}{4\ V_0/I_0} \right)^{\frac{1}{3}} \tag{3}$$

which is a function of the ratio between the alternating-current impedance of the circuit, K, and the direct-current impedance of the beam, V_0/I_0. The circuit impedance, K, which is of concern here, is defined[3] as the useful field in the beam region per unit transmitted power:
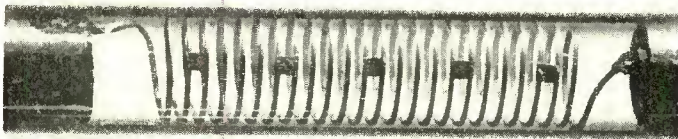

Fig. 5—Type-B filter helix with periodically shorted turns. This corresponds to Figure 1d.

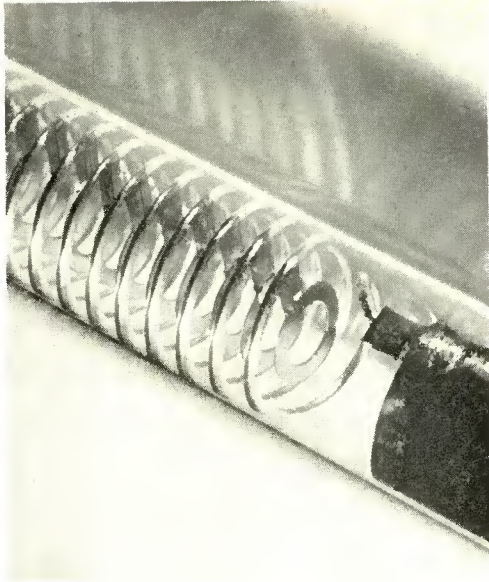Fig. 6—Type-C filter helix, showing periodic loading by added local reactances consisting of loop-tabs attached at the insides of the helix. This corresponds to Figure 1e.
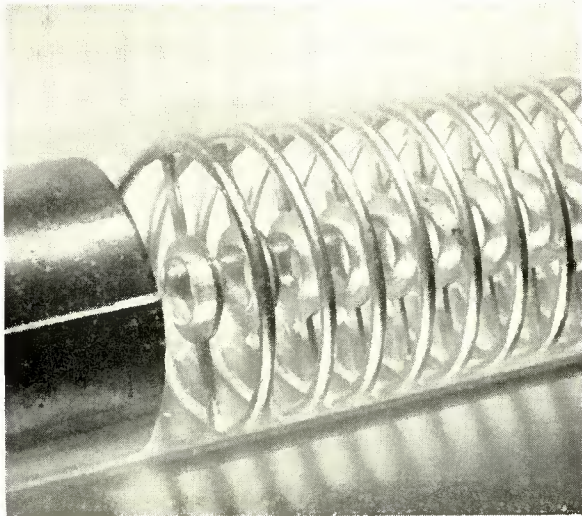

Fig. 7—Type-C filter helix with inner loops periodically attached to opposite sides of the helix turns. This corresponds to Figure 1f. It is a complex circuit with many of the characteristics of the type shown in Figure 1e.

$$K = \frac{E^2}{2\beta^2 P} = \frac{E^2}{2\beta^2 W v_g} \tag{4}$$

where $E =$ useful field in the beam region,

$P =$ transmitted power,

$W =$ total stored energy,

$\beta = \omega/v =$ circuit propagation constant,

$v_g =$ group velocity,

$v =$ phase velocity.

For a given phase velocity, v, the circuit impedance, K, is proportional to the useful field per unit of stored energy, E^2/W, and inversely proportional to the group velocity, v_g, where

$$v_g = \frac{v}{1 - \frac{\omega}{v}\frac{\partial v}{\partial \omega}}. \tag{5}$$

It can be shown that periodic insertion of discontinuities along a uniform helix leads (to a first approximation) to

$$E^2/W = \text{constant} \tag{6}$$

if the discontinuities are chosen so as to transform the helix into a filter helix of type B. Therefore, the increase of impedance in this type is nearly proportional to the decrease of group velocity, i.e.,

$$\frac{K}{K_0} \doteq \frac{v_{g0}}{v_g} \doteq \frac{v}{v_g} \tag{7}$$

where the index "0" refers to the parameters of the uniform helix. Thus, by increasing the delay line dispersion $(-\partial v/\partial \omega)$, the impedance K can be raised above that of the uniform helix at the expense of the amplification bandwidth $(\Delta\omega/\omega)$. For the beam-voltage range below 1000 volts, which is the desired range for a practical low-power amplifier tube, the helix is the best circuit (see Reference (3), p. 91) as regards its radio-frequency impedance K, under broadband condition $v = v_g$. Thus, by increasing the impedance K of such a helix

according to Equations (5) and (7), exchanging higher impedance for smaller bandwidth, this helix will still remain the best circuit for the given amplification bandwidth. The filter-helix type B is believed to approximate this optimum circuit closely. It may be pointed out here, that any physically realizable helical conductor can be regarded as being in itself a degenerated type-B filter helix. The periodically recurring inhomogeneities of the helical conductor are the turns of the helix wire[7, 8] themselves.

A FILTER HELIX MODEL

In this section the passive behavior of an infinitely long filter helix is studied. The simplifying assumption of infinite length will be
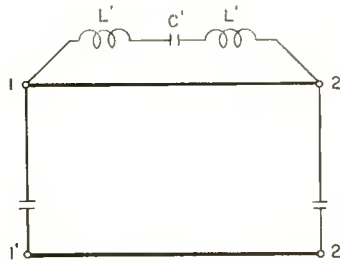

Fig. 8—An approximate equivalent circuit for the type-C filter helices shown in Figures 1e, 6 and 7, consisting of a uniform transmission line with a lumped-element bypass path.

dropped later. We replace the actual filter helix (Figure 1) by a simplified model consisting of an infinite chain of identical four-pole units. A unit might, for example, be composed of different sections of transmission line and different lumped susceptances. For the filter helices of Figures 1e and 1g, a simplified equivalent filter-network unit would be that shown in Figure 8. The simplest equivalent network for a unit of the variable impedance filter helix of Figure 1a is shown in Figure 9. The discussion of the basic properties of filter helices will be based upon the equivalent filter unit of Figure 9. It represents also a useful approximation for the circuits in Figures 1b and 1c, and also for 1e and 1g as long as the shunt susceptance represented by L' and

---

[7] Samuel Sensiper, "Electromagnetic Wave Propagation on Helical Conductors," Ph. D. Thesis, Electrical Engineering Department, Massachusetts Institute of Technology, May, 1951.

[8] P. K. Tien, "Helix Impedance of Traveling-Wave Tubes," Tech. Rep. No. 50, June 27, 1952, Stanford University, Electr. Res. Lab., Contract N6 ONR-251.

C' between lumped elements (Figure 8) is negligible. The model, therefore, consists of sections of different impedance, Z_1 and Z_2, and different electrical length or angles, θ_1 and θ_2. It is chosen to be symmetrical for computational reasons only.

ELECTRICAL ANGLE	$\theta_1/2$	θ_2	$\theta_1/2$
IMPEDANCE	Z_1	Z_2	Z_1
CHAIN MATRIX	(m_1)	(m_2)	(m_1)
PHASE VELOCITY	v_1	v_2	v_1
PHYSICAL LENGTH	$\ell_1/2$	ℓ_2	$\ell_1/2$

I FILTER ELEMENT   FIG. 9a

TOTAL EL ANGLE	θ
CHARACTERISTIC IMPEDANCE	Z
CHAIN MATRIX	(M')
PHASE VELOCITY	v
GROUP VELOCITY	v_g
PHYSICAL LENGTH	ℓ_o

$y_o = \dfrac{1}{Z}$ jB FIG. 9b
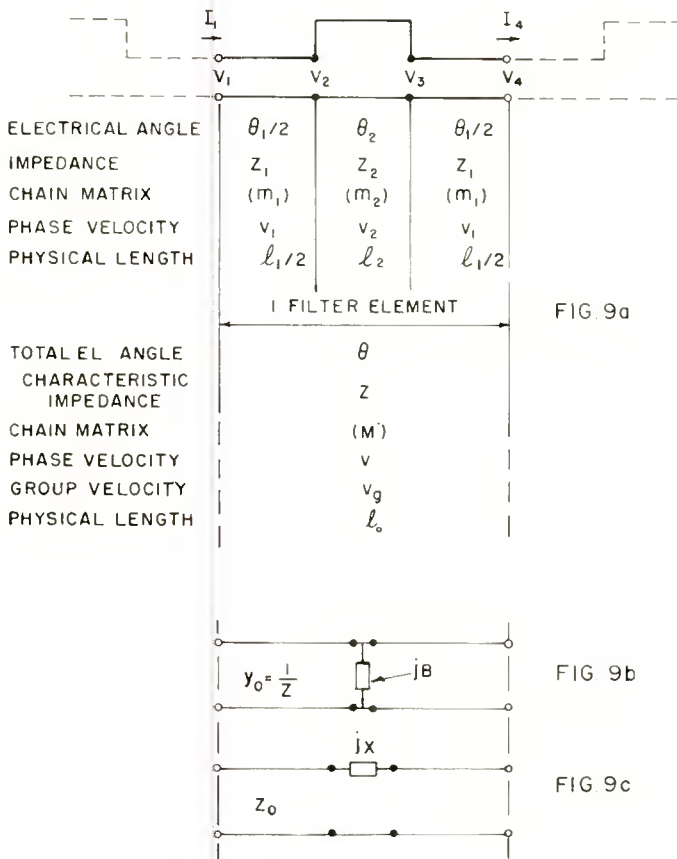
jx FIG. 9c

Z_0

Fig. 9—(a) Equivalent circuit for filter helices with changing impedance, as, e.g., those of Figures 1a and 1c; (b and c) equivalent circuits for filter helices with periodic lumped shunt susceptances and series reactances, as, e.g., those in Figures 1b and 1e.

The electrical angles θ_1 and θ_2 are determined by the physical length of the two sections, l_1 and l_2, and their respective phase velocities, v_1 and v_2, which may be different. For example, the axial phase velocity of a helix changes with its distance from a surrounding shield as seen

in Figure 10[*] where the relative phase velocity, v/c, is plotted in normalized form for various shield-to-helix diameter ratios, d/a, versus the helix design parameter,
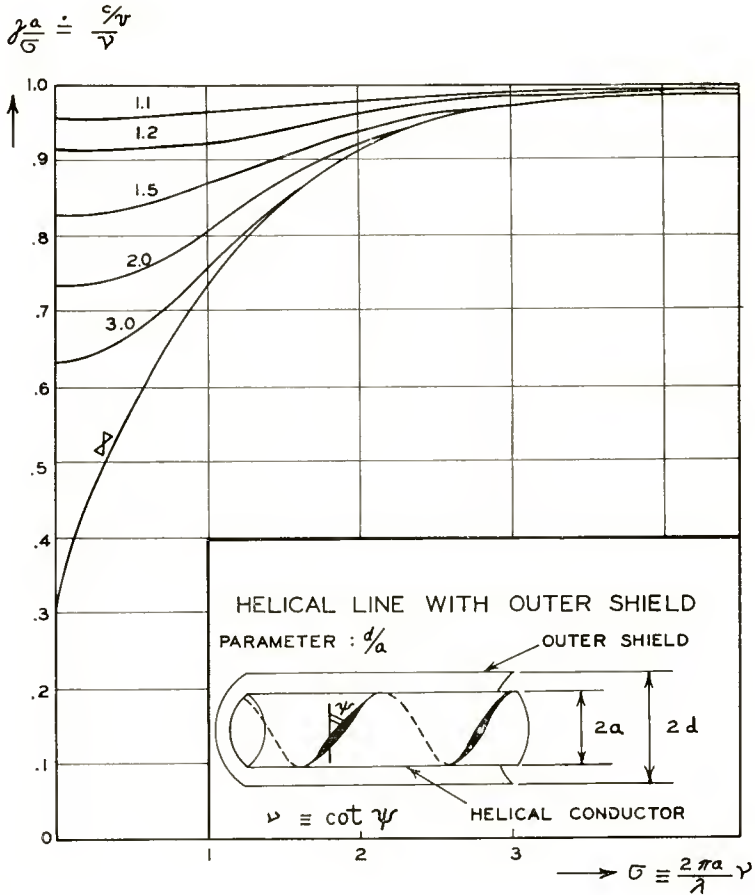
$$\sigma = \frac{2\pi a}{\lambda} \cot \psi \qquad (8)$$

Fig. 10—Effect of outer shield upon the phase velocity of a helix.

where λ is the free space wave length, $2a$ the helix diameter and ψ the winding angle.

The evaluation of the characteristic behavior of the filter-helix model of Figure 9 is based upon standard matrix analysis of chain filters[9] and linear lattices.[10]

The symmetrical filter unit of Figure 9 contains three sections of uniform transmission line joined together. In each section there exists the amount of forward and of backward traveling energy necessary to match the boundary conditions. If the voltage of the forward traveling energy of a piece of line of impedance Z and electrical length ϕ is V^+ and the voltage of the reflected energy is V^-, then their sum represents the input voltage V_a and output voltage V_b:

$$V_a = V_a{}^+ + V_a{}^- = V_a{}^+ + V_b{}^- e^{-j\phi}$$
$$V_b = V_b{}^+ + V_b{}^- = V_a{}^+ e^{-j\phi} + V_b{}^-. \tag{9}$$

The corresponding reflected current, $I^- = V^-/Z$, however, subtracts from the forward traveling current, $I^+ = V^+/Z$:

$$ZI_a = V_a{}^+ - V_a{}^- = V_a{}^+ - V_b{}^- e^{-j\phi}$$
$$ZI_b = V_b{}^+ - V_b{}^- = V_a{}^+ e^{-j\phi} - V_b{}^-. \tag{10}$$

Eliminating the forward and backward traveling components, the relation between input and output quantities may be written as

$$V_a = V_b \cos\phi + jI_bZ \sin\phi$$
$$I_a = (jV_b/Z) \sin\phi + I_b \cos\phi \tag{11}$$

or in chain matrix form

$$\begin{pmatrix} V_a \\ I_a \end{pmatrix} = (m) \begin{pmatrix} V_b \\ I_b \end{pmatrix} = \begin{pmatrix} \cos\phi & jZ \sin\phi \\ \dfrac{j}{Z} \sin\phi & \cos\phi \end{pmatrix} \begin{pmatrix} V_b \\ I_b \end{pmatrix} \tag{12}$$

The whole filter unit of Figure (9a) consists of three such line sections. By multiplying their respective chain matrices (m_n) one obtains the equations relating input quantities V_1, I_1 and output quantities V_4, I_4:

$$\begin{pmatrix} V_1 \\ I_1 \end{pmatrix} = (m_1) \ (m_2) \ (m_1) \begin{pmatrix} V_4 \\ I_4 \end{pmatrix} = (M) \begin{pmatrix} V_4 \\ I_4 \end{pmatrix} \tag{13}$$

---

[9] L. A. Pipes, "The Matrix Theory of Four-Terminal Networks," *Phil. Mag.*, Vol. 36, Seventh Series, p. 370, 1940.

[10] A. W. Lines, "Some Properties of Waveguides with Periodic Structure," *Proc. Inst. Elec. Eng.*, Vol. 97, Part III, p. 263, July, 1950.

where

$$(M) = \begin{bmatrix} \cos \dfrac{\theta_1}{2} & jZ_1 \sin \dfrac{\theta_1}{2} \\[2ex] jZ_1{}^{-1} \sin \dfrac{\theta_1}{2} & \cos \dfrac{\theta_1}{2} \end{bmatrix} \begin{pmatrix} \cos \theta_2 & jZ_2 \sin \theta_2 \\[1ex] jZ_2{}^{-1} \sin \theta_2 & \cos \theta_2 \end{pmatrix}$$

$$\begin{bmatrix} \cos \dfrac{\theta_1}{2} & jZ_1 \sin \dfrac{\theta_1}{2} \\[2ex] jZ_1{}^{-1} \sin \dfrac{\theta_1}{2} & \cos \dfrac{\theta_1}{2} \end{bmatrix} \tag{14}$$

$$(M) = \begin{pmatrix} A & B \\ C & D \end{pmatrix} = \begin{pmatrix} \cos \theta & jZ \sin \theta \\ jZ^{-1} \sin \theta & \cos \theta \end{pmatrix} \tag{15}$$

The multiplication (14) carried through yields the following coefficients for the matrix (15):

$$A = D = \cos \theta_1 \cos \theta_2 - \zeta \sin \theta_1 \sin \theta_2 \tag{15a}$$

$$B = jZ_1 \left\{ \sin \theta_1 \cos \theta_2 + \sin \theta_2 \left(\frac{Z_2}{Z_1} \cos^2 \frac{\theta_1}{2} - \frac{Z_1}{Z_2} \sin^2 \frac{\theta_1}{2} \right) \right\} \tag{15b}$$

$$C = jZ_1{}^{-1} \left\{ \sin \theta_1 \cos \theta_2 + \sin \theta_2 \left(\frac{Z_1}{Z_2} \cos^2 \frac{\theta_1}{2} - \frac{Z_2}{Z_1} \sin^2 \frac{\theta_1}{2} \right) \right\} \tag{15c}$$

where
$$\zeta \equiv \frac{1}{2} \left(\frac{Z_1}{Z_2} + \frac{Z_2}{Z_1} \right) \tag{16}$$

The complete description of the filter-chain unit of Figure (9) is contained in (15).

The phase angle θ of the unit cell is, according to (15a),

$$\theta = \cos^{-1} A \tag{17}$$

and the characteristic impedance of the infinite filter chain becomes

$$Z_0 = \sqrt{\frac{B}{C}}. \tag{18}$$

PHASE AND GROUP VELOCITY

If, for convenience, we let the electrical lengths of the line sections (Figure 9) be

$$\theta_1 = \alpha \theta_0$$
$$\theta_2 = (1 - \alpha) \; \theta_0 \tag{19}$$

where $\theta_0 = \theta_1 + \theta_2$, then the phase angle per unit cell, θ, of the infinite filter chain becomes, with (15a),

$$A = \cos \theta = \cos \alpha \, \theta_0 \cos (1 - \alpha) \; \theta_0 - \zeta \sin \alpha \, \theta_0 \sin (1 - \alpha) \; \theta_0 . \tag{20}$$

This can be transformed into

$$\cos \theta = \frac{\zeta + 1}{2} \cos \theta_0 - \frac{\zeta - 1}{2} \cos \left(\theta_0 \, (1 - 2\alpha) \right) \tag{21}$$

or simplified still further into

$$\cos \theta = (1 + \epsilon) \cos \theta_0 - \epsilon \cos \left(\theta_0 \, (1 - 2\alpha) \right) \tag{22}$$

where

$$\epsilon \equiv \frac{\zeta - 1}{2} = \frac{(Z_1 - Z_2)^2}{4 \, Z_1 \, Z_2} \geq 0. \tag{22a}$$

Denoting the right-hand side of Equation (20) or (21) by y, its solution can be written

$$\theta = \theta' + 2\pi n = \cos^{-1} y \tag{23}$$

$$n = \cdots - 2, -1, 0, 1, \cdots \cdots$$

A detailed display of the multivalued solution (23) of Equation (21) is given in Figure 11. Although computed for this particular filter model, Figure 11 contains all basic characteristics of any repetitive filter chain or one-dimensional lattice. The pass-bands of the filter chain would, for example, correspond to the different energy bands in the one-dimensional model of a solid, etc. Figure 11 was plotted for the special parameters

$$\zeta = 2 \; (\text{or} \; Z_1/Z_2 = 3.75) \; \text{and} \; \alpha = 3/8.$$

The left-hand and the right-hand sides of Equation (20) or (21) were plotted in the upper part of Figure 11 on the left and on the right sides of the vertical axis respectively. For every value of θ_0 for which $|y| \leq 1$, there is an infinite set of real solutions of θ. This is shown clearly in the upper family of curves where θ is plotted directly
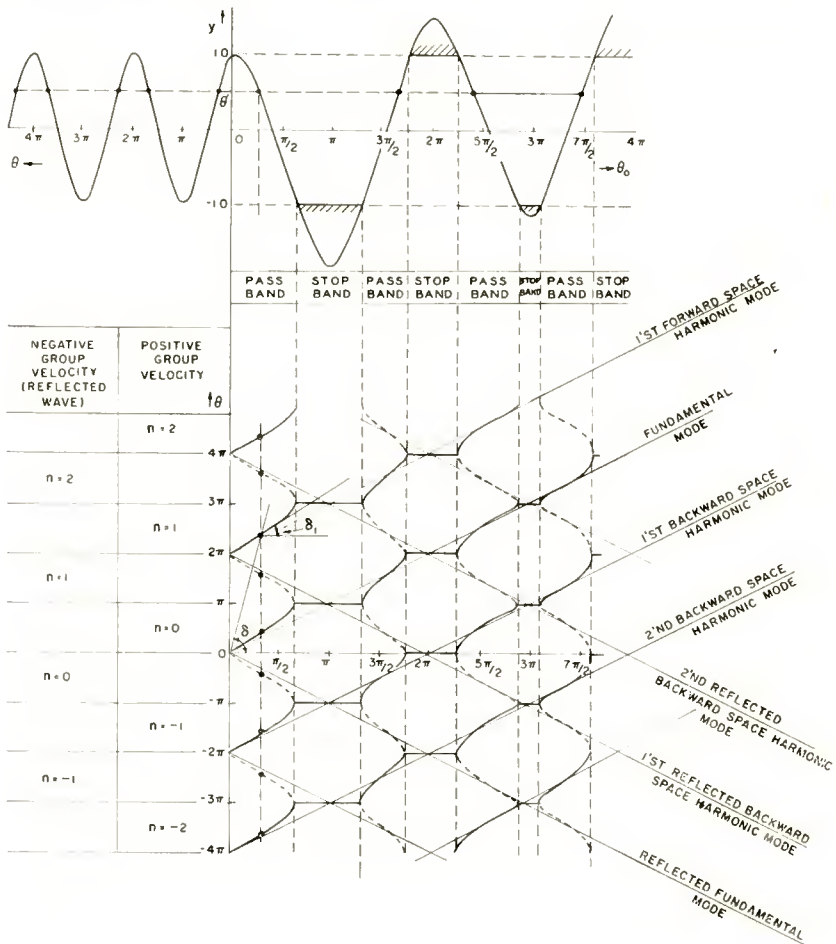

Fig. 11—Display of the solutions of the lattice Equations (21)-(23) showing the pass and stop bands, and the forward and backward propagating modes.

as a function of θ_0. Whenever $|y|$ is larger than unity, no real solution of (23) for θ exists, i.e., in those regions no unattenuated power propagation along the infinite filter chain is possible. The regions are therefore called "stop bands," while the regions which permit unattenuated power transfer are known as the "pass bands."

The edges of the bands or the cutoff frequencies, $\theta_0 = \theta_c$, are obviously obtained from the condition:

$$\cos \theta = \pm 1 \tag{24}$$

or

$$(1 + \epsilon) \cos \theta_c - \epsilon \cos (\theta_c (1 - 2\alpha)) = \pm 1 \tag{25}$$

where

$$\theta = m\pi \quad (m = 0, 1, 2 \cdots \cdots).$$

At the cutoff frequencies, the electrical length of one filter unit is just a half-wave length or that multiple thereof which causes destructive interference of the primary and the reflected waves along the filter array.

The total phase angle per filter unit of physical length l_0 ($l_0 = l_1 + l_2$) determines the *phase velocity* v along the delay line of Figure 9:

$$\theta = \omega \frac{l_0}{v}. \tag{26}$$

The sum of the electrical lengths of the two line sections can be expressed as

$$\theta_0 = \omega \left(\frac{l_1}{v_1} + \frac{l_2}{v_2} \right) \tag{27}$$

In many filter-helix constructions, the difference between the phase velocities of the two line sections, v_1 and v_2, is sufficiently small that we can assume

$$v_1 = v_2 = v_0. \tag{28}$$

Under this condition, (27) becomes

$$\theta_0 = \omega \left(\frac{l_1}{v_1} + \frac{l_2}{v_2} \right) = \omega \frac{l_0}{v_0} \tag{29}$$

and the ratio between the actual phase velocity along the filter line, v, and the phase velocity v_0 for an equally long homogeneous line becomes, with Equation (23),

$$\frac{v}{v_0} = \frac{\theta_0}{\theta} = \frac{\theta_0}{\theta' + 2\pi n} = \cot \delta \qquad (30)$$

$$n = \cdots - 2, -1, 0, 1 \cdots$$

From Figure 11 it is seen that the relative phase velocity v/v_0 is given by the slope (angle δ) of the connecting line between an arbitrary point of the phase curves and the origin. v decreases with increasing mode number n.

Similarly it can be readily shown that the slope of the phase curves themselves (angle δ_1 in Figure 11) represents the *group velocity*

$$v_g = v \left(1 - \frac{\omega}{v} \frac{\partial v}{\partial \omega} \right)^{-1} \qquad (5)$$

By differentiating (30) one obtains

$$\frac{\partial \theta}{\partial \theta_0} = v_0 \frac{\partial}{\partial \omega} \left(\frac{\omega}{v} \right) = \frac{v_0}{v^2} \left(v - \omega \frac{\partial v}{\partial \omega} \right) = \frac{v_0}{v_g}$$

and therefore (Figure 11)

$$\frac{\partial \theta_0}{\partial \theta} = \cot \delta_1 = \frac{v_g}{v_0} \qquad (31)$$

which is the same for all mode numbers n at a given frequency, θ_0.

With (30) and (31) it is now easy to identify the different branches of the phase curves in Figure 11 as the different modes of the four basic wave types tabulated below in Table I.

Table I

	Positive Group Velocity	Negative Group Velocity
Positive Phase Velocity	Forward Wave	Reflected Forward Wave
Negative Phase Velocity	Backward Wave	Reflected Backward Wave

For the fundamental mode of the forward wave which is used most often in traveling-wave type amplifiers, the relative phase velocity is

plotted in the upper portion of Figure 12. The same parameters were chosen here as for Figure 11:

$$\zeta = 2 \ (Z_1/Z_2 = 3.75), \qquad \alpha = 3/8.$$

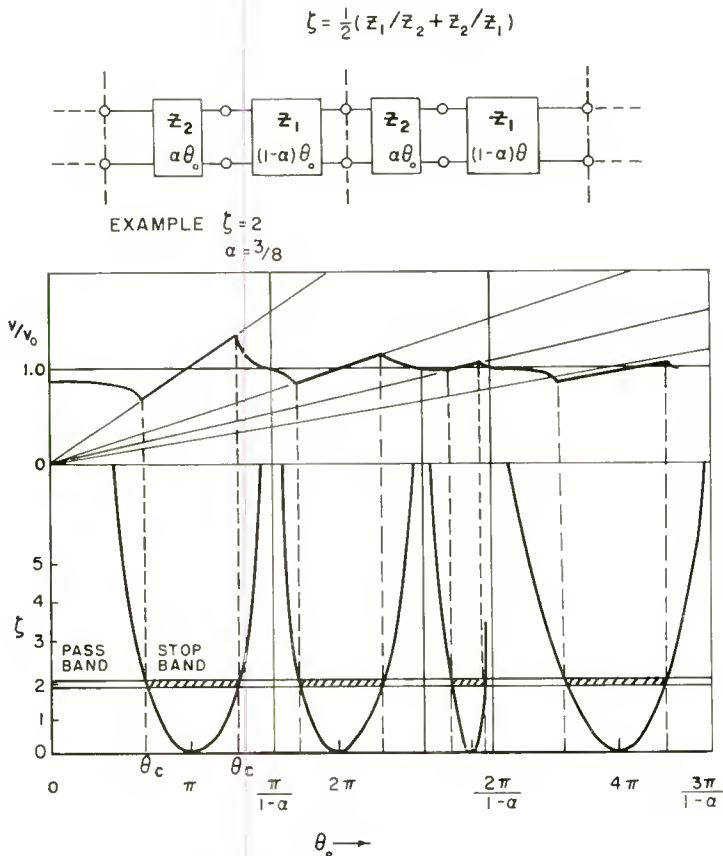The more detailed relative phase velocity curves computed for the con-

Fig. 12—Relation between the relative phase velocity and the pass bands of a particular filter.

figurations $\alpha = 1/2$ and $\alpha = 1/4$ will be discussed later (Figures 15 and 16).

In the lower portion of Figure 12, the boundaries between stop and pass bands, i.e., the cutoff phase angles θ_c, are plotted as functions of the line-impedance ratio Z_1/Z_2. The relation is found from (25) yielding:

$$\epsilon \equiv \frac{\zeta - 1}{2} = \frac{\pm 1 - \cos \theta_c}{\cos \theta_c - \cos \theta_c (1 - 2\alpha)} . \tag{32}$$

A detailed plot of the cutoff frequencies (or phase angles $\theta_0 = \theta_c$) versus ζ for several values of the relative line-section length, α, is presented in Figure 13a. All these curves which separate pass band from
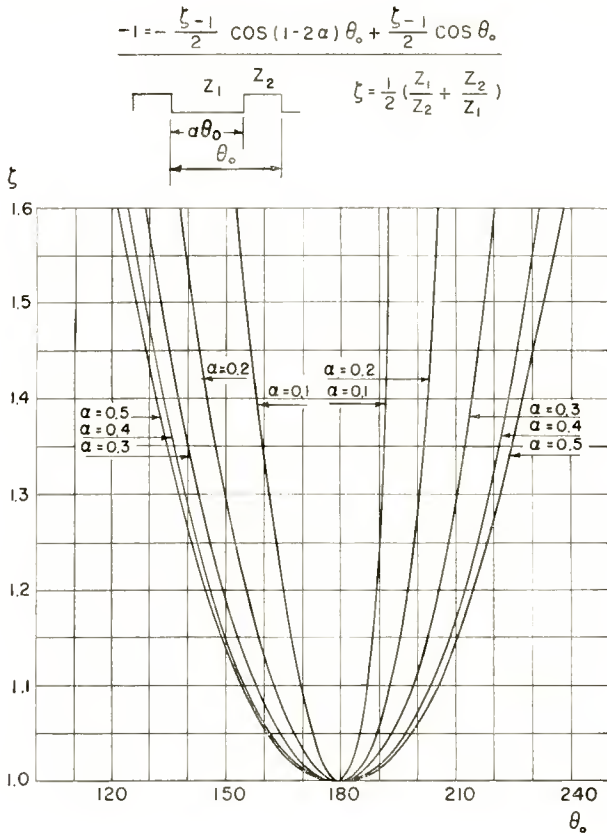
Fig. 13a—Parametric chart for locating the first stop band of a two-element linear lattice from the impedance and length ratios of the subelement lines.

stop band regions go through the points $m\pi$ $(m = 1, 2, 3 \cdots \cdots \cdots)$ at $\epsilon = 0$ or $\zeta = 1$ where $Z_1 = Z_2$. The widest stop band at any given ζ value is obtained for $\alpha = 0.5$, where the two sections of different impedance Z_1 and Z_2 have the same electrical length, $\theta_1 = \theta_2 = \theta_0/2$. In Figure 13b, these same band-edge curves are plotted versus the electrical length, θ_1, of the first subelement.

An enlarged picture of the first quadrant near the origin of Figure
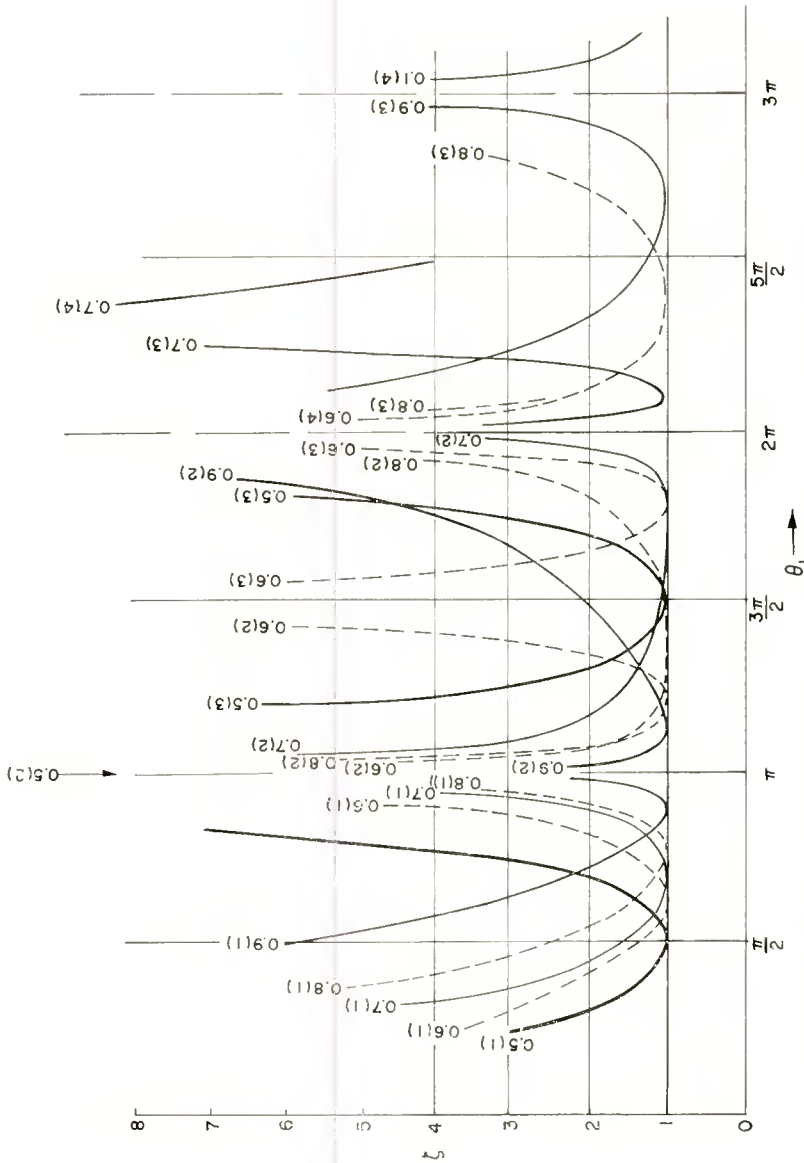
Fig. 13b—Parametric chart for locating stop and pass bands of a two-element linear lattice in terms of the first subelement length. The first numbers indicate the subelement length ratio, α. The numbers in parentheses denote the 1st, 2nd, 3rd . . . stop band.

11 is drawn up in Figure 14 where the total phase angle per unit cell, θ, is computed from (23) for various ζ and plotted against relative phase angle θ_0/θ_c. θ_c is the upper cutoff angle of the lowest pass band. The plot actually shows the fundamental mode ($n = 0$) of the forward wave. By imaging Figure 14 on the top and bottom frame line, all other modes existing in the lowest pass band can be obtained. Detailed curves of relative phase velocity were computed for two sectional-length ratios $\alpha = 1/2$ and $\alpha = 1/4$ for the forward fundamental mode ($n = 0$)
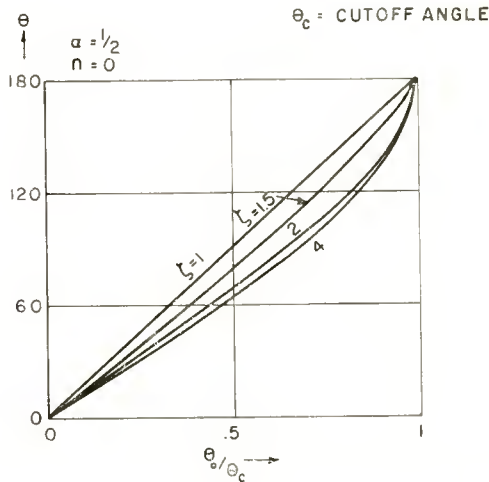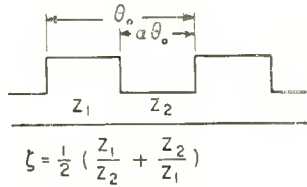
Fig. 14—Enlargement of the phase characteristic of the fundamental mode as shown in Figure 11 for the lowest pass band, with several values of impedance ratio.

and the first backward mode ($n = 1$) as shown in Figures 15 and 16. The negative phase velocities of the backward waves were imaged at the abscissa from the fourth into the first quadrant for convenience.

The limiting value of the phase velocity at very low frequencies ($\theta_0 \to 0$) is, from (30),

$$\lim_{\theta_0 \to 0} \frac{v}{v_0} = \lim_{\theta_0 \to 0} \frac{\theta_0}{\theta} = \frac{\partial \theta_0}{\partial \theta}\bigg|_{\theta_0 = 0} = \frac{v_g}{v_0}\bigg|_{\theta_0 = 0} \tag{33}$$
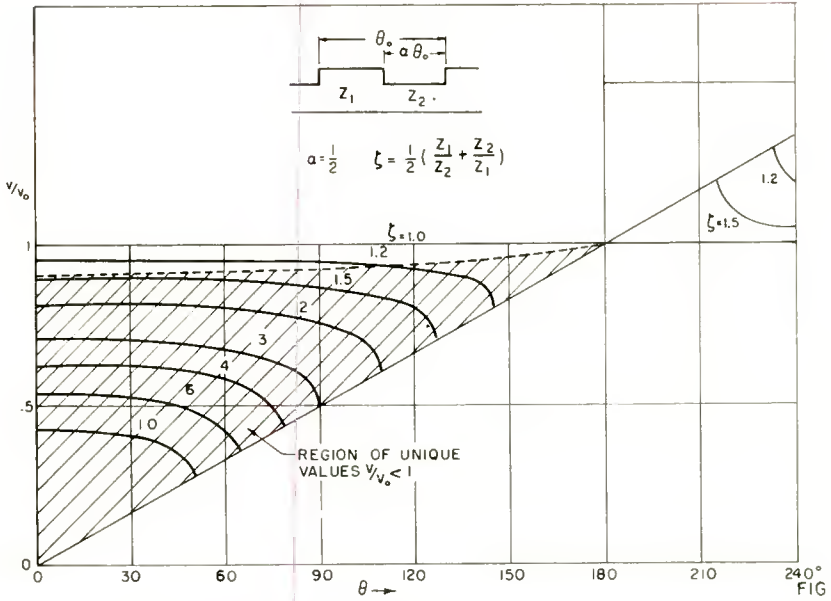
Fig. 15—These and the following curves show the variation of relative phase velocity with frequency or electrical angle for a filter with equal subelement lengths.
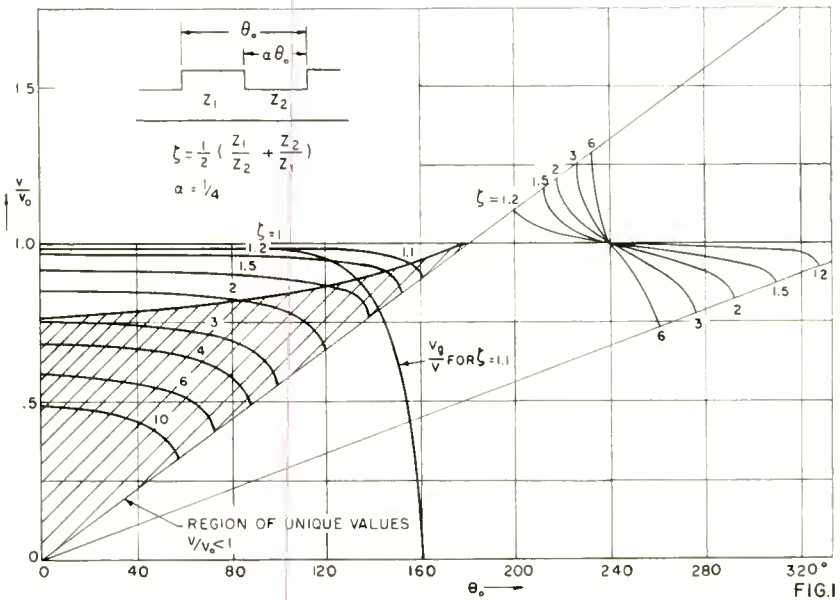

Fig. 16—Similar to Figure 15 but with a shorter second subelement.

Writing (22)

$$\cos \theta = (1 - \sin^2 \theta)^{\frac{1}{2}} = (1 + \epsilon)\ (1 - \sin^2 \theta_0)^{\frac{1}{2}}\ - \epsilon\ (1 - \sin^2 (1 - 2\alpha)\, \theta_0)^{\frac{1}{2}}$$

in a series expansion and letting

$$\sin \theta \rightarrow \theta$$

$$\sin \theta_0 \rightarrow \theta_0$$

then

$$\lim_{\theta_0 \rightarrow 0}\ \frac{v_0}{v} = (1 + 4\alpha\ (1 - \alpha)\ \epsilon)^{\frac{1}{2}}. \tag{34}$$

The relative group velocity v_g/v_0 was computed and plotted in Figure 16 for the impedance ratio $Z_1/Z_2 = 1.6$ ($\zeta = 1.1$) from (31) which yields together with (22)

$$\frac{v_g}{v_0} = \frac{\partial \theta_0}{\partial \theta} = \frac{\sqrt{1 - \{((1 + \epsilon)\ \cos \theta_0 - \epsilon \cos\ [\theta_0\ (1 - 2\alpha)\,]\}^2}}{(1 + \epsilon)\ \sin \theta_0 - \epsilon\ (1 - 2\alpha)\ \sin\ [\theta_0\ (1 - 2\alpha)\,]} . \tag{35}$$

If the relative length of α of the shorter line section of the filter unit decreases more and more, it finally degenerates into a lumped shunt susceptance $B = \omega C$ as in the filter helices of Figures 1b and 1c. With $\alpha \rightarrow 0$, the phase angle, Equation (20), becomes

$$\cos \theta = \cos \theta_0 - \zeta\, \alpha\, \theta_0 \sin \theta_0 \tag{36}$$

with $\lim (\zeta \alpha\, \theta_0) = \lim (\zeta\, \theta_1) = \dfrac{B_c}{Y_0}\ \dfrac{\theta_0}{\pi} = 2h\ \dfrac{\theta_0}{\pi}$ (37)

where $B_c = \omega C$ represents the lumped susceptance at the first cutoff angle θ_c, and Y_0 the characteristic admittance of the homogenious line. The relative phase velocity $v/v_0 = \theta_0/\theta$ for such a filter chain is plotted in Figure 17 for various values of $h = B_c/2Y_0$. The relative group velocity is shown only for one particular parameter value, $h = 0.3$.

For the application of a filter chain as a delay line in a traveling-wave tube, it is important that the frequency region, where interaction with the beam and gain occurs, be limited to the matched operating band. As interaction only takes place if beam and phase velocity are about the same, it is evident that there should not exist any frequency outside of the matched operating band where the phase velocity is the same as within that band.

Figures 11 and 12 indicate that the largest deviations of v with

respect to v_0 occur in the first two pass bands, the lowest relative phase velocity appearing in the first, the highest in the second pass band.

For filter helices, the phase velocities $v > v_0$ are not unique. This is a result of the "natural" dispersion of all helical lines which causes an increase of $v_0(f)$ toward lower frequencies, as seen from Figure 10. Therefore there always exists a frequency f' in the first pass band and a frequency f'' in the second pass band for which
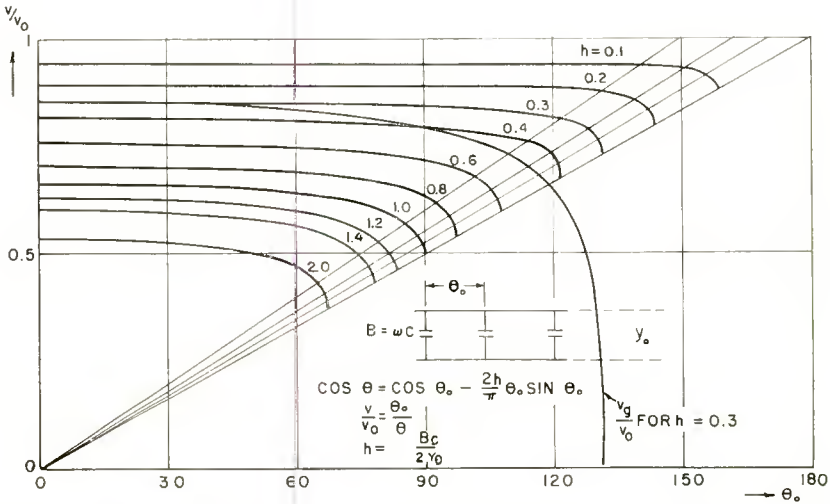

Fig. 17—Relative phase velocity versus frequency or electrical angle for a line periodically loaded with shunt susceptances.

$$v(f') = v(f'') \tag{38}$$

because

$$\left(\frac{v}{v_0}\right)_{f'} \times v_0 \, (f') = \left(\frac{v}{v_0}\right)_{f''} \times v_0 \, (f''). \tag{39}$$

For this reason the region of unique phase velocity in a filter helix is limited to a part of the lowest pass band. In Figures 15 and 16 the region of unique relative phase velocity $v/v_0 < 1$ is cross hatched.

For amplification of shortest waves, higher spatial harmonic modes ($\pm n = 1, 2 \cdots$) have been used to operate with comparatively larger circuit structures.[11] These higher spatial modes have extremely low

---

[11] S. Millman, "A Spatial Harmonic Traveling-Wave Amplifier for Six Millimeters Wavelength," *Proc. I.R.E.*, Vol. 39, pp. 1034-1043, September, 1951.

velocities in filter-helix circuits. They have not yet been utilized practically. Backward wave modes (See Table I) with positive group velocity but negative phase velocity have been discussed by Pierce[3] and recently widely employed by R. Kompfner and others[12] in electronically tunable oscillators. Filter helices of type C, especially in the design of Figure 1g, produce a large backward-wave field component $(n = -1)$ and have been successfully used as tunable oscillator circuits.
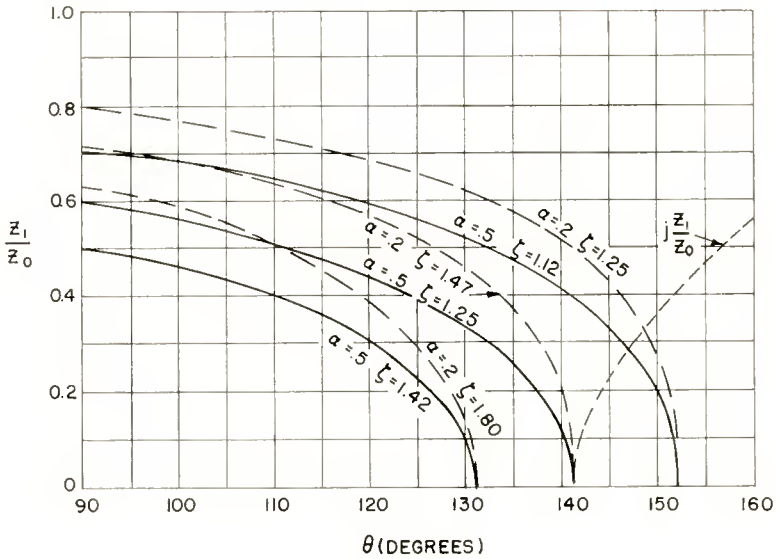

Fig. 18—Variation of normalized admittance with frequency or electrical angle in the low-pass region for several filter parameters. Pairs of associated parameters are shown which produce filters with the same first cutoff frequency.

FILTER HELIX IMPEDANCE AND MATCHING

The phase angle θ, and therefore the phase velocity v, are independent of the characteristic impedance, Z_0, of a chain filter. This is readily seen from Equations (16) and (17).

There exists, therefore, an infinite number of filters with different characteristic impedance which have a given cutoff frequency. This is shown for three different cutoff angles in Figure 18. The relative impedance according to Equation (18) can be written

---

[12] Herbert Heffner, "Analysis of the Backward-Wave Traveling-Wave Tube," Stanford University, 1952.

$$\left(\frac{Z_0}{Z_1}\right)^2 = \frac{\sin\theta_0 - \dfrac{\zeta-1}{\zeta+1}\sin\left[\theta_0\left(1-2\alpha\right)\right] + 2\sqrt{\dfrac{\zeta-1}{\zeta+1}}\sin\alpha\theta_0}{\sin\theta_0 - \dfrac{\zeta-1}{\zeta+1}\sin\left[\theta_0\left(1-2\alpha\right)\right] - 2\sqrt{\dfrac{\zeta-1}{\zeta+1}}\sin\alpha\theta_0} \quad (40)$$

where Z_1 is the first subelement impedance. This expression is plotted for two types of filters: one with subelement length ratio $\alpha = \theta_1/\theta_0 = 0.5$, the other with $\alpha = 0.2$. The impedance ratio ζ was chosen such that identical cutoff frequencies $\theta_0 = \theta_c$ are obtained. It should be noted (Figure 18) that the characteristic impedance, Z_0, is always larger than the first subelement impedance, Z_1. There are two different second-subelement impedances, Z_2, which make ζ, and therefore the characteristic impedance Z_0, the same. One of these values of Z_2 is larger than Z_1 and the other is smaller.

In general, relatively high circuit impedance is favorable to large amplification if the circuit is used in a traveling-wave-tube amplifier. There exists an optimum, however, as the losses increase with the amount of stored energy which is responsible for the higher impedance. The optimum practical impedance is, therefore, dependent upon the specific mechanical construction of the filter and is inversely related to the loss per unit line length.

A further limitation may be placed upon the choice of Z_0 by the required matching bandwidth between the filter helix and the input and output lines.

It will be shown in subsequent papers that there is little insertion loss necessary in the stable operation of filter-helix traveling-wave tubes with a narrow amplification bandwidth. Therefore, any mismatch at the tube output is reflected back to the input. The reflection coefficient at the input of a filter helix which is loss free and terminated by a line having the same impedance as the input line will now be computed. It is assumed that the impedance of the input and output lines does not change with frequency. The reflection coefficient at the input will be calculated with respect to some reference operating frequency point at which the filter is exactly matched to the input and output lines. The characteristic impedance of the filter will be different at frequencies away from the operating point and the filter helix mismatched at both ends. The reflection coefficient, seen at the input gives the reflected and the transmitted power, therefore the insertion loss of the loss-free filter helix.

If the characteristic impedance of the input and output lines, and the characteristic impedance of the filter at the reference operating

point is Z_{0m}, and the impedance looking into the filter plus output line is Z_{in}, then the reflection coefficient at the input will be

$$q = \frac{Z_{in} - Z_{0m}}{Z_{in} + Z_{0m}}. \tag{41}$$

As shown, for example, by Pipes (Reference (9), p. 385) the transformation effected by a filter of "n" sections having a characteristic impedance

$$Z_0 = Z(\omega)$$

can be written

$$\frac{Z_{in} - Z_0}{Z_{in} + Z_0} = - K^n \frac{Z_0 - Z_{0m}}{Z_0 + Z_{0m}} \tag{42}$$

where

$$Z_0 = \sqrt{\frac{B}{C}} \tag{18}$$

$$K = \frac{A - CZ_0}{A + CZ_0} = \frac{A - \sqrt{BC}}{A + \sqrt{BC}} \tag{42a}$$

K^n represents the transformation of the output match through the filter array, to the input. As before, the matrix

$$(M) = \begin{pmatrix} A & B \\ C & D \end{pmatrix} \tag{15}$$

describes the unit cell of the filter array. A symmetrical, lossless filter unit will be assumed, and therefore

$$A = D$$
$$AD - BC = 1. \tag{43}$$

The reflection coefficient at the output presented by the termination Z_{0m} to the filter-helix line with impedance Z_0 is defined as

$$q_0 = \frac{Z_0 - Z_{0m}}{Z_0 + Z_{0m}}. \tag{44}$$

Then the reflection coefficient seen from the input line into the filter will be, by combining Equations (41), (42), and (44)

$$q = q_0 \frac{1 - e^{-2jn\theta}}{1 - q_0^2 \, e^{-2jn\theta}} . \tag{45}$$

The cold insertion loss of the loss-free filter helix then will be

$$L = -10 \log \, (1 - |q|^2) = 10 \log \, (1 + |q|^2). \tag{46}$$

From (45) we have

$$1 - |q|^2 = \frac{1}{1 + \mu \sin^2 n\theta} \tag{47}$$

where

$$\mu = \frac{4q_0^2}{(1 - q_0^2)^2} = \tfrac{1}{4} \left(\frac{Z_{0m}}{Z_0} - \frac{Z_0}{Z_{0m}} \right)^2 \tag{47a}$$

with (47), the insertion loss of the filter in decibels will be

$$L = -10 \log \, (1 - |q|^2) = 10 \log \left[1 + \tfrac{1}{4} \left(\frac{Z_{0m}}{Z_0} - \frac{Z_0}{Z_{0m}} \right)^2 \sin^2 n\theta \right] \tag{48}$$

Table II lists a number of filter parameters and matching points for which insertion loss curves were computed. These parameter values were chosen because of their relevance to the design of filter-helix traveling-wave amplifiers which were found experimentally to have good performance.

Table II

Case No.	Value of θ_0 at which $Z_0 = Z_{0m}$	α	Z_2/Z_1	ζ
I	136°	0.5	2.0	1.25
II	126°	0.5	2.4	1.42
III	146°	0.5	1.6	1.12
IV	146°	0.2	2.0	1.26
II A	129°	0.5	2.4	1.42
II B	123°	0.5	2.4	1.42

$n = 20$ in all cases

Figure 19a (Case I and Case II) illustrates the effect of changing the subelement impedance ratio while holding the subelement-length ratio, α, constant. In each case the filter was matched to the input and output lines at the same fraction of the cutoff angle. The larger impedance ratio is associated with the lower cutoff angle, as indicated on the stop and pass-band domains of Figure 12, *et seq.* Otherwise, the curves are similar.

Figure 19b (Case III and Case IV) shows the different insertion loss curves which result from altering a particular filter design to keep
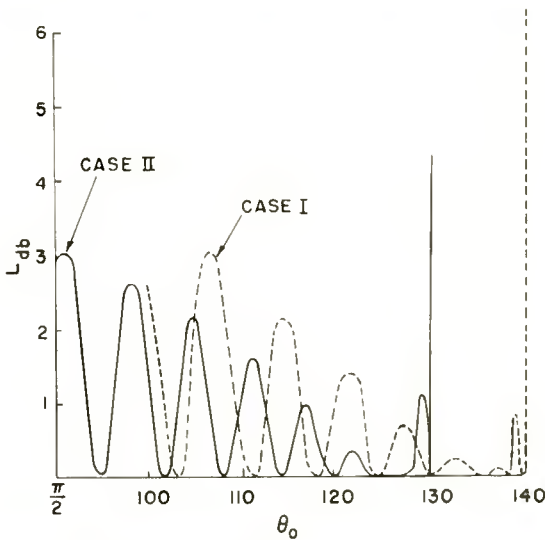
Fig. 19a—Insertion loss of two filter helices matched to constant-impedance input and output lines at frequencies near the first cutoff. The two filters have the same subelement length ratio but different subelement impedance ratios.

the cutoff angle constant. It is clear from these and the preceding examples that moderate changes in filter parameters cause only minor changes of the reflection amplitudes in the pass-band if the frequency of matching is kept at the same relative distance from the cutoff frequency, i.e., if θ_{0m}/θ_c remains constant.

As would be expected, however, major changes in the insertion-loss curve are brought about by changes in the relative angle θ_{0m}/θ_c at which a given filter is matched. If the input and output lines are matched to the filter at an angle (or frequency) close to cutoff, where the filter characteristic impedance is changing rapidly, the bandwidth for a given maximum amount of reflective insertion loss will be nar-
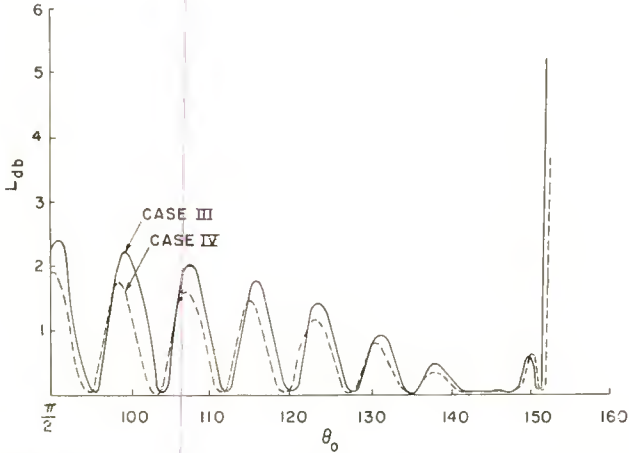
Fig. 19b—Insertion loss curves similar to those of Figure 19a for two different filters matched at the same frequency.

rower than for a matching point farther from cutoff. This is illustrated in two ways in Figures 20a and 20b. In Figure 20a, a single filter, with an intrinsic cutoff angle of $\theta_c = 131°$, is matched successively to its
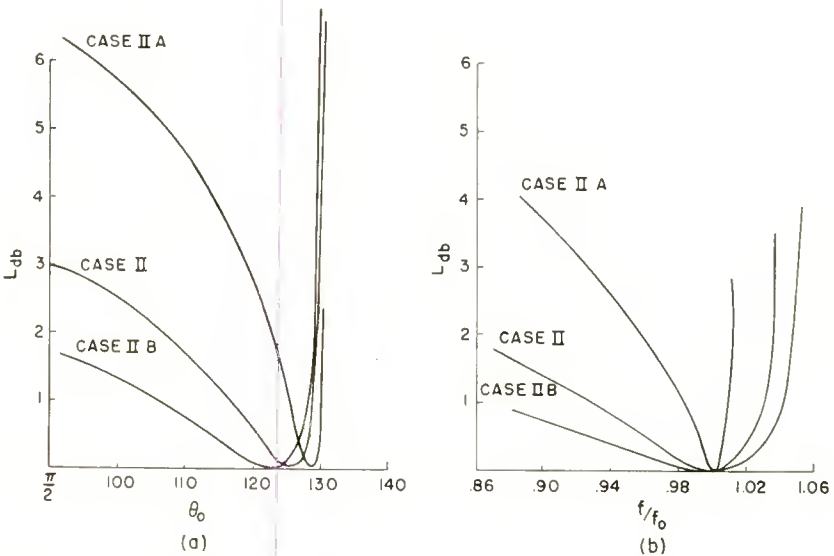
Fig. 20—Insertion loss of a filter helix matched to input and output lines at different frequencies. In (a), the insertion loss curves are plotted versus the electrical angle θ_0. In (b), the same curves are plotted versus normalized matching frequency to illustrate how the bandwidth decreases the closer the matching frequency approaches the cutoff frequency.

input and output lines at $\theta_{0m} = 123°$, $126°$, and $129°$. The matching bandwidth decreases as the matching point is moved into regions of more rapid variation of filter impedance versus phase angle. The envelopes of the maxima only are shown. The same phenomenon is illustrated in Figure 20b. Here it is assumed that the filter parameters have been so chosen that the angles $\theta_{0m} = 123°$, $126°$, and $129°$ correspond to the same frequency f_0. These three different filters therefore are matched at f_0, and the resultant envelopes of the maxima in the reflection curve again show that the filter with the highest and most rapidly-varying impedance gives the narrowest matching bandwidth.

It should be emphasized that these impedance-matching and insertion-loss computations refer to "cold" filter helices. Their characteristics under "hot," i.e., operating conditions, in traveling-wave tube circuits will be treated in later papers.

CONCLUSIONS

In this first of a series of papers on filter-helix traveling-wave tubes, the filter helix is introduced as a new type of interaction circuit. Its characteristics can be described quite accurately by using a one-dimensional lattice model. The stop and pass-band frequency regions, and the phase and group velocity characteristics are computed for this model.

This new interaction circuit offers numerous advantages for use in low-voltage traveling-wave tubes. It allows the gain per unit circuit length to be increased at the sacrifice of some frequency bandwidth. Also, with the filter helix one can limit at will the amplification bandwidth of the amplifier by choosing the appropriate dispersion in the operating range of frequencies. The filter helix also makes possible the construction of relatively large and rugged circuits for amplification of very short waves. Photographs show a selection of filter helices actually tested in developmental traveling-wave tubes.

RADIATION PATTERN SYNTHESIS*

By

Edmund A. Laport

Chief Engineer, RCA International Division,
New York, N. Y.

Summary—The radiation patterns for an array of nondirective radiation sources are first discussed from the standpoint of controlling the directions of the minimums. Further pattern control is introduced by substituting directive sources (secondary array) for each nondirective element of the original (primary) array. It is shown that precise solutions are possible by direct synthesis procedures giving at least two zeros by each stage of evolution in substituting directive for nondirective elements. The development of binomial linear arrays is introduced and then combined with the foregoing method to obtain wide angles of radiation suppression and desired pattern shapes to satisfy the rigorous requirements of present-day radiation engineering, with the zeros distributed in any specified manner. The same method is expanded to embrace the solution for radiation patterns for uniform current sheets of any aperture, and the equivalence of this approach to the Fourier cosine transform is demonstrated.

Pattern Synthesis

CONSIDER a primary (basic) array of identical vertical radiators numbered 1 to n, geometrically disposed and synchronously excited in any manner. Let No. 1 be the reference radiator with respect to which all amplitude, space and time differences are measured. Radiator m is located a distance S_m (in electrical degrees) from No. 1 in a direction β_m with respect to a chosen reference direction such as true north. The current in radiator m has a phase difference ϕ_m with respect to that in No. 1.

By virtue of the fact that the radiators are identical in form and their currents are measured at corresponding points, their individual field-strength contributions will be proportional to their respective currents. Therefore their field-strength ratios are represented by their current ratios.

When all the currents are equal in amplitude, the shape of the horizontal field-strength pattern in the Fraunhofer region can be expressed by the scalar value of the equation

$$F_0(\beta) = 1 + e^{j\psi_2} + e^{j\psi_3} + \cdots e^{j\psi_n}, \tag{1}$$

in which each wave-interference angle, ψ, is

---

* Decimal classification: R120.

533

$$\psi_m = S_m \cos (\beta - \beta_m) + \phi_m.$$

The azimuth angle, β, is measured from the reference direction (usually clockwise), and ϕ ranges through all four quadrants.

INDIVIDUAL RADIATION SOURCES

Each radiation source for each term in this primary array pattern has a circular field-strength pattern. If $f(\beta)$ is the pattern for each source, then in Equation (1) it is implied that $f(\beta) = 1$. Later this restriction will be removed for practical cases. The symbol $f_m(\beta)$ will be used to indicate patterns for pairs of order m.

DISCUSSION OF ZEROS

$F_0(\beta)$ will, in general, contain a number of maximums and minimums which may occur regularly or irregularly. In an array with random parameters, zeros, if they occur at all, will be at random azimuths. In various systematic arrays, one, two, or several zeros can be systematically oriented. Array patterns of this kind are required to satisfy particular allocation problems. The designer must search for practical parameters that will yield a desired distribution of zeros, or minimums, in a horizontal pattern; and when the number of radiators exceeds two, the problem may become formidable because of the multiplicity of independent variables. Computers such as the Antennalyzer[1] are useful in searching for such solutions.

EQUI-CURRENT PAIR AS A RADIATION SOURCE

When an array consists of only two radiators, Equation (1) represents a pair with equal currents. Then

$$F_1(\beta) = 1 + e^{j\psi}. \tag{2a}$$

However, there are conveniences to shifting the zero reference point in the system from radiator No. 1 to the geometrical center of the pair. When this is done for the equi-current pair,

$$F_1(\beta) = \frac{e^{j\frac{\psi}{2}} + e^{-j\frac{\psi}{2}}}{2} = \cos \frac{\psi}{2} = \cos \left(\frac{S}{2} \cos \beta + \frac{\phi}{2} \right) \tag{2b}$$

---

[1] G. H. Brown and W. C. Morrison, "The RCA Antennalyzer—An Instrument Useful in the Design of Antenna Systems," *Proc. I.R.E.*, Vol. 34, pp. 992-999, December, 1946.

when the axis of the pair is coincident with the reference direction. When the pair axis has an orientation β_0,

$$f_1(\beta) = \cos \left[\frac{S}{2} \cos (\beta - \beta_0) + \frac{\phi}{2} \right] \quad \text{(normalized)}. \tag{2c}$$

The pattern resulting from Equation (2) has certain fundamental properties:

(1) zeros occur at angles $\pm \beta$ where $\psi = 90, 270$, etc.;

(2) $f_1(\beta)$ is symmetrical with respect to the pair axis;

(3) if the pattern contains only one zero, its direction is along that of the pair axis;

(4) an even number of zeros in the pattern are symmetrically located with respect to the pair axis;

(5) an odd number of zeros places one in line with the axis and the others in symmetrical pairs;

(6) two zeros can be placed at any desired azimuths by proper choice of spacing S, phase difference ϕ, and orientation β_0.

Generalized Primary Array

Equation (1) can be further generalized to embrace a wider scope of patterns by changing the strength of each radiation source by altering the current ratio(s). Then, if B, C, etc. be successive current ratios in radiators 2, 3, etc.,

$$F_2(\beta) = A \left(1 + Be^{j\psi_2} + Ce^{j\psi_3} + \cdots Xe^{j\psi_n} \right), \tag{3}$$

where A is a scale factor affecting the magnitude of the pattern, or a normalizing factor. The scalar coefficients B, C, etc. may have any finite positive values. All phase factors are included in ψ.

This pattern contains another order of randomness in the location of the minimums in $F_2(\beta)$, due to the range of each coefficient. The difficulty of designing an array of this type for a specific distribution of the minimums is increased by the introduction of these additional independent variables, while at the same time the range of desirable possibilities is also increased. Under certain conditions the minimums can be zeros.

Systematic Arrays

Methods for the direct solution of any particular distribution of zeros that may be required in an engineering problem will now be

considered. One of the simplest methods is to substitute a secondary array pattern $f_2(\beta)$ for, and centered on, each radiator in the primary array, with the axes of all secondary arrays oriented identically. This transforms Equation (3) to

$$F_3(\beta) = A \, f_1(\beta) \, F_2(\beta). \tag{4}$$

Here there is a set of zeros due to the secondary array $f_2(\beta)$ as well as those of the primary array $F_2(\beta)$. These two sets are independently adjustable. If $f_2(\beta)$ consists of a pair of radiators centered on the location of each original radiator in the primary array, there are at least two zeros that can be brought into coincidence with two prescribed azimuths. If the primary array also consists of a basic equi-current pair, $F_2(\beta)$ can also provide at least two more. Therefore four radiators can always be arranged to provide at least four zeros distributed in any manner. The array becomes a 4-element equi-current parallelogram. In extreme cases, the parallelogram can become compressed into a linear array.

If the problem requires six zeros distributed at random, each radiator in the parallelogram array can again be replaced by a cocentered tertiary array having the pattern $f_3(\beta)$ that will provide an exact solution for the two additional zeros in the horizontal pattern. The equation for this third stage of pairing becomes

$$F_4(\beta) = A \, f_3(\beta) \, f_2(\beta) \, F_2(\beta). \tag{5}$$

When each factor is the pattern for a basic equi-current pair, the final array will also have equal current amplitudes in all radiators. Therefore the pattern can also be expressed exactly by Equation (1) after inserting the proper space and phase parameters.

LOCATION OF ZEROS

If zeros are required at azimuths $\beta_1, \beta_2 \cdots \beta_6$, and the pattern of Equation (5) is to be employed, each stage of pairing can satisfy any pair of the desired zeros. For example, $F_2(\beta)$ may provide the zeros at β_2 and β_5, $f_2(\beta)$ the ones at β_1 and β_6, and $f_3(\beta)$ those at β_3 and β_4. A different array results from each combination of pairs of zeros.

The available choice of parameters that will certainly satisfy the specifications with regard to the zeros presents a choice of designs, at least one of which will usually provide desired shapes and distributions of the maximums. An illustration of the solution of such a problem is included in the Appendix.

WIDE ANGLES OF SUPPRESSION

Having demonstrated a technique for meeting any conditions imposed by the distribution of the zeros, a means is available for satisfying the requirement for patterns having very wide angles of radiation suppression. By distributing a number of zeros at small angular separations, it is possible to suppress the growth of radiation lobes between them. The degree of suppression can be controlled by the zero spacings, and by their number. Furthermore, at least two wide-angle null zones in two principal directions can be provided by a linear array. Any number of stages of pairing can be used to provide any specified width, orientation and degree of suppression.

SYSTEMATIC CURRENT DISTRIBUTIONS

In Equations (3), (4), and (5) there were no restrictions placed upon the values of the coefficients B, C, D, etc. By assigning suitable systematic values to these coefficients and to their associated values of ϕ, other useful means of pattern shaping and array synthesis are available. For example, consider the effects on pattern shape when $f(\beta)$ is squared, or raised to any integral power, p. The new pattern will have smaller subsidiary lobes, wider null zones and sharper main lobes. This leads to a binomial current distribution obtained by a linear array of $p + 1$ radiators equally spaced. The resulting binomial current distribution is vectorial. Only when the currents in the basic pair are cophased ($\phi = 0$) are the binomial coefficients algebraic.

Binomial current distributions used for both primary and secondary (as well as higher-order) arrays provide means for directly designing a very great variety of patterns with controlled zero azimuths and at the same time, controlled widths of the null zones   Previously these two objectives could be accomplished separately — now, by this technique, they can be accomplished simultaneously.

The binomial current distribution can be modified in the following manner: From a basic equi-current pair of radiators having the pattern

$$f_a(\beta) = \cos\left(\frac{S_a}{2}\cos\beta + \frac{\phi}{2}\right), \tag{6}$$

values of S_a and ϕ can be chosen that will bring two zeros at a specified angular separation. The axis of the pair will bisect the angle between them. Once a value has been chosen for S_a, different values of ϕ will vary the angle between the two zeros. Therefore, if wide nulls are

required for either one or two directions, an array can be synthesized that will have the pattern

$$f_a(\beta) = \cos\left(\frac{S_a}{2}\cos\beta + \frac{\phi_1}{2}\right)\cos\left(\frac{S_a}{2}\cos\beta + \frac{\phi_2}{2}\right)\cos\left(\frac{S_a}{2}\cos\beta + \frac{\phi_3}{2}\right)$$

. . . . etc.   (7)

In this equation there are three successive pairings indicated using ϕ_1, ϕ_2, and ϕ_3 in turn to bring zeros at specified angles sufficiently close together to prevent the growth of radiation lobes between them. The current distribution in a linear array of $p+1$ radiators (where p is the number of stages of pairing) which provides such a pattern is systematic, and resembles a vector binomial distribution of currents. This may be called a quasi-binomial distribution, obtained when all pairs have the same orientation, S_a is constant, and ϕ is the independent variable manipulated systematically.

Fundamentally, the binomial and quasi-binomial arrays are parallelogram arrays that have been compressed into a linear array. The spacings are such that, when compressed into a linear array, two or more radiators merge into one The current in each radiator is the vector sum of those in the radiators that were merged. This can be demonstrated as follows:

Let the pattern for a primary array be

$$F_1(\beta) = \cos\left(\frac{S_0}{2}\cos\beta + \frac{\phi_0}{2}\right).$$ (8)

When each primary radiator is replaced by an identical pair oriented at an angle β_0 with respect to the primary-array axis, the resulting 4-element equi-current parallelogram array pattern will be

$$F(\beta) = \cos\left[\frac{S_0}{2}\cos\beta + \frac{\phi_0}{2}\right]\cos\left[\frac{S_0}{2}\cos(\beta - \beta_0) + \frac{\phi_0}{2}\right].$$ (9)

However, when $\beta_0 = 0$, this equation becomes

$$F(\beta) = \cos^2\left(\frac{S_0}{2}\cos\beta + \frac{\phi_0}{2}\right),$$ (10)

which is the pattern for a (3-element) binomial array of second degree. Two radiators of the parallelogram array have merged into one in the middle of the binomial array. Therefore, binomial and quasi-binomial arrays are special cases for the more general paralellogram arrays. The attractive feature of these special arrays is the economy of radiators and therefore economy of space, because each pairing adds only one radiator.

Where additional pattern control of a nature not provided by the simplest binomial and quasi-binomial primary array patterns is needed, secondary arrays that are basic pairs (or more extensive arrays) can be substituted for each radiator in the primary array. When this substitution is made, the amplitude and phase factors for the primary array have to be preserved. This gives a pattern of the generic type of Equation (4) except that the spacings, phasings, orientations and coefficients for the primary array have been systematized binomially. The secondary arrays can also be binomially derived if necessary. Such patterns are generated by parallelogram arrays of six or more elements.

These techniques permit the direct synthesis of arrays under almost any conditions imposed by modern geographic allocations. The problem is facilitated by the frequent condition that certain pattern "zeros" can, in fact, be minimums instead of zeros, and a sufficient suppression of radiation at some azimuths may be obtained incidentally, without special provision.

The systematic array is not always the simplest that will meet a specified case because there are certain random conditions of array geometry and current distribution that may provide an acceptable pattern with fewer radiators. When they exist, these configurations are found by cut-and-try methods.

RADIATION PATTERN FOR A UNIFORM FLAT CURRENT SHEET

Continuous distributions of currents may be considered as resulting from an infinite number of parallel linear currents. The current distribution is usually computed as a Fourier integral, and its radiation pattern as the Fourier transform of the continuous current distribution.

In this section it will be shown that the radiation pattern for a continuous flat current sheet with uniform current in one of its dimensions, say its length, can be computed in much the same way as developed previously in this paper.

A uniform flat sheet of cophased currents having an electrical length of $2L$ is considered as two halves, and the middle of each half is considered to be the center of a linear radiating element. The pat-

tern for this first cophased pair of radiators will be (measuring β now from the normal to the pair instead of the axis)

$$\cos\left(\frac{L}{2}\sin\beta\right).$$

Each radiator of this pair can now be replaced with a cocentered cophased pair with a spacing such that the two pairs comprise four equally-spaced parallel radiators in the plane of the sheet. Each of these secondary pairs will have the pattern

$$\cos\left(\frac{L}{4}\sin\beta\right).$$

Performing this substitution with a third stage of pairing to simulate the sheet with a uniform array of 8 equi-spaced equi-current radiators, each of the tertiary pairs will have the pattern

$$\cos\left(\frac{L}{8}\sin\beta\right).$$

The pairing break-down can proceed to any desired number of stages, and after each stage the current distribution for the array approaches nearer to the length $2L$ and to a continuous distribution. At any stage of pairing, such as the three developed preceding, the pattern for the distribution is

$$F(\beta) = \cos\left(\frac{L}{2}\sin\beta\right)\cos\left(\frac{L}{4}\sin\beta\right)\cos\left(\frac{L}{8}\sin\beta\right)$$

$$\cdots \cos\left(\frac{L}{2^n}\sin\beta\right), \qquad (11)$$

where n is the number of stages of pairing, counting the original primary pair.

At any stage of pairing, the error in the pattern is that due to the final term

$$f_n(\beta) = \cos\left(\frac{L}{2^n}\sin\beta\right) \neq 1.$$

As $\dfrac{L}{2^n} \to 0$, the amount of the difference decreases until $f_n(\beta) = 1$. As the number of stages of pairing increases, $F(\beta) \sim \dfrac{\sin{(L_0 \sin \beta)}}{(L_0 \sin \beta)}$, the Fourier transform[2-4] for a uniform flat current distribution when L_0 is its electrical half-length in radians.

Therefore

$$\underset{f_n(\beta)\,\to\,1}{\text{limit}} \left| \cos\left(\frac{L_0}{2}\sin\beta\right)\cos\left(\frac{L_0}{4}\sin\beta\right)\cos\left(\frac{L_0}{8}\sin\beta\right) \right.$$

$$\cdots \cos\left(\frac{L_0}{2^n}\sin\beta\right) = \frac{\sin{(L_0 \sin \beta)}}{L_0 \sin \beta}. \qquad (12)$$

Appendix — Applicational Examples

Figures 1 and 2 are presented to show two of many possible arrays that provide zeros at 20, 66, 264 and 350 degrees. The two examples illustrate at once a certain latitude of choice of the pattern shapes that satisfy the specified zero distribution

Figure 3 graphically illustrates the evolution of a pattern for three degrees of evolution for a basic equi-signal pair that leads to a binomial array.

Figure 4 shows the use of a second-degree binomial array (the middle pattern of Figure 3) as a primary array in conjunction with an equi-current pair used as a secondary array. The resulting 6-element parallelogram array pattern shows wide angles of radiation suppression with desired major and minor lobes and five zeros at selected azimuths.

Figure 5 illustrates the use of a primary array consisting of an equi-current pair and a secondary array consisting of a second-degree binomial array designed specifically to produce a split beam with very wide angle of radiation suppression using only six radiators.

In all these figures the zero reference for phase relations is the center of the primary array.

[4] J. F. Ramsay, "Fourier Transforms in Aerial Theory," *Marconi Review*, Vol. 9, pp. 139-145, October-December, 1946.

[2] R. M. Foster, "Directive Diagrams for Antenna Arrays," *Bell Sys. Tech. Jour.*, Vol. 5, pp. 292-307, January, 1926.

[3] I. Wolff, "Determination of the Radiating System which will Produce a Specified Directional Characteristic," *Proc. I.R.E.*, Vol. 25, pp. 630-643, May, 1937.

Figure 6 illustrates a quasi-binomial array where the phase angle is adjusted in 20-degree steps from 30 to 90 degrees with a basic-pair spacing of 120 degrees to produce a consecutive distribution of zeros that provides almost complete suppression of radiation over an angle of ±92 degrees, using five radiators. The blind angle can be increased
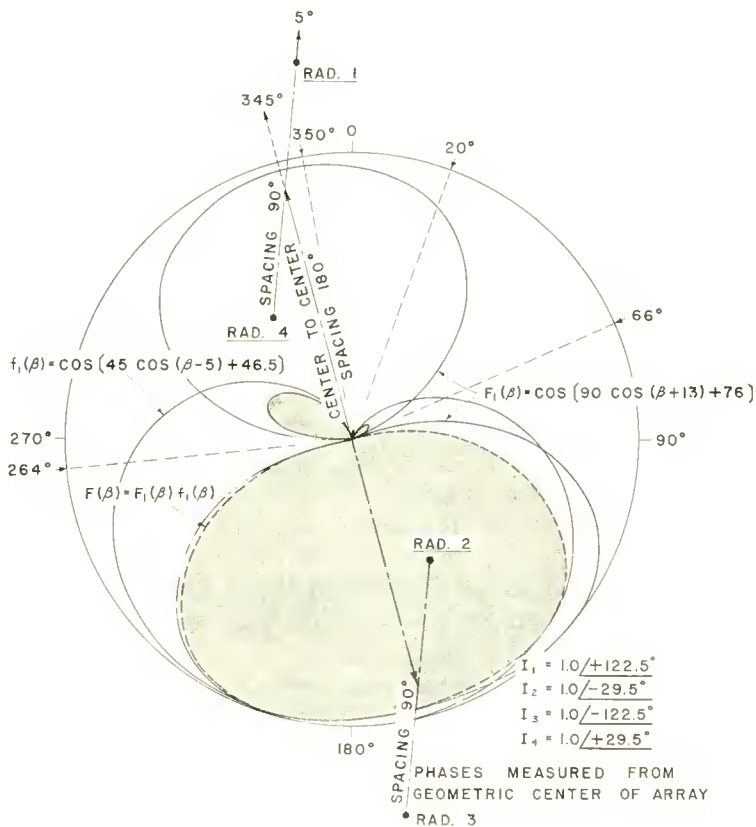
Fig. 1—A possible solution for radiation pattern with zeros at 20, 66, 264 and 345 degrees, with the array.

(a) by using larger phase-angle differentials in each stage with less complete suppression in the blind region, or (b) by using additional stages of pairing.

Table I demonstrates the approximation to the Fourier transform pattern for a uniform current sheet having three wavelengths total width, using only four stages of pairing.
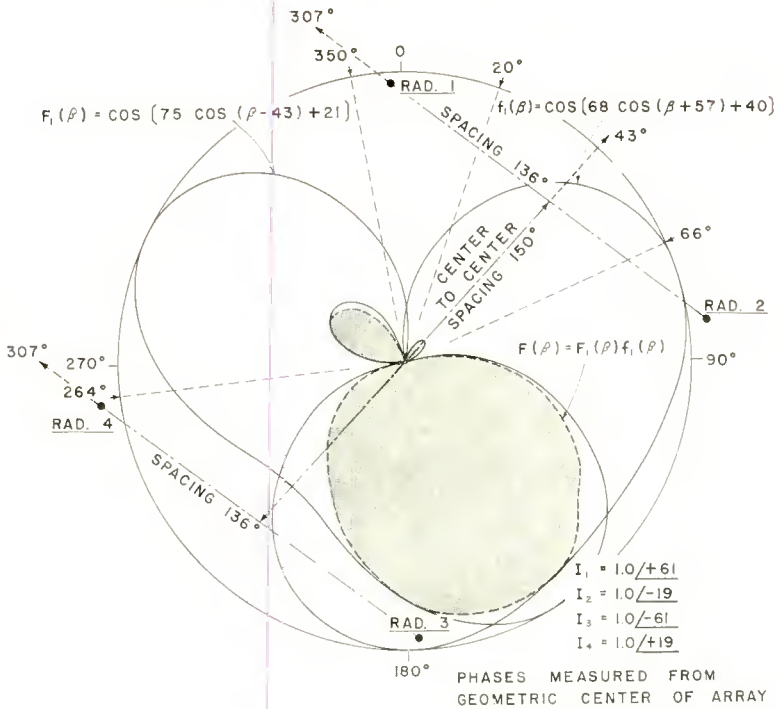
Fig. 2—A possible solution for radiation pattern with zeros at 20, 66, 264 and 345 degrees, with the array.
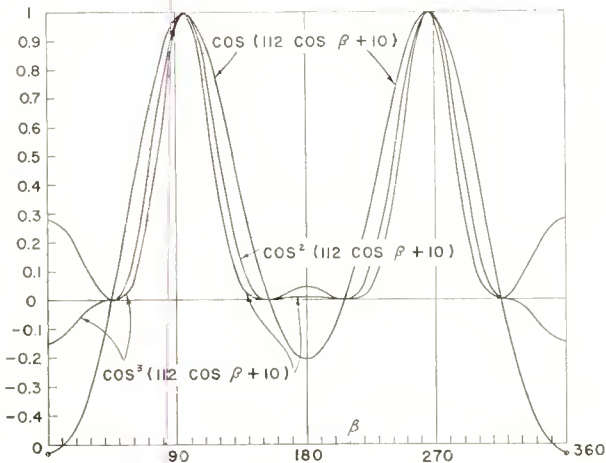
Fig. 3—Example of secondary-lobe reduction, null broadening and beam sharpening using binomial current grading.
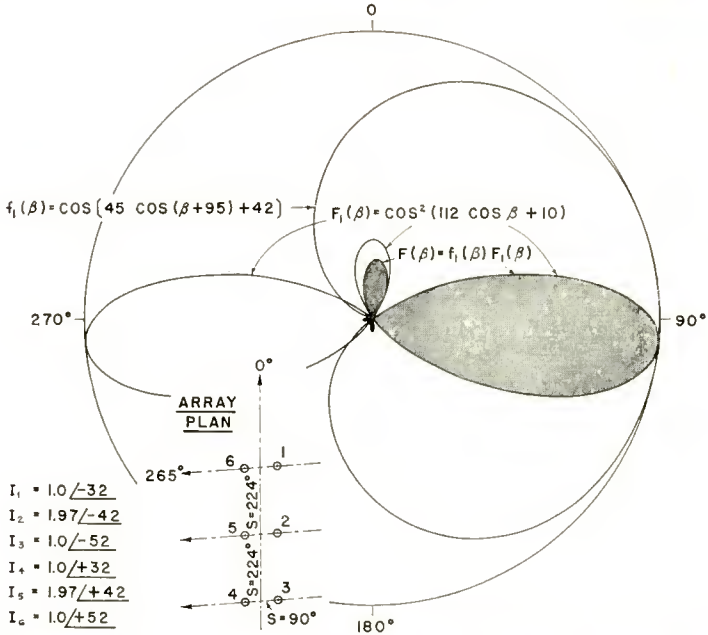
Fig. 4—Example of pattern shaping using a second-degree binomial primary array with directive secondary array pairs.
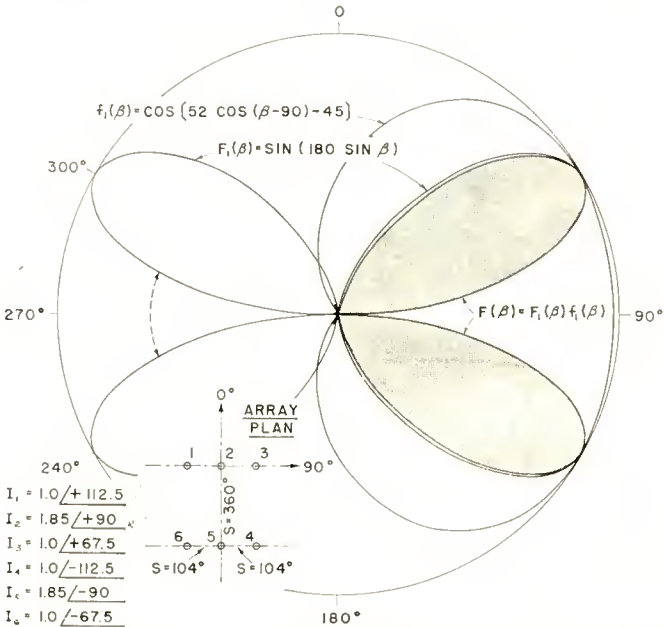
Fig. 5—Example of pattern shaping using a primary pair array with second-degree binomial secondary arrays.
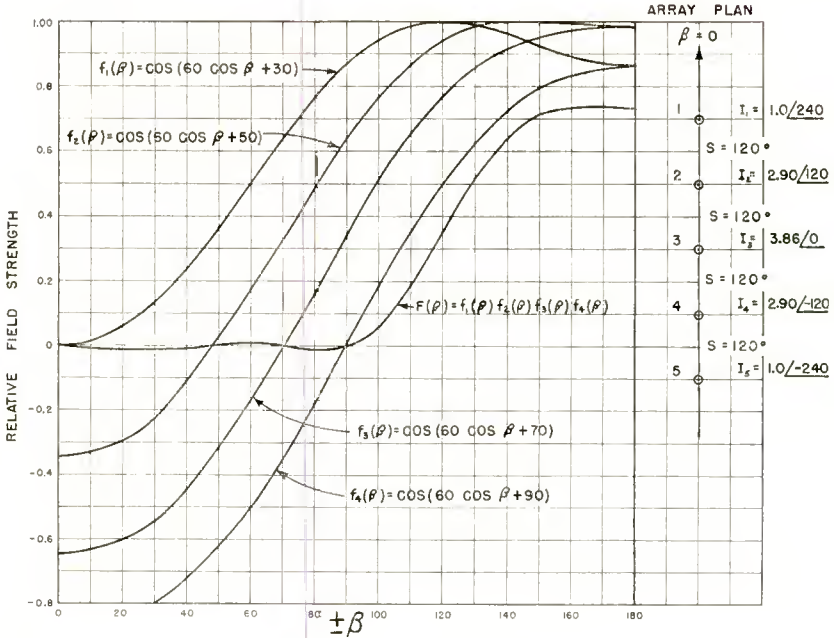
Fig. 6—Example of null broadening using quasi-binomial current grading in a linear array.

Table I—Comparison of the Approximation $\cos (1.5\pi \sin \beta) \cos (0.75\pi \sin \beta)$ $\cos (0.375\pi \sin \beta) \cos (0.1875\pi \sin \beta)$ with the Fourier Cosine Transform

$$\frac{\sin (3\pi \sin \beta)}{3\pi \sin \beta}.$$

β (degrees)	Approximation	Fourier Transform
0	1,000	1,000
10	0.612	0.608
20	—0.0268	—0.0271
30	—0.225	—0.212
40	—0.041	—0.0372
50	0.116	0.135
60	0.122	0.115
70	0.063	0.059
80	0.0159	0.0150
90	0	0

PARTICLE COUNTING BY TELEVISION TECHNIQUES*

By

L. E. FLORY AND W. S. PIKE

Research Department, RCA Laboratories Division,
Princeton, N. J.

Summary—Television scanning methods offer considerable promise as a means of counting small particles. An experimental unit based upon a standard closed-circuit television system has been built to count red blood cells. In this equipment the television signal produced by scanning a field of cells is applied to a count-rate meter which gives a reading proportional to the number of cells in the field. To obtain a reading independent of cell size, the average diameter of the cells is measured electronically and the count-rate meter reading automatically compensated therefor. The equipment for accomplishing this is described and test results are presented.

INTRODUCTION

THE problem of counting the number of microscopic particles in a given area appears to be important in many fields of scientific endeavor. Red blood cells, white blood cells, bacterial cultures, and the grains of photographic emulsions are but a few of the many types of particles which must often be counted, and still others will doubtless occur to the reader. At present the counting of such particles is a laborious and time-consuming process since a technician must view the field of particles in a microscope and count them visually with the aid of a mechanical totalizer such as a counter or similar device. There are, in addition, many chances for error in such a process as particles may easily be overlooked or counted more than once.

As long as the particles are regular in size and not clustered too closely together, television scanning techniques offer considerable promise for rapidly and accurately counting them. Figure 1 shows, in block form, the elements of a counting system using this technique. The particles to be counted are placed under the microscope and suitably illuminated. The camera of a closed-circuit television system is substituted for the eye of the observer at the microscope eyepiece. Focus and illumination are adjusted by observation of the monitor kinescope of the television system. The video output of the latter is applied to a count-rate meter. The particles to be counted will produce video pulses at the output of the television system, and the count-rate meter will

---

546

give an indication proportional both to the number and size of the particles in the field of the microscope. To make the reading independent of particle diameter, compensation is applied as follows.

Figure 2a depicts a small area of a field of particles being scanned by a television system. The horizontal lines represent the path of the scanning beam and the circles represent the particles. An electrical pulse will be produced in the output of the television system each time the scanning beam intercepts a particle. The pulses corresponding to
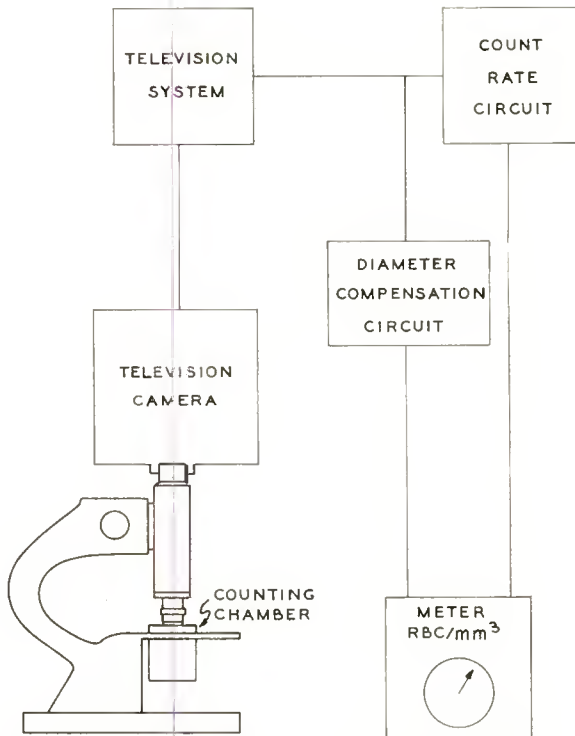
Fig. 1—Block diagram of particle counter.

line 15 of Figure 2a, for example, are shown in Figure 2b. Typically, the system magnification is such that each particle is cut by more than one line of the raster. If each particle is cut by n lines, there will be n pulses per particle in the output of the system, and large particles will produce more pulses than small ones. Thus the count rate meter, without compensation, cannot distinguish between a large number of small particles and a small number of large particles.

An oscilloscopic analysis of the video pulses in the output of a television system scanning a field of randomly distributed circular

particles uniform in size, showed that the time durations of these pulses peaked quite sharply at a mean value slightly less than the time duration to be expected if each raster line cut particles exactly on their diameters. A probability analysis by E. G. Ramberg confirmed this and clearly demonstrated that the mean time duration of the pulses was directly proportional to the particle diameter, and thus to the number of raster lines cutting each particle and the number of video pulses produced by each particle. A circuit may be added to the count-rate meter to measure the mean time duration of the pulses and thus the mean diameter. The count-rate meter scale factor may be made to vary inversely with this value so that the meter reading is completely independent of particle size. This circuit is called the diameter compensation circuit.

Fig. 2—(a) Portion of field of particles showing scanning raster; (b) Pulses from line 15.

EXPERIMENTAL ERYTHROCYTE COUNTER

The first experimental application of this counting technique has been to the counting of red blood cells, or erythrocytes. Figure 3 is a photograph of the monitor screen with a suspension of erythrocytes in a counting chamber under the microscope. Dark-field illumination has proven more convenient to use with these cells, but would not necessarily be so with other particles. The television chain is a standard early production industrial television equipment which is built around the recently announced Vidicon photoconductive pickup tube.

Figure 4 shows the first version of the equipment as set up for operation and Figure 5 is a close-up of the latest model of the counting meter itself. This device has been dubbed the "Sanguinometer." The differences between the two models are principally in the arrangement of the controls, the later model incorporating an easier-to-use arrangement of the pulse-width measuring circuit controls suggested by Dr. Leon Hellman of Sloan-Kettering Institute. To make a red-cell count the technician follows the usual clinical procedure for obtaining and diluting the blood sample and places a measured quantity of the dilute
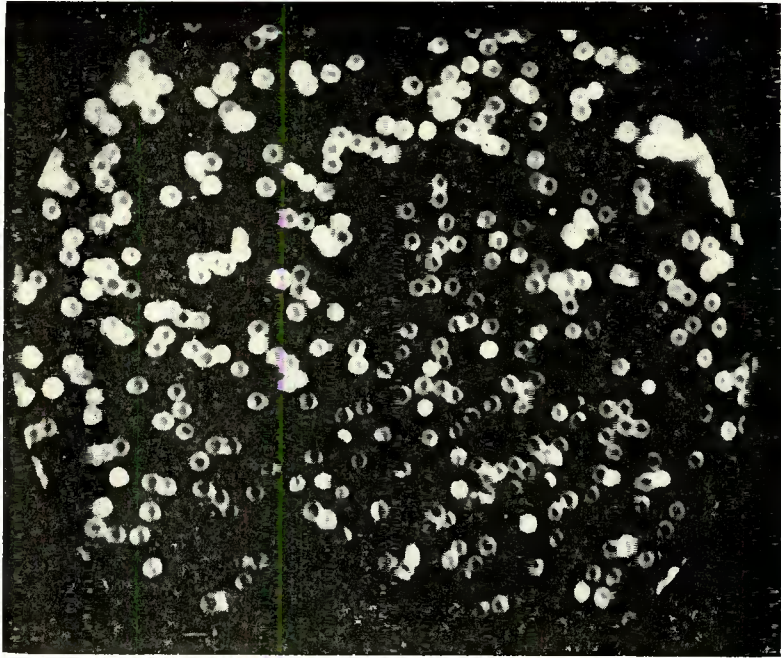
Fig. 3—Solution of erythrocytes as seen on the monitor screen.
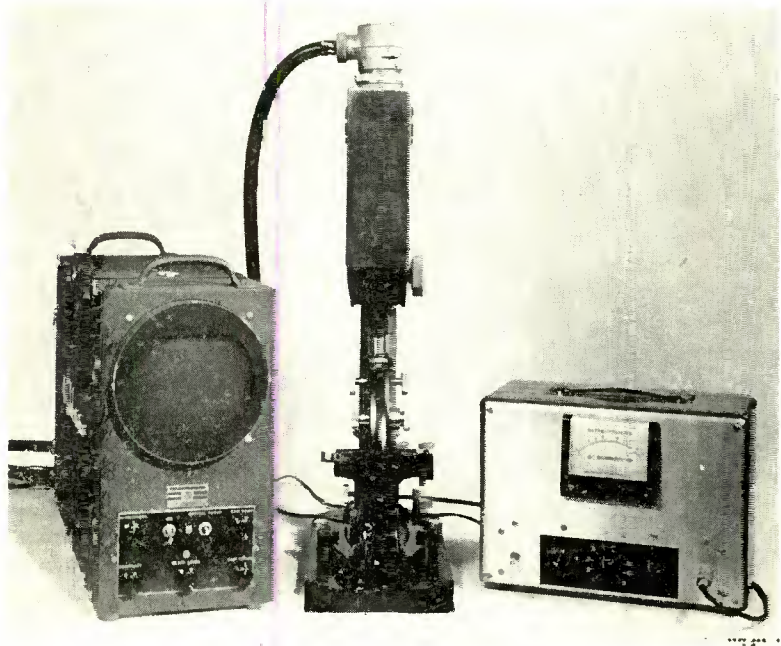
Fig. 4—Early experimental particle counter.

solution in an unruled counting chamber of standard volume under the microscope. After focussing the latter, the technician rotates the "Width" control (lower center Figure 5) on the counter until the electric eye tube (upper right Figure 5) closes. This operation compares the length of the video pulses from the cells with a standard adjustable delay line built into the counter. Closure of the eye indicates coincidence between the delay line length and the mean pulse length. A calibrated shunt across the count-rate meter movement is ganged with the delay line switch so that the operation of determining the pulse width simultaneously adjusts the meter sensitivity to the correct
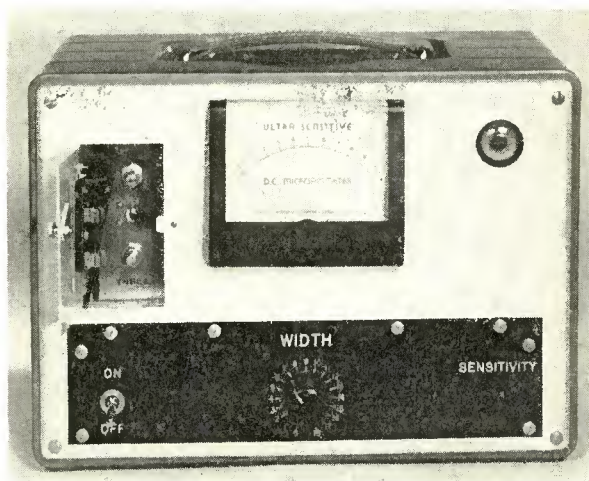
Fig. 5—Later model of counting meter.

value for proper diameter compensation. The operator then reads the meter to determine unambiguously the number of cells in the field of the microscope. Obviously the meter may be calibrated in any convenient units, and for a specialized application such as erythrocyte counting may be calibrated to include the effect of the original and standardized dilution of the blood sample if desired.

CIRCUIT DESCRIPTION

The circuit of the current version of the erythrocyte counter is shown in Figure 6. Positive video pulses from the television equipment are brought in at J1. V1 through V6 comprises the diameter compensation circuit, and V7 through V11 the count-rate meter. V7 amplifies and inverts the incoming video pulses which vary in amplitude and width. These pulses are converted by a pair of cascaded regenerative clippers comprising V8 through V11 into positive pulses at the plate

of V11. Each clipper is a form of monostable multivibrator. The "Threshold" bias controls of these clippers are adjusted before operation so that the clippers are just below the point of self-oscillation. The standardized pulses at the plate of V11 are applied to the count-rate meter circuit proper, comprising diodes D5 and D6 and their associated components. This circuit will be familiar to most readers and its operation need not be discussed beyond stating that the meter reading is proportional to the number of pulses per second at its input. C24 is a calibrating adjustment and R44 through R61 make up the variable
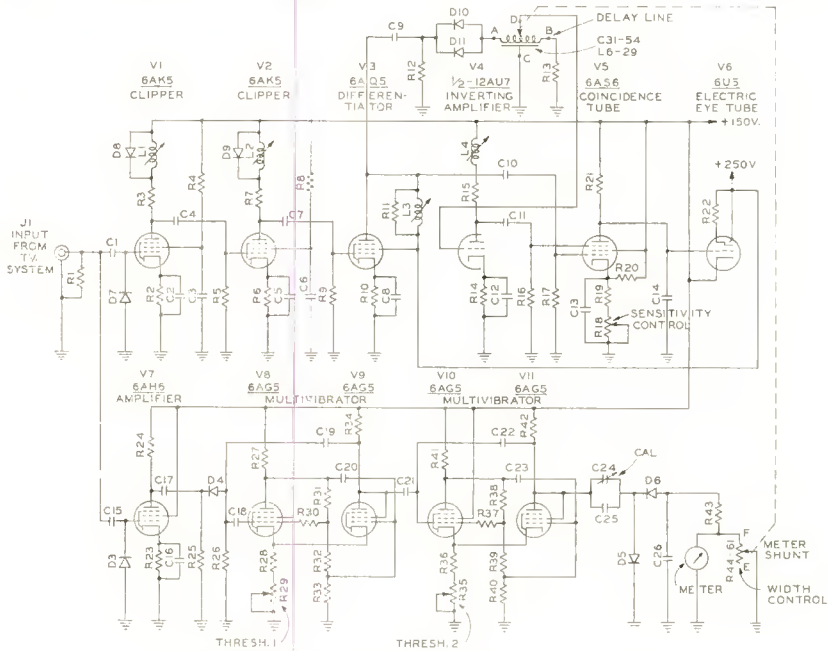
Fig. 6—Circuit diagram of sanguinometer.

shunt across the meter movement which is controlled by the diameter compensation circuit. The calibration and threshold controls, which are infrequently used, are accessible to the operator through the small door in the front panel visible in the upper left corner of Figure 5.

In the diameter compensation circuit the incoming pulses are amplified and clipped by V1 and V2, but the pulse width is not changed. The video response of these amplifiers is maintained to about 10 megacycles per second. A small amount of ringing is permitted in the peaking coils L1 and L2, but is damped in each case after the first half cycle by diodes D8 and D9. This arrangement seems to assist in maintaining good rise times. V3 drives an inductive

differentiating circuit consisting of L3 and R11. At the plate of V3, narrow negative pips occur which correspond in time with the leading edges of the incoming pulses, and narrow positive pips which correspond with the trailing edges of the original pulses. The positive pips are applied directly to G1 of normally off coincidence tube, V5. The negative pips are applied via diodes D10 and D11, and adjustable delay line comprising L6 through L29 and C31 through C54 and an inverting amplifier, V4, to G3 of V5. When the delay-line length is adjusted to coincide with the mean length of the incoming pulses, the pips at G1 and G3 of V5 will be in time coinci-
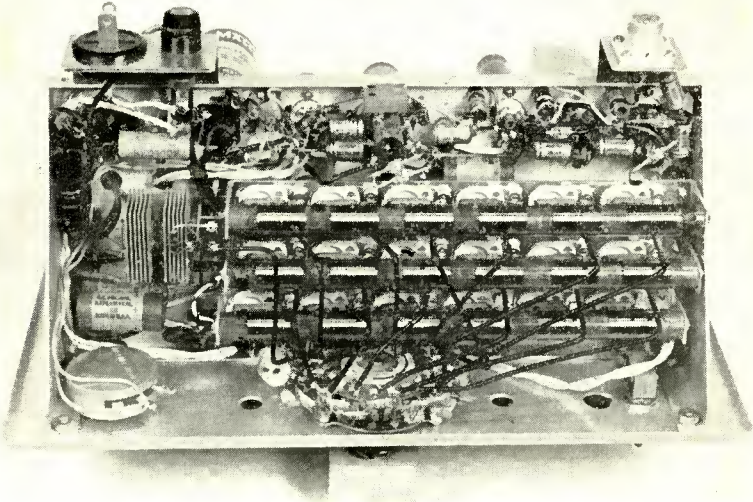
Fig. 7—Underside of sanguinometer chassis.

dence and plate current will flow. This is indicated to the operator by electric eye tube, V6, which is directly connected to an integrating circuit in the plate of V5. Potentiometer R18 adjusts the bias and thus the sensitivity of the coincidence circuit.

  Figure 7 is a photograph of the underside of the erythrocyte counter chassis. The hand-wound precision resistors of the adjustable meter shunt are visible mounted directly on one deck of the 20-point "Width" switch. Only 19 of the contacts of this switch are used. The second deck of the switch varies the electrical length of the delay line in 0.025-microsecond increments. Three units of this line, each comprising 6 sections of conventional lumped constant "m-derived" construction are visible directly above the switch. A fourth identical unit is located above the chassis. The total delay

of the line is 0.6 microsecond, and the line impedance is about 1000 ohms. A 0.15-microsecond length of line (one unit) is always in the circuit. The diameter compensation circuit can thus accommodate particles whose resulting pulse widths lie between 0.15 microsecond and 0.6 microsecond. This range is ample for erythrocyte counting if the optical magnification of the system is adjusted so that the field of the microscope embraces approximately the same area of the counting chamber that is viewed by a technician in making a manual count according to the usual clinical procedure.
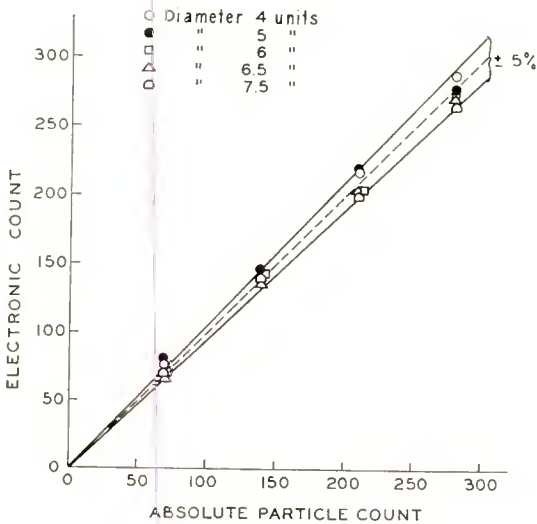
Fig. 8—Electronic count of simulated particles of various diameters.

TEST RESULTS

For convenience, early testing was accomplished using simulated fields of particles. The television camera and a slide projector were set up side by side and focused on a screen. A microscope was not used. Slides simulating the appearance of fields of particles were made by punching appropriate sizes and numbers of holes in pieces of opaque paper. These were then sandwiched between glass plates and inserted in the slide carrier of the projector. By suitable adjustment of the relative positions of screen, television camera and slide projector a range of pulse widths and numbers of particles entirely comparable to that obtained during actual erythrocyte counting could be obtained. The results of these tests are shown in Figure 8, in which it is seen that good agreement between the electronic counter readings and the actual number of simulated

particles was obtained over about a two-to-one range of particle diameters. The electronic count, but for a few exceptions, is within ± 5 per cent of the true number of simulated particles.

With the cooperation of Dr. Leon Hellman of Sloan-Kettering Institute, the instrument was tested on samples of real blood. The results are summarized in Figure 9. In this graph the ordinate is the electronic count and the abscissa the count of a skilled technician upon the same sample. The technician's error is thus included in the data and is not separable from errors in the electronic counter. The most obvious difference in the functioning of the counter
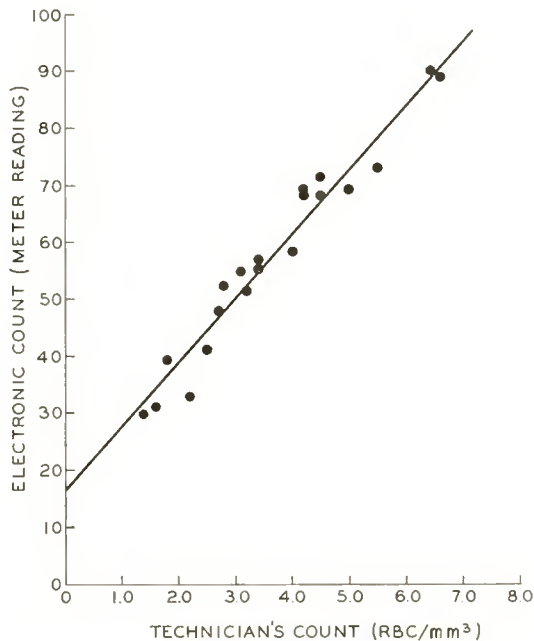
Fig. 9—Electronic count of erythrocytes as compared to manual count of same sample by technician.

on real blood as compared with its performance on simulated particles is the noticeable zero offset. This is apparently due to a poorer signal to noise ratio on the real blood. Aside from this, the accuracy may be considered satisfactory. During these tests the calibration of the counter was checked from time to time on a calibration slide. This slide consisted of a sample of erythrocytes which had been placed in the same type of counting chamber used during an actual count and then chemically fixed with a special solution and sealed up to

make a permanent calibration slide. To enable the operator to return, during each calibration, to exactly the same region of the calibration slide, a photographic negative of the appearance of the television monitor screen for this region of the calibration slide was prepared. This negative was adjusted in size so that it could be held up before the kinescope screen while the calibration slide was moved about on the microscope stage to obtain registry between the negative and the picture on the monitor. The calibration procedure thus was made relatively simple and foolproof and using it the inevitable slow drifts in the entire system could be readily detected.

The rapidity with which counts can be made with this equipment has underlined a well known phenomenon which can easily lead to inaccuracies in the present method of manual erythrocyte counting. This is the effect of nonuniform distribution of the red cells in the dilution. Using the electronic counter, readings taken at various points over the surface of a given sample were often found to vary by as much as 20 per cent. With the electronic counter it is an easy matter to take a number of such readings on a given sample and average the results, a process which would be prohibitively laborious and time consuming in manual counting.

Although the present instrument has thus far been used only on erythrocytes, there are many interesting possibilities for other uses of it. One application which has been suggested but not yet tried is that of counting different types of white cells selectively. For example, stains are available which are selectively absorbed by different types of these cells. The availability of these stains suggests the interesting possibility of staining the various types of white cells in a given sample of different colors and then counting the various types by means of appropriate color filters in the television camera. Such a technique would apparently be of considerable use in certain cases where it is important to determine the relative number of each type of white cell in a given sample.

Conclusion

Rapid electronic counting of microscopic particles with sufficient accuracy for many purposes is technically feasible using a standard closed circuit television chain plus a count-rate meter equipped with diameter compensation. The future application of the system to such fields as routine erythrocyte counting probably depends more on economic factors than on technical possibilities. With the increasing availability of inexpensive closed circuit television chains,

it is possible that widespread application of the technique may come about.

ACKNOWLEDGMENT

THE TANGIER RADIO RELAY SYSTEM*

By

Carl G. Dietsch

Engineering Department, RCA Communications, Inc.,
New York, N. Y.

Summary—Long-range radio communications in the short-wave band are adversely affected by magnetic disturbances, aurora, and solar activity. The effects are most severe near the polar regions. In order to circumvent this difficulty in circuits between New York and parts of Europe and Asia, a relay station has been set up at Tangier. This paper examines the reasons for choosing Tangier as the site, and describes the equipment necessary to meet the requirements of a modern communications system offering high-speed telegraph, telephone, and radiophoto services.

INTRODUCTION

THE first commercial radiotelegraph circuits were operated in the long-wave band between 15 and 500 kilocycles. While these circuits could provide communications over virtually the entire world, they had several rather serious drawbacks. Foremost among these was the noise, or "static" as it was then called, which sometimes made long distance communications difficult, or even impossible. This noise was chiefly due to electrical storms, and so was particularly annoying in the tropics and other areas where such storms commonly occur.

The most obvious method of increasing the signal-to-noise ratio was by increasing the power output of the transmitters. In some cases, the use of directional receiving and/or transmitting antennas would provide additional improvement. Both of these approaches were followed, but rather severe practical limitations restricted their usefulness.

Communications in the long-wave band requires large amounts of power because of the low efficiency of antennas used for these wave lengths. The radio-frequency generator must supply some 10 to 20 times the power actually radiated by the antenna. As a result, 200-kilowatt and even 500-kilowatt alternators were common in the early days of radiotelegraph. At these levels, the power increase which would be needed to provide a significant improvement in signal-to-noise ratio at a distant point, would be entirely out of the question from an economic standpoint.

Similarly, the improvement which was theoretically possible with

---

* Decimal Classification: R480.

directive antennas was difficult to achieve in practice. The beam width of a directive antenna is roughly proportional to the number of wave lengths contained in the radiating elements. Because of the long wave lengths involved, highly directive antennas were not feasible. For example, at 20 kilocycles the physical length of a wave length is 9.3 miles. The construction of gigantic structures required to support a reasonably efficient transmitting antenna of that type was impractical.

Another growing pain experienced by the wireless communication industry was the lack of space in the radio spectrum. Because of the large demand for frequencies in the long-wave region, there was little chance for expansion of commercial communication services.

As a result of these difficulties, communications engineers turned their attention toward the short-wave bands (4 to 22 megacycles) which were known to have certain advantages over the longer waves, and where much of the spectrum was unused. During the early 1920's, considerable effort was expended in the development of short-wave radio techniques, so that in 1925 it was possible to establish a direct short-wave radiotelegraph circuit between New York and Buenos Aires. This proved to be superior to the existing long-wave circuits in several respects. Less power was required, smaller antennas could be used, and the disruption of service by noise was much less frequent.

The success of this initial installation brought about the replacement with short-wave equipment of most of the long-wave gear used for circuits to South America. In addition, short-wave circuits were established for traffic with several European cities. On these European circuits, however, certain effects were discovered which were not present on the South American circuits. Large, rapid changes in signal intensities were observed, and occasionally there would be complete absence of signals for extended periods of time. There were also wide variations in signal intensities received from day to day and from hour to hour. These effects were in addition to the normal fading found on most long-range, short-wave circuits. The disturbances appeared to be most severe in circuits between New York and the northern countries of Europe. It was also found that circuits to the Orient in which the great-circle paths passed over the north polar region were completely obliterated most of the time.

Within a few years, techniques had been developed which permitted reliable short-wave communications on the European circuits during all but the most severe of the disturbances. Perhaps the most important single development in this respect was space diversity reception,[1] which

---

[1] H. H. Beverage and H. O. Peterson, "Diversity Receiving System of RCA Communications, Inc. for Radiotelegraphy," *Proc. I.R.E.*, Vol. 19, pp. 531-561, April, 1931.

consists of a system of two or more directional receiving antennas spaced a sufficient distance apart so that the signal intensity on one antenna usually increases when there is a decrease in the signal received on another. The signals from these antennas are fed into a diversity receiver which automatically selects the one of greatest intensity, thus reducing the effects of signal fading. By using long-wave circuits during the disturbed periods, continuously reliable communications were possible.

PROPAGATION STUDIES

Extensive studies were made of the vagaries of short-wave propagation. These seemed to indicate a correlation between field intensities and conditions of terrestrial magnetism.[2] Short-wave propagation over long distances depends on reflections of the transmitted wave by the E and F layers of ionization which form the ionosphere. When these layers are disturbed by ionospheric "storms," propagation is erratic in the disturbed areas. This effect had not been evident in the long-wave circuits.

Further studies showed that the periods of greatest ionospheric storms were also periods of greatest sunspot activity, and that the intensity of the storms was greatest near the north magnetic pole, in the Northern Hemisphere. Since means of predicting sunspot activity were known, this offered an approach to the prediction of short-wave propagation conditions. As a result of these discoveries, it was possible to establish zones which were designated as "effective," "disturbed," and "dead" with respect to a fixed communication center. Figure 1 is a chart of these zones about New York for the year 1942. There is no indication of the degree of disturbance, but actually there is an inverse relationship between the severity of the disturbance and the distance to the disturbed zone for all circuits outside of the zone. The intensity also varies with solar activity, but the location of the maximum disturbance in the zone does not change appreciably. The zones illustrated conform with actual propagation conditions experienced during 1942.

It can be seen from Figure 1 that the cities of northern Europe and India lie in the disturbed zone. One method of obtaining reliable short-wave communications between these cities and New York is to employ a relay station at a location which does not lie near the disturbed zones of either New York or the cities of northern Europe.

---

[2] H. E. Hallborg, "Terrestrial Magnetism and Its Relations to World-Wide Short-Wave Communication," *Proc. I.R.E.*, Vol. 24, pp. 455-471, March, 1936.
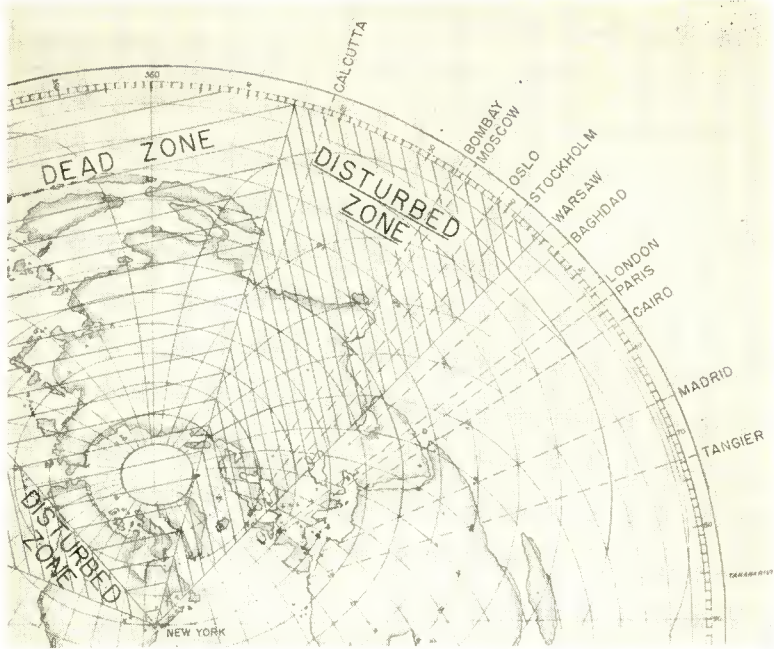
Fig. 1—Average disturbed and dead zones about New York
for short-wave signals during 1942.

The seaport of Tangier is so situated. Figure 2 is a chart showing
propagation zones with respect to Tangier. It might be supposed that
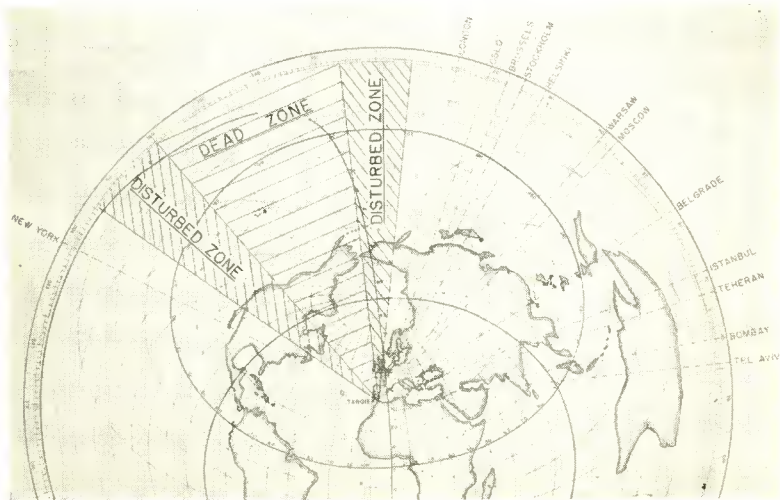
Fig. 2—Average disturbed and dead zones about Tangier
for short-wave signals during 1942.

a location farther from the magnetic pole would be more desirable, but as the distance from the equator decreases, the noise increases. While the noise is much less troublesome on the short-wave than on long-wave circuits, it can, nevertheless, become a limiting factor in the tropics. On a noise scale which ranges from 1 to 5, Tangier has an annual average of $2\frac{1}{2}$.[3] Approximately the same figure applies to Riverhead, Long Island, New York, where the RCA Communications main receiving station is located. Tangier, then, represents a good compromise between the opposing factors.
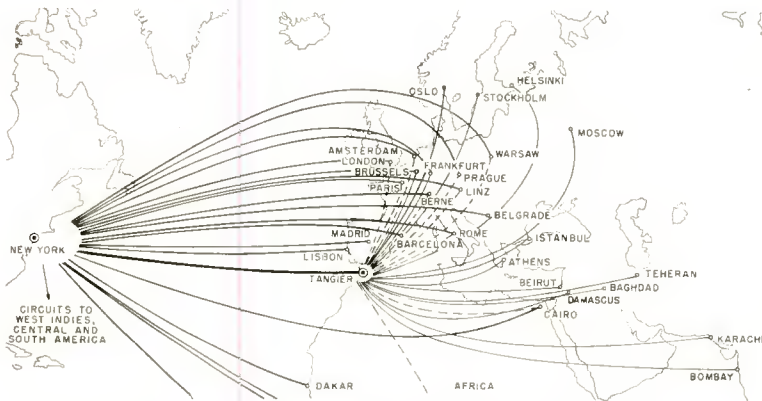
Fig. 3—Circuits between New York and Europe and the
Near and Middle East.

The utility of a relay station in northern Africa was demonstrated by the U. S. Army station which was put into operation in Algiers in 1944. This station enabled considerably more reliable Morse and teletype service between the United States and our armed forces in Europe than had been possible on direct circuits.

THE TANGIER RELAY STATION

In early 1946, RCA Communications Inc. installed a relay station on the northwest tip of Africa in the Tangier International Zone. The site of the station is approximately 16 miles south of the city of Tangier, Morocco. Figure 3 shows the traffic circuits that pass through the station. The principal purpose of the installation was to serve as a link in the New York–Moscow and New York–Bombay circuits, enabling continuous reliable short-wave communications between these

---

[3] "Ionospheric Radio Propagation," *National Bureau of Standards Circular #462*, pp. 151-162, U. S. Government Printing Office, Washington, D. C.

cities. Soon after inauguration of this service, its usefulness was
established for relaying traffic between New York and other cities in
Northern Europe during periods when the space paths of the direct
circuits were adversely affected by severe ionospheric storms and
auroral phenomena. The value of the station is indicated by the fact
that its facilities have increased approximately sixfold since 1946.

A plan of the station is shown in Figure 4. The administrative
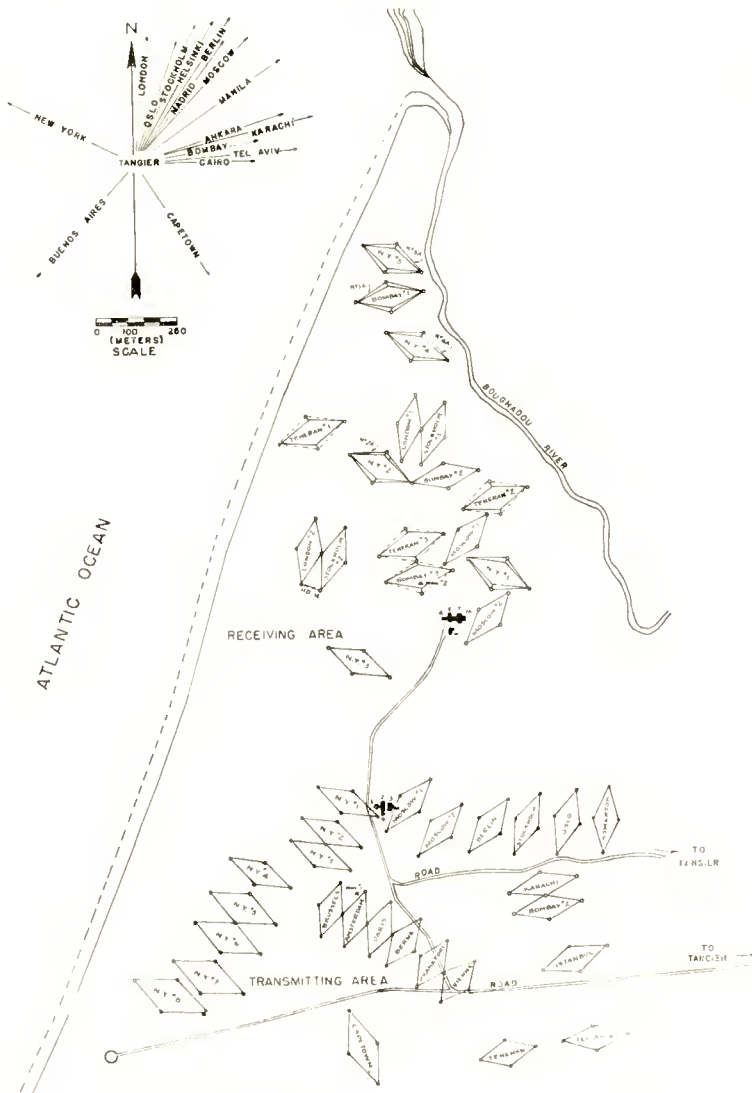
Fig. 4—Plan of the Tangier Relay Station.

offices are located in the receiving area in the northern part of the property, and the diesel-electric power station and the fresh water supply and pumping station are in the transmitter area in the southern part. The main diesel-electric unit is a low-speed machine capable of delivering approximately 400 kilowatts of 230-volt, 3-phase, 60-cycle power. This is shown in Figure 5. In addition, there are 8 standby units, each rated at 50 kilowatts. There are provisions for synchronizing the standby units so that they may be added to the main line
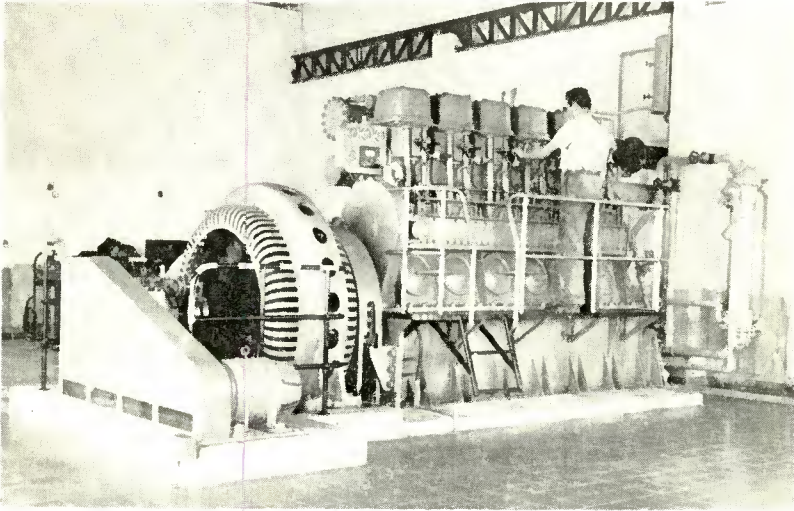
Fig. 5—400-kilowatt diesel-driven generator.

without interrupting the power supply. Step-up transformers provide 2300-volt power for transmission to the central radio office and receiving station. This is carried by two underground cables, either of which is capable of supplying the entire load. The voltage is stepped-down to 230 volts for use at these locations.

Fresh water is obtained from a deep well owned by the Tangier Administration. In order to ensure an adequate supply, it was necessary to install pumping facilities and more than a mile of cast iron pipe.

OPERATIONS

Communications between Tangier and New York are conducted over four sets of four-channel send/receive electronic time-division multiplex equipment. The five-unit teletype system is employed, with an operating speed of 60 words per minute. In addition to the time-division equipment, there is a four-channel send/receive frequency-

division multiplex system which is operated in conjunction with single-sideband transmitting and receiving equipment. Except for short maintenance periods, the multiplex equipment is kept in continuous operation. A five-unit "solo" printer channel is used for the exchange of information and instructions between the operating personnel in New York and Tangier.

Most of the traffic between Tangier and the cities of Europe and the East is in the form of five-unit teleprinter signals.[4] At Tangier, the received signals from the first leg of the circuit are punched on a tape. They are then read off the tape and fed into the second leg of the circuit. For the few remaining circuits which still employ Morse signals, a rapid system has been developed for converting five-unit teletype signals into Morse so as to minimize conversion delays.

The volume of traffic between New York and certain European cities is such that multiplex channels are being planned for use between Tangier and the cities in question. A set of four-channel time-division electronic multiplex equipment is already in use between Tangier and London. On this circuit, the aggregate signal is relayed—that is, the signal is received at Tangier, demodulated, regenerated, and re-transmitted on another frequency. This method has the advantage that both noise and distortion are eliminated. Extensive use of this technique in the future is indicated.

For leased-channel services between New York and several cities in Europe, five-unit teletype single-channel signals are relayed automatically. A regenerative telegraph repeater unit is used for each such channel at the output of the multiplex unit. This serves to restore the signals as nearly as possible to their original form prior to retransmission.

On occasion, Morse signals have also been automatically relayed. The signal is demodulated and then applied to a keying device which modulates the relay transmitter. This method has the disadvantage that both noise and distortion are relayed along with the signal, but a minimum of equipment is required at Tangier.

RECEIVING EQUIPMENT

The receivers employed at Tangier include twenty triple-diversity receivers,[5] nine dual-diversity receivers, and one triple-diversity single-

---

[4] S. Sparks and R. G. Kreer, "Tape Relay System for Radiotelegraph Operation," *RCA Review*, Vol. VIII, pp. 393-426, September, 1947.

[5] J. B. Moore, "Recent Developments in Diversity Receiving Equipment," *RCA Review*, Vol. II, pp. 94-116, July, 1937.

sideband receiver. The last is used in conjunction with the frequency-division multiplex equipment. Each of the receivers is equipped with an antenna patching panel so that it may be connected to any of the numerous receiving antennas. In addition, each receiver has an adapter for receiving frequency-shift telegraph signals. The frequency-shift system of keying has notable advantages over the off/on system,[6] and is used on nearly all of the signals relayed through Tangier. Figure 6 is an interior view of the receiving station.
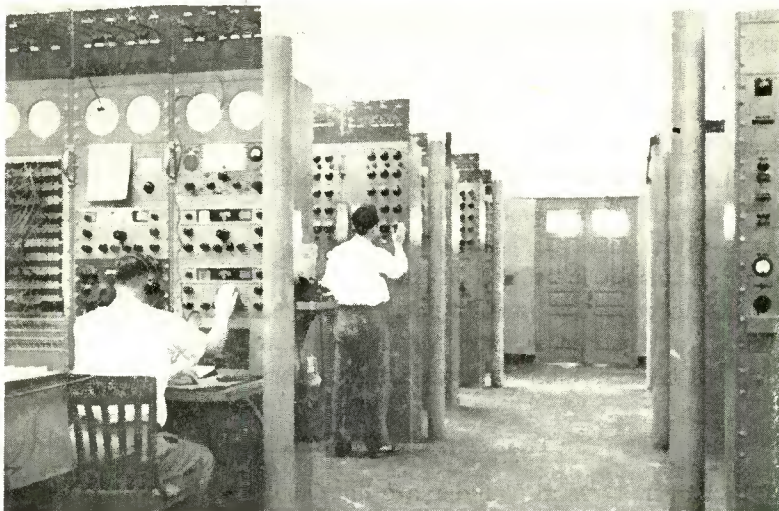
Fig. 6—Tangier receiving station. The control center is at the left.

Rhombic receiving antennas are used almost exclusively. The location of the 22 rhombics now in use or nearing completion can be seen in Figure 4. The large number of antennas required is due to the wide band of frequencies which must be covered (4 to 22 megacycles), the directivity requirements, and the need for space diversity.

Ten of the antennas are in the form of five dual units. Each unit employs four masts to support two rhombic antennas. One of the pairs is for a "day" frequency, and the other for a "night" frequency, connected so that both can be used simultaneously. The night frequency antenna is mounted at the top of the masts, and the day frequency antenna at approximately 2/3 of the mean height of the night antenna. The remaining twelve rhombics are single units. The distribution of the antennas, in terms of direction, is as follows:

---

[6] H. O. Peterson, J. B. Atwood, H. E. Goldstine, G. E. Hansell, and R. E. Schock, "Observations and Comparisons on Radiotelegraph Signalling by Frequency Shift and On/Off Keying," *RCA Review*, Vol. VII, pp. 11-31, March, 1946.

    4 "night" antennas for New York
    5 "day" antennas for New York
    1 "night" antenna for the Middle East
    3 general purpose antennas for the Middle East
    3 general purpose antennas for the Near East
    6 general purpose antennas for Middle, North, and Far
        Northern Europe.

In addition to the rhombics, there are several dipole and 2 experimental V-type antennas.

All of the rhombics are of standard design. Four-wire transmission lines[1] are used to carry the signals to the antenna line termination structure adjacent to the receiver building. From there two-wire lines pass through plate glass lead-in ports, into the receiving building and distribute the signals to the various receiving locations. The interior two-wire lines are transposed at intervals of approximately two feet. The characteristic impedance of each transmission line from the output end of the exponential line of a particular rhombic antenna to the input terminals of a particular receiver is maintained at approximately 200 ohms. All transmission lines are carefully balanced to ground.

Transmitting Equipment

The transmitters at Tangier are housed in two adjacent buildings with a combined floor area of 5700 square feet. Some of the transmitters may be seen in Figure 7. There are a total of 25 transmitters as follows:

            8 15-kilowatt transmitters
            5 10-kilowatt transmitters
            4 5-kilowatt transmitters
            1 3-kilowatt transmitter
            2 2-kilowatt transmitters
            5 1-kilowatt transmitters

Either frequency-shift or on/off keying may be used on each transmitter. When using frequency-shift keying, a quartz crystal oscillator unit is employed to hold the transmitter frequency constant.

Twenty-six transmitting antennas are employed, all of which are rhombics. Four "day frequency" and four "night frequency" antennas are directed toward New York, twelve antennas are directed toward cities in Europe, five toward points in the Near and Middle East, and one toward Capetown.

Radio-frequency power from the transmitters is carried by two-wire balanced transmissions through glass lead-in ports to a central-transmission-line cross-connect frame outside of the main transmitter building. Two-wire open transmission lines lead from this frame to the main outdoor transmission-line trunks. The lines for the individual antennas branch off from the main trunk. The outdoor transmission lines are supported by wooden poles.

Fig. 7—Interior view of the transmitting station.

RELAYING RADIOPHOTO AND RADIOTELEPHONE SIGNALS

While the facilities at Tangier were installed primarily for the purpose of relaying message traffic and leased channel services, they have, on occasion, also been used to relay radiophoto and radiotelephone signals. In the case of radiophoto, complete control is exercised from the two terminals involved, the facilities at Tangier being simply a means of linking together the two space paths. Voice circuits are used to send operating instructions. Good results have been obtained in relaying signals to and from points in North Europe, and the Near and Middle East. Figure 8 shows a picture received in New York from Helsinki via Tangier. This was sent during the 1952 Olympic Games at a time when it was not possible to send a satisfactory picture over the direct circuit. Radiotelephone signals can be relayed in the same manner as radiophoto signals.

Fig. 8—Photoradio picture relayed to New York via Tangier.

ACKNOWLEDGMENT

APERTURE COMPENSATION FOR TELEVISION CAMERAS*

By

R. C. Dennison

Engineering Products Department, RCA Victor Division,
Camden, N. J.

Summary—Aperture distortion in television pickup equipment is caused by the finite size of the scanning aperture. Its effect on the image is a reduction in resolution and detail contrast. Compensation of aperture distortion can be accomplished through the use of a dispersionless wave filter of the transversal type. Simple equations for designing both fixed and variable boost aperture compensators are developed, and a procedure for achieving optimum compensation is discussed. Photographs are included to illustrate the benefits obtained through proper use of aperture compensation.

Introduction

ALTHOUGH methods of compensation for the effects of aperture distortion have been available for many years, such devices have not been extensively employed in commercial television equipment. The reason for this is that most television pickup tubes have insufficient signal-to-noise reserve to allow the full benefits of aperture compensation to be enjoyed. The vidicon, however, is essentially noiseless. When used with a low-noise cascode preamplifier and at the moderately high light levels which are provided by standard television film projectors, the vidicon permits optimum utilization of aperture compensation.[1, 2] This has led to a renewal of interest in aperture compensation.

Aperture Distortion

Aperture distortion is caused by the finite size of the scanning beams employed in television camera tubes and kinescopes and by lens aberrations in the optical system. It is apparent that a large scanning aperture will cover several picture elements simultaneously, reproduc-

---
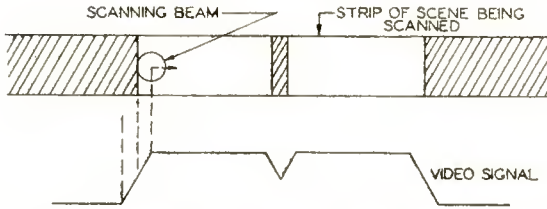
Fig. 1—Effect of aperture distortion on sharpness of relief and detail contrast.

ing them as a blur. Horizontal resolution thus improves as the size of the scanning aperture is decreased, provided that the bandwidth of the system is sufficient to pass the higher video frequencies thereby generated.

The size of the scanning aperture also limits the ability of a television system to reproduce sharp transitions in picture brightness. This is illustrated in Figure 1. As the scanning beam starts to cross a black picture element, the receiver scanning spot starts to turn darker. Total extinction of the receiver scanning spot does not occur until the camera scanning spot is completely on the black picture element. If the diameter of the scanning beam exceeds the width of the picture element, the leading edge of the beam will start to leave the picture element before total extinction has occurred. This causes a reduction in the detail contrast of the image and is manifest in those areas of the image containing fine detail in the horizontal direction; e.g., the horizontal-resolution wedges of a resolution test chart.

The effect of aperture distortion is quasi-analogous to inserting a low-pass filter in the video channel of the television system. Mathematical analysis[3] shows that the attenuation and phase shift due to aperture distortion are of the form shown in Figure 2. The actual
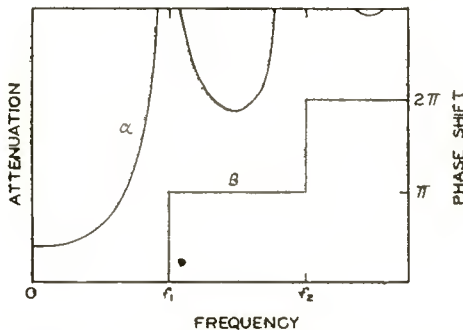
Fig. 2—The nature of attenuation and phase shift due to aperture distortion.

---

[3] Pierre Mertz, "Television—The Scanning Process," *Proc. I.R.E.*, Vol. 29, p. 529, October, 1941.

shape of the attenuation curve depends somewhat on the cross-sectional shape of the scanning beam and the density distribution of the electrons composing it.

It is of interest to correlate the data of Figure 2 with the physical effects of aperture distortion. If the horizontal-resolution wedge of a televised test chart is carefully examined, it will be observed that the lines and spaces merge together into a uniform gray blur in the region corresponding to frequency f_1 since the attenuation of the signal is high at this frequency. Beyond this point the lines may be resolved again but with reversed polarity; that is, a line will be found where there should be a space. This is due to the 180 degree phase shift which occurs at f_1. In the region of f_2 there will be another fade-out of resolution. In typical television systems, only the first "zero" of resolution is apparent.

Aperture Correction

The foregoing discussion of aperture distortion allows one to prescribe performance specifications for an aperture compensator. While an exact solution has not been discovered, the following approximation provides greatly enhanced resolution and detail contrast. Thus the device should

(a) Provide a controllable boost in video gain, rising with frequency and having a peak at or near f_1. The shape of this rising gain characteristic should be substantially complementary to the attenuation caused by the aperture distortion. In practice, a cosine-shaped response has been found to be a satisfactory approximation.

(b) Introduce a phase shift which is either identically zero or which varies linearly with frequency.

Aperture Correcting Processes

According to the phase-area theorem,[4] the phase shift of a network of the minimum phase shift type is determined by its amplitude response. Recognition of this fact led to the development of the so-called "negative aperture process."[5] In this system, the signal is split and passes through two parallel channels. One channel has a flat response

[4] Stanford Goldman, *Transformation Calculus and Electrical Transients*, Prentice-Hall, Inc., New York, N. Y., 1949, p. 241.

[5] O. H. Schade, "Electro-Optical Characteristics of Television Systems; Part II—Electro-Optical Specifications for Television Systems," *RCA Review*, Vol. 9, p. 245, June, 1948.

while the other is given a response similar to that of the aperture. After suitable phase correction, a certain fraction of the latter signal is subtracted from the unmodified signal. Due to the difficulty of providing the required phase correction, such systems are neither easy to design nor flexible in operation.

A second method, known as the "cascade aperture process," passes the signal through a stage which has a rising gain characteristic and then through an all-pass phase correcting network. The gain ascension is provided by either plate or cathode *high-peaking* and the phase correction is achieved by means of a lattice or other balanced phase shift networks.[6-7]

A third method of aperture compensation employs a special wave-filter system which has the required transmission characteristic yet exhibits a constant delay at all frequencies.[8-13] These filters avoid the necessity of phase-correction circuits through clever application of networks which are not subject to the laws governing minimum phase shift circuits. The most important networks falling in this category are those involving distributed parameters, e.g., transmission lines. Fortunately, it is possible to closely approximate the behavior of such lines with carefully designed artificial delay lines. Kallman[11] has given the name "transversal filter" to transmission line devices which afford such dispersionless* filtering.

TRANSMISSION-LINE PHENOMENA[14]

The aperture corrector described in this paper depends on certain interesting effects resulting from wave reflections at the open end of a lossless transmission line. Figure 3 shows such a line connected to a generator whose internal resistance is equal to the characteristic

[6] E. D. Goodale and R. C. Kennedy, "Phase and Amplitude Equalizer for Television Use," *RCA Review*, Vol. 10, p. 35, March, 1949.

[7] E. D. Goodale, "Phase Amplitude and Aperture Correction in Television Systems," presented at the Spring Technical Conference, I.R.E. Cincinnati Section, Cincinnati, Ohio, April 19, 1952.

[8] N. Wiener and Y. W. Lee, U. S. Patent 2,124,599. Filed July 18, 1936.

[9] Y. W. Lee and N. Wiener, U. S. Patent 2,128,257. Filed July 7, 1936.

[10] A. D. Blumlein, H. E. Kallman, and W. S. Percival, U. S. Patent 2,263,376. Filed June 28, 1938.

[11] Heinz E. Kallman, "Transversal Filters," *Proc. I.R.E.*, Vol. 28, p. 302, July, 1940.

[12] J. C. Wilson, U. S. Patent 2,273,163. Filed August 15, 1940.

[13] M. S. Corrington and R. W. Sonnenfeldt, "Synthesis of Constant-Time Delay Networks," presented at ninth annual National Electronics Conference, September 28-30, 1953, Chicago, Ill.

* Sometimes loosely referred to as "phaseless".

[14] L. A. Ware and H. R. Reed, "Communication Circuits," 3rd Ed., John Wiley and Sons, Inc., New York, N. Y., 1949, Chapter VI.

impedance of the line. The sending-end impedance of a lossless open-circuited transmission line is given by

$$Z_s = - j R_0 \cot \theta \qquad (1)$$

where R_0 is the characteristic impedance of the line, and θ is the electrical length of the line in radians. The voltage across the sending-end of the line is

$$e_1 = \frac{Z_s}{R_0 + Z_s} e \sin \omega t = e_i \cos \theta \; \underline{/- \theta} \qquad (2)$$

and the voltage across the receiving-end of the line is

$$e_2 = \frac{e_1}{\cos \theta} = e_i \; \underline{/- \theta}. \qquad (3)$$
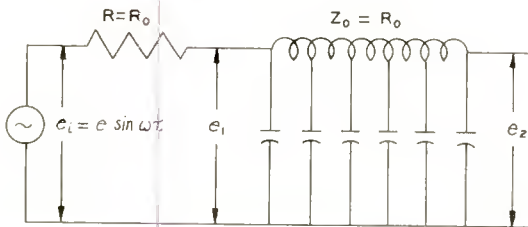
Fig. 3—An open-circuited lossless transmission line connected to a generator whose internal resistance is equal to the characteristic impedance of the line.

This result appears somewhat amazing since it shows the receiving-end voltage to be in phase with the sending-end voltage and to have a magnitude independent of frequency. For a simple physical explanation of these phenomena, the reader is referred to the author's prior paper on aperture compensation.[15]

Theory of the Transversal Aperture Corrector

Figure 4 shows the basic arrangement used in the aperture corrector. The signals from the two ends of the transmission line are amplified and combined to obtain an output voltage given by

[15] R. C. Dennison, "Aperture Compensation for Television Pick-up Equipment," presented at ninth annual National Electronics Conference, September 28-30, 1953, Chicago, Ill.

$$e_o = -e_2 G_2 + e_1 G_1 \tag{4a}$$

$$= -G_2 (e_2 - K e_1) \tag{4b}$$

$$= -e_i G_2 (1 - K \cos \theta) \; \underline{/-\theta} \tag{4c}$$

where

$$K = \frac{G_1}{G_2}. \tag{5}$$

The gain of this circuit is thus

$$G = \frac{e_o}{e_i} = -G_2 (1 - K \cos \omega\tau) \; \underline{/-\omega\tau} \tag{6}$$
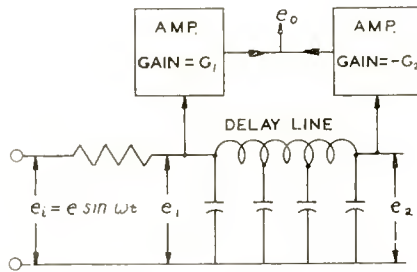
Fig. 4—The basic circuit arrangement used in the transversal aperture corrector.

where τ is the delay time of the transmission line. If the aperture compensator is to be built as a separate unit so that it can be connected into any camera chain, the basic circuit of Figure 4 will require input and output stages. If we let the gain due to these stages be $-G_r$, then the over-all gain of the complete aperture compensator is

$$G_o = G_r G_2 (1 - K \cos \omega\tau) \; \underline{/-\omega\tau}. \tag{7}$$

Equation (7) is plotted in Figure 5 for values of $G_r G_2 = 2.5$ and $K = 0.6$. The gain rises cosinusoidally with frequency attaining a maximum value at a frequency f_p at which the delay line is one-half wavelength long ($\omega\tau = \pi$). Thus the required line delay is

$$\tau = \frac{\theta_p}{\omega_p} = \frac{\pi}{2\pi f_p} = \frac{1}{2f_p}. \tag{8}$$

If the line is properly designed, so that τ is independent of frequency, there will be no phase distortion. Thus the scheme shown fulfills the specifications outlined for satisfactory aperture equalization.

The maximum boost in gain is evidently (see Figure 5)

$$B_m = \frac{(G_o)_{\omega\tau=\pi}}{(G_o)_{\omega\tau=0}} = \frac{1+K}{1-K}. \tag{9}$$

Ordinarily the value of B_m is chosen by the designer. Then K is determined from

$$K = \frac{B_m - 1}{B_m + 1}. \tag{10}$$
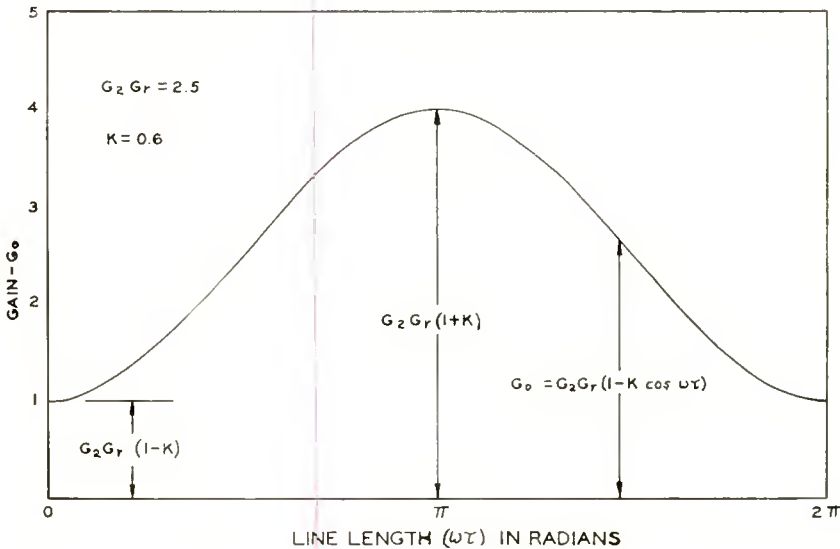
Fig. 5—The gain of the aperture compensator as a function of the electrical length of the line. The maximum occurs when, at frequency f_p, the line is one-half wavelength long.

FIXED-BOOST APERTURE EQUALIZER

The amplifiers indicated in Figure 4 may conveniently take the form of a differential amplifier[16] as shown in Figure 6. The gain from

[16] G. E. Valley, Jr. and H. Wallman, *Vacuum Tube Amplifiers*, M.I.T. Radiation Laboratory Series, McGraw-Hill Book Company, Inc., New York, N. Y., 1948, p. 442-443.

grid No. 1 to plate No. 2 is given by

$$G_1 = \frac{\mu}{1 + \dfrac{2r_p}{R_L} + \dfrac{r_p\,(r_p + R_L)}{R_L R_K\,(\mu + 1)}} \tag{11}$$

and the gain from grid No. 2 to plate No. 2 is

$$G_2 = \frac{\mu + \dfrac{\mu}{\mu + 1} \cdot \dfrac{r_p}{R_K}}{1 + \dfrac{2r_p}{R_L} + \dfrac{r_p\,(r_p + R_L)}{R_L R_K\,(\mu + 1)}}. \tag{12}$$
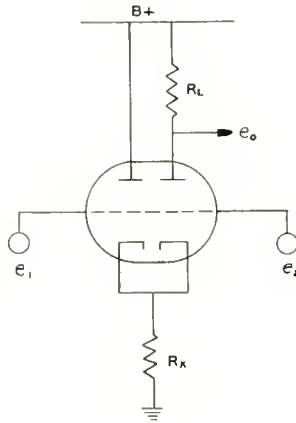
Fig. 6—Schematic diagram of a differential amplifier.

The ratio of G_1 to G_2 is (note Equation (5))

$$\frac{G_1}{G_2} = K = \frac{\mu}{\mu + \dfrac{\mu}{\mu + 1} \cdot \dfrac{r_p}{R_K}} \doteq \frac{g_m R_K}{1 + g_m R_K} \tag{13}$$

where use has been made of the approximation

$$\frac{\mu + 1}{r_p} \doteq \frac{\mu}{r_p} = g_m. \tag{14}$$

Equating Equations (10) and (13) gives the value of R_K required to produce any desired boost. Thus

$$R_K = \frac{B_m - 1}{2g_m}. \tag{15}$$

Equation (15) is subject to the approximation given in Equation (14) which introduces an error of about 2.4 per cent when a 6BQ7-A tube is employed.

Now let the value of $g_m R_K$ from Equation (15) be substituted into Equation (12). Then

$$G_2 = \frac{\mu R_L (B_m + 1)}{(B_m + 1) R_L + 2r_p B_m} \tag{16}$$

where the approximation of Equation (14) has been employed. However, the error in this case is much smaller than it is in Equation (15) due to the constant terms which are added to the terms containing the approximations and also because the approximation occurs both in the numerator and the denominator. A further simplification of Equation (16) is obtained by dropping the term in the denominator containing R_L. This yields

$$G_2 = \frac{g_m R_L}{2} \left(\frac{B_m + 1}{B_m} \right) \tag{17}$$

The error due to this approximation increases with B_m and R_L, reaching about 4.3 per cent when $B_m = 10$ and $R_L = 500$ ohms.

The value of G_r required to make the over-all gain of the aperture corrector unit equal to unity at zero frequency may be obtained by substituting Equations (10) and (17) into Equation (7) and setting $G_o = 1$ and $\omega = 0$. Then

$$G_r = \frac{B_m}{g_m R_L}. \tag{18}$$

VARIABLE BOOST APERTURE EQUALIZER

For many purposes, it is desirable that the boost be variable. Equation (15) shows that the boost can be varied by changing R_K. If this method is used, however, Equation (18) shows that G_r must simultaneously be varied if it is desired to maintain constant background contrast, i.e., a constant value for G_o at $\omega = 0$.

A simple circuit[17] which avoids this defect is shown in Figure 7. A dual potentiometer allows the voltage due to i_{p2} to be decreased while simultaneously increasing the voltage due to i_{p1}. Note that these signals are of opposite polarity. Inspection of Equations (11) and (12) reveals that G_1 and G_2 vary nearly linearly with plate load resistance provided $\Delta R_L \ll r_p$. The output voltage may be found by means of the superposition theorem by considering the effects of i_{p1} and i_{p2} individually. The output voltage due to i_{p2} may be seen to be (from Equation (4-c))

$$e'_o = -e_i G_2 (1 - N)(1 - K \cos \omega\tau) \,/\!\!-\omega\tau \tag{19}$$
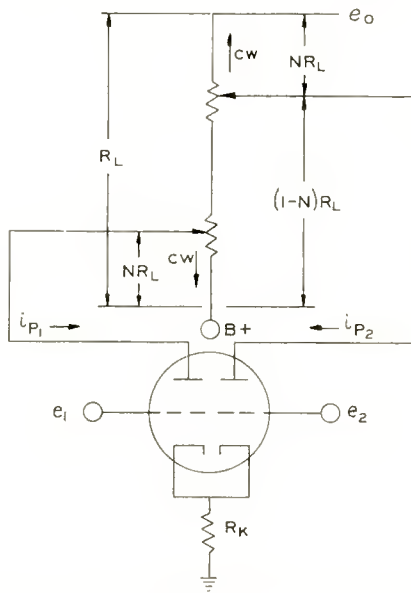
Fig. 7—The variable-boost amplifier circuit.

and the output voltage due to i_{p1} is

$$e''_o = e_i G_2 N (K - \cos \omega\tau) \,/\!\!-\omega\tau. \tag{20}$$

If these two voltages are added, the result is

$$e_o = -e_i G_2 \{1 - N(1+K) + [N(1+K) - K]\cos \omega\tau\} \,/\!\!-\omega\tau. \tag{21}$$

The gain including the input and output stages is

---

[17] Morris Specialties Company, "Model 100A Aperture Equalizer," a brochure.

$$G = G_2 G_r \{1 - N(1+K) + [N(1+K) - K] \cos \omega\tau\} \underline{/-\omega\tau}. \qquad (22)$$

At zero frequency, $\cos \omega\tau = 1$, and the quantity inside the braces reduces to $(1 - K)$ which is independent of the value of N. This is precisely the condition required in order that a change in boost shall not affect the low-frequency contrast.

Following the method used to obtain Equation (9), the boost B as a function of N is

$$B = \frac{(G)_{\omega\tau=\pi}}{(G)_{\omega\tau=0}} = \frac{1 - N(1+K) - [N(1+K) - K]}{1 - N(1+K) + [N(1+K) - K]} = \frac{1+K}{1-K}(1-2N). \qquad (23)$$

The boost is maximum when $N = 0$, and is

$$B_m = \frac{1+K}{1-K}. \qquad (24)$$

Substituting Equation (24) into Equation (23) gives

$$\frac{B}{B_m} = 1 - 2N \qquad (25A)$$

or

$$N = \frac{1}{2}\left[1 - \frac{B}{B_m}\right] \qquad (25B)$$

For maximum boost, $B = B_m$ and $N = 0$. This occurs when the potentiometer in Figure 7 is rotated to its maximum clockwise position. For *flat response*, $B = 1$ so that

$$N' = \frac{B_m - 1}{2B_m}. \qquad (26)$$

This condition occurs before the potentiometer reaches the full counterclockwise position; however, this can be remedied by inserting a fixed resistance between the two sections of the dual-potentiometer.

Substituting Equations (8), (10), (17), and (18) into Equation (22) gives
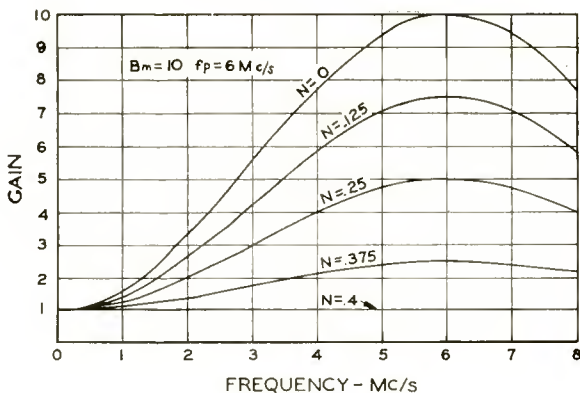
Fig. 8—The frequency response of the variable-boost aperture equalizer for various values of N. It is seen that the low-frequency gain is constant. $N = (100 — P)/200$ where P is the percentage of full clockwise rotation of the dual-potentiometer boost control.

$$G = \frac{1}{2}\left\{ [B_m(1-2N)+1] - [B_m(1-2N)-1]\cos\pi\left(\frac{f}{f_p}\right)\right\} \Big/ -\pi\left(\frac{f}{f_p}\right)$$

$$(27)$$

The scalar magnitude of this equation is plotted for several values of N in Figure 8 for the case where $B_m = 10$ and $f_p = 6$ megacycles.

FIXED BOOST WITH "IN-OUT" PROVISION

Figure 9A represents the circuit equivalent to the variable boost circuit of Figure 7 when N has been set equal to N' to get a flat
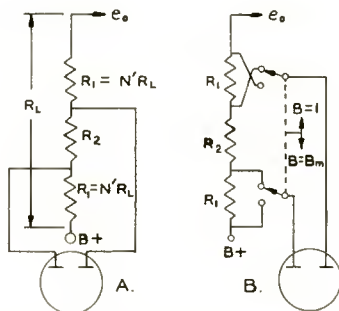
Fig. 9—(A) A special case of the variable-boost amplifier with its boost fixed at unity. (B) The circuit arranged so that the boost may be switched "IN" or "OUT".

response ($B = 1$). Substituting the value of N' from Equation (26) into the equation for R_1 (see Figure 9A) gives

$$R_1 = N'R_L = \frac{B_m - 1}{2B_m} R_L \qquad (28)$$

and hence

$$R_2 = R_L - 2R_1 = \frac{R_L}{B_m} . \qquad (29)$$

It is often possible to choose a value for R_L such that standard readily available values may be employed for R_1 and R_2.

The use of resistor R_2, to get a flat response when the potentiometer in the variable boost circuit of Figure 7 is turned all the way counterclockwise, has been mentioned. Another practical application is shown in Figure 9-B. In one position of the switch, the aperture equalization is effective and provides a maximum boost of B_m. In the other position of the switch, a flat response is obtained; furthermore, the low-frequency gain remains constant so there is no change in the background contrast of the picture.

OPTIMUM EQUALIZATION

The aperture correction circuits described provide a cosinusoidal modification of the response curve of the camera chain to which they are applied. The aperture response of a camera tube, on the other hand, is a transcendental function. Optimum compensation, therefore, involves a process of curve matching. This may be carried out on a graphical trial and error basis. The two parameters which are at the designer's disposition are B_m and f_p.

As an example, the optimum compensation was determined for a 6198 Vidicon. The response of the Vidicon[1] multiplied by the response of the aperture corrector was plotted against frequency for various values of B_m and f_p. Comparison of these curves showed that optimum compensation required $B_m = 4$ and $f_p = 10$ megacycles. Figure 10 shows the response of the 6198 Vidicon with and without aperture compensation. With compensation, the response is flat within ± 1 decibel out to 4.6 megacycles which frequency corresponds to approximately 370 lines resolution. Without compensation, the response is down 9 decibels at 4.6 megacycles.

Figures 11A and 11B show the improvement in resolution and detail contrast when aperture compensation is applied to a monoscope camera. In this test, $B_m = 5$ and $f_p = 10$ megacycles.

The Delay Line

To prevent phase distortion, it is necessary to use a dispersionless line, that is, one in which τ is independent of frequency up to the top of the useful video band. The m-derived, π-section lines of the Batchelder[18] or Golay[19] type give good results. These lines lend themselves to compact design since adjacent coils are coupled together.

The degree to which the performance of an artificial line approaches that of an ideal distributed-constant line improves with the number of sections used; however, good results can be obtained with only three or four sections provided f_p is not too low compared to the useful video
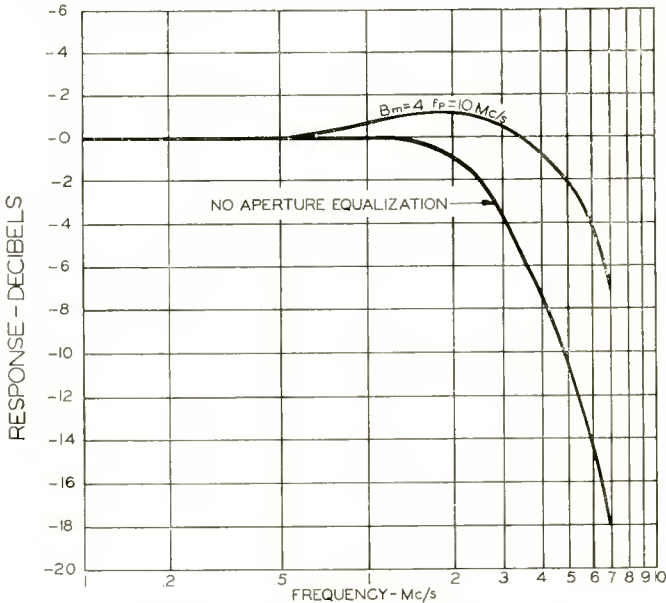
Fig. 10—Aperture response of the 6198 Vidicon (lower curve) and over-all system response with optimum equalization.

bandwidth. A simple line employing mutual inductance compensation is shown in Figure 12. The design equations are as follows:

$$L = \frac{0.4\,R_0}{n\,f_p} \tag{30}$$

$$C = \frac{0.5}{n\,f_p R_0} \tag{31}$$

---

[18] L. Batchelder, U. S. Patent 2,250,461. Filed May 28, 1938.
[19] M. J. E. Golay, "The Ideal Low-Pass Filter in the Form of a Dispersionless Lag-Line," Proc. I.R.E., Vol. 34, p. 138, March, 1946.
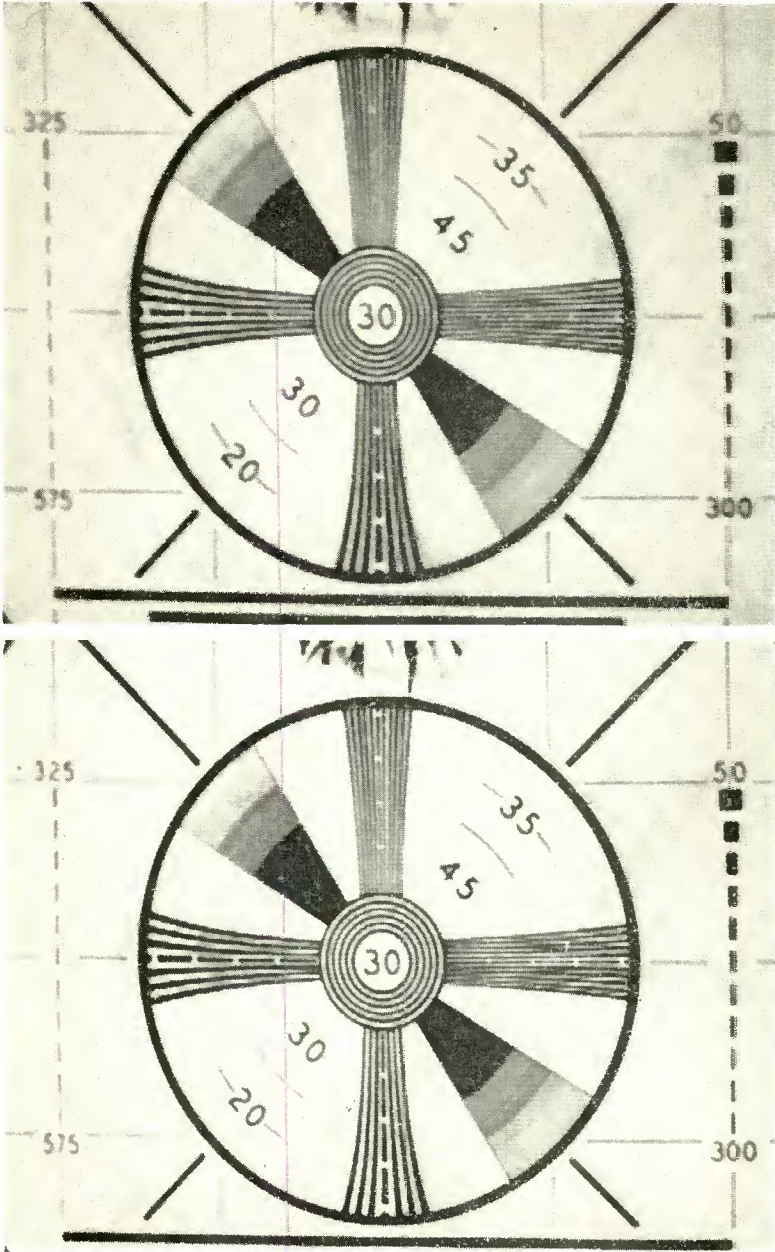
Fig. 11—(A) (above) The effect of aperture distortion on resolution and detail contrast. This is a standard monoscope camera pattern as displayed on an aluminized ten-inch kinescope; (B) (below) The improvement due to using aperture compensation. In this exhibit, $B_m = 5$ and $f_p = 10$ megacycles; everything else is the same as in 11A.
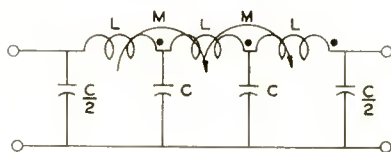
Fig. 12—A simple m-derived, π-section line employing mutual inductance compensation to minimize phase dispersion. The coils are all wound in the same direction.

$$k = \frac{M}{L} = 0.125 \qquad (32)$$

where n is the number of sections and k is the coefficient of coupling between adjacent coils. The sending-end and receiving-end voltages and the normalized time delay for a four section line are shown in Figure 13. It will be observed that the artificial line closely approximates the behavior of the ideal transmission line over a considerable range of frequencies; furthermore, if the line is lossless it may be shown that the sending-end and receiving-end voltages are exactly in phase.
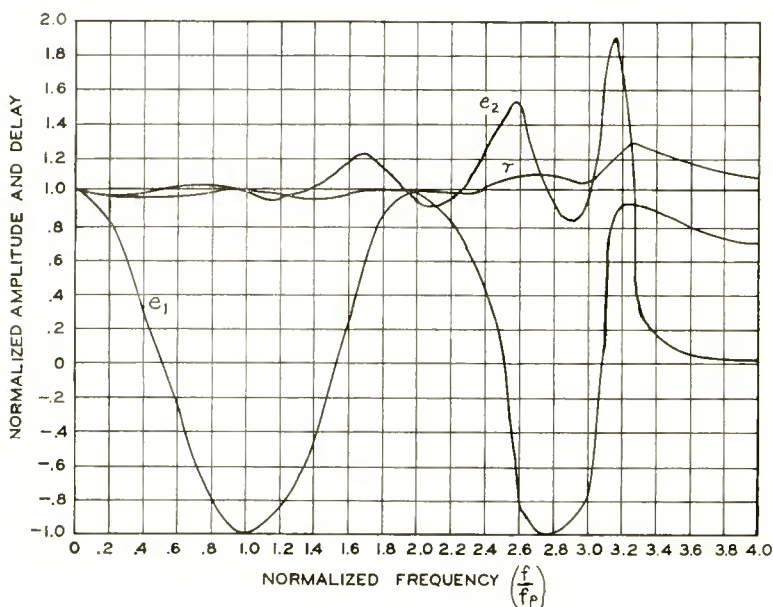
Fig. 13—The theoretical performance of a four-section delay line of the type shown in Figure 12. The line is assumed lossless and is terminated only at its sending end.

Conclusions

Aperture compensators of the open-line transversal-filter type may be designed with facility once the required values of B_m and f_p are known. These quantities may be determined by a graphical trial and error process. Properly applied, aperture compensation imparts a "snap" to the image which gives it a more lifelike appearance. The improvement is readily discernible and is equally beneficial to monochrome and color television systems.

Acknowledgments

A P-N-P TRIODE ALLOY JUNCTION TRANSISTOR FOR RADIO-FREQUENCY AMPLIFICATION*†

BY

C. W. MUELLER AND J. I. PANKOVE

Research Department, RCA Laboratories Division,
Princeton, N. J.

Summary—The performance of alloy junction transistors falls off as the frequency increases. Heretofore, the chief cause of this has been the resistance–capacitance low-pass filter effect in the base–emitter input. The effect is produced by the germanium resistance (between the external base connection and the active junction region) and the emitter-to-base diffusion capacitance. The latter may be extraordinarily high because of the relatively slow diffusion of charge carriers into the base region which must be charged up and discharged with minority carriers. In the new transistor design described, resistance and capacitance have been reduced by using a thick wafer of low-resistance germanium and placing the active junctions on a very thin section produced by drilling a well into the wafer. The junctions are about .0005 inch apart. Other capacitances are reduced by using small diameter junctions. To prevent limitation due to transit-time dispersion, nearly planar junctions are obtained by using germanium–indium alloy discs from which the junctions are formed.

The new unit will give 39 decibels gain (neutralized) at 455 kilocycles, 12 decibels (unneutralized) at 10 megacycles, and has an oscillation limit of 75 megacycles. At 1 megacycle, a noise factor as low as 4 decibels has been obtained.

INTRODUCTION

IN normal broadcast receiver design, an amplifier giving good gain in the frequency region of 0.5-3 megacycles is desirable. In order to fulfill this need, keep power consumption to a minimum, and retain the simplicity and versatility of the triode alloy-junction transistor, a development was undertaken to extend the frequency range of this type of transistor.

To follow the course of the present development, it is desirable to discuss first the important factors which limit the frequency response of the triode transistor such as the TA-153.[1] The important factors stem from a combination of two effects; one inherent to transistor operation, and the other extrinsic to transistor action but arising from

---

the constructional details. In the operation of this type of transistor it is well known that minority charge carriers, after injection by the emitter, flow to the collector by a process of diffusion through the base region and receive little or no aid from electric fields. Such diffusion currents flow under the influence of a density gradient, i.e., different carrier charge densities in different regions of the base layer. Thus, when a signal is applied to the transistor, the number of carriers in the base region must vary in accordance with the signal so that the diffusion current flow to the collector will reproduce the signal in the output circuit. This change in the charge of the base region induced by the applied signal acts as an emitter-to-base capacitance. Furthermore, because this charge flow in and out of the base region is a diffusion flow, an extraordinarily high capacitance results (of the order of 0.01 microfarad in the TA-153 transistor[1]).

This capacitance is much greater than that associated with the transition region of the emitter junctions. The "diffusion" capacitance is given approximately by

$$C_{b'e} = \frac{q}{kT} \frac{W^2 I_E}{2D}$$

where

$C_{b'e}$ = input capacitance of the common-emitter representation of Figure 1,

W = effective thickness of the base region,

I_E = d-c emitter current,

D = diffusion constant for minority carriers in the base region,

q = electronic charge,

k = Boltzmann's constant,

T = absolute temperature.

When I_E is expressed in milliamperes, and W in mils, this formula gives the capacitance in farads as

$$C_{b'e} = \begin{matrix} 2.8 \times 10^{-9} \ W^2 I_E \ \text{(for p-n-p units)} \\ 1.3 \times 10^{-9} \ W^2 I_E \ \text{(for n-p-n units)}. \end{matrix}$$

Since this capacitance is proportional to the square of the thickness of the base region, it is important to minimize this dimension in tran-

sistors designed for high-frequency applications. Note that this capacitance is proportional to the d-c current and does not involve the junction area. It is evident that a measurement of $C_{b'e}$ will provide a measure of the effective thickness of the base region.

Now, in the construction of the alloyed junction transistor, the external base connection to the germanium wafer is made at some distance from the active junction region. The resistance of the germanium between the base connection and the active junction constitutes a series base lead resistance ($r_{bb'}$ of Figure 1) through which the input signal must pass, with consequent attenuation before it can be applied to the intrinsic transistor. Furthermore, the charging current for the emitter-to-base capacitance discussed above must also flow through this resistance. This combination of series resistance and emitter-to-base capacitance constitutes a low-pass filter which is one of the most important limiting factors of transistors of the type under discussion.

The presence of this base lead resistance in addition to diminishing the input signal available to the actual transistor junctions, is also a feedback element, and its presence in the transistor leads to a reduction in the over-all output resistance and an increase in the over-all output capacitance of the transistor.

In addition to the input circuit effects discussed above, there are further consequences resulting from the fact that charge carriers flow from emitter to collector by a diffusion process. Diffusion flow is essentially a random process with the individual carrier making many collisions and changing direction of motion many times during its travel across the base region. Directivity to this random motion is supplied by the concentration gradient discussed above. Thus, the transit time for the individual carriers must vary widely, giving rise to a dispersive effect in the transfer function (i.e., transconductance). This transit time dispersive effect in the transfer of carriers to the output circuit also limits the frequency response of transistors but, for transistors such as the TA-153, its effect is not as detrimental as the input circuit effects discussed above.

The transit-time dispersion effects in the transfer function have been discussed as resulting only from diffusion phenomena. There may be a similar effect due to different path lengths caused by nonplanar geometries and end effects. The difference in path length may be minimized by small emitter-to-collector spacings, planar junctions, and accurate centering.

This picture of the consequences of diffusion flow in the base region has tended to separate the effects on the input circuit from those con-

cerned with the transfer generator, leading quite naturally to the π equivalent-circuit representation (Figure 4). It may be well to point out that in other representations such as an equivalent T circuit, the transfer generator (alpha) involves both the transfer transit-time dispersion effects and base-charge variation effects. This is as it should be, for alpha is the current gain amplification factor, and must account for changes of current between the input and output. Indeed, the collector-to-emitter current gain cutoff frequency is related to $C_{b'e}$ by

$$f_{ca} = \frac{q}{2\pi kT} \frac{I_E}{C_{b'e}}$$

and a measurement of $C_{b'e}$ at low frequencies may be substituted for a measurement of f_{ca} at considerably higher frequencies.

Another frequency-limiting factor which may become significant as transistors are designed to minimize the above effects is the presence of other capacitances, such as collector-to-base and collector-to-emitter. The collector-to-base capacitance may be reduced by reducing the area of the collector junction. There is also a contribution to this capacitance due to transit-time variation effects caused by a variation of the effective base thickness with the instantaneous collector voltage.

These considerations will be applied to the development of a p-n-p medium-frequency transistor. Similar considerations would also apply to n-p-n transistors.

Factors Governing Design

As will now be understood from the preceding discussion, in the design of high-frequency transistors it is important that, in addition to satisfying the requirements for good transistor action at audio frequencies, particular attention must be given to the following parameters:

1. Thickness of base layer.
2. Series base lead resistance.
3. Capacitance.

As pointed out in the general discussion, the value of $C_{b'e}$ (or f_{ca}) is degraded in proportion to the square of the distance between the emitter and collector junctions. This distance should be as small as can conveniently be obtained, and a reasonable value of spacing to aim for is .0005 inch.

In the alloy type transistor, an emitter-to-collector spacing of .0005

inch can be obtained in two ways: (a) by using a thick base wafer and a large impurity alloy penetration, or (b) by using a thin germanium base wafer with small impurity alloy penetration. With method (a), however, the junctions are hemispherical rather than parallel planes, and consequently the possible hole path lengths may vary considerably. In method (b) the junctions are more nearly flat and parallel and this method was therefore chosen. With thin base wafers it is necessary that the impurity alloy depth of penetration be small. Accurate control is then necessary to prevent emitter-to-collector shorts.

The factors governing the penetration of indium by solution into the germanium base material have been discussed.[1] A shallow penetration as desired here can be secured by: (1) a short firing time, i.e., shorter than that required for an equilibrium solution of the alloying action, (2) using a small volume of indium, (3) using a disc of indium–germanium alloy. The method described in this paper is a combination of all three, but depends principally on the latter two.

In order to secure plane parallel junctions, heating at a high temperature is desirable to secure rapid wetting over the entire region of the junction. Various combinations of alloy disc composition and temperature are possible and several have been tried. However, as the atomic percentage of germanium in the indium–germanium alloy is raised above 10 per cent, it is more difficult to secure a homogeneous alloy, and the mechanical properties of the alloy become poorer. The alloy which has been found most advantageous at the present time contains 5 atomic per cent germanium in indium, and this is the alloy used in all experiments described here.

As previously pointed out, it is important that $r_{bb'}$, the resistance of the germanium connecting the active junctions and the base tab, be as small as possible. This resistance is shown in the input equivalent circuit of Figure 1a. The values of this equivalent circuit can be measured by means of specially designed bridges.[2]

The series resistance, $r_{bb'}$, consists of two regions, as shown in Figure 1b: region "A" directly between the junctions, and region "B" between the junctions and the base connection. Obviously, the resistance of both these regions is reduced by using a base material with the lowest possible resistivity. In the "B" region, no limitation on resistivity exists. However, on the "A" region, two good junctions must be formed.

---

[2] L. J. Giacoletto, "Equipments for Measuring Junction Transistor Admittance Parameters for a Wide Range of Frequencies," RCA Review, Vol. XIV, pp. 269-296, June, 1953.

Shockley[3] has shown that in order to have a good hole emitter, the conductivity of the emitter section must be much higher than that of the base region. Experimentally, it is found that as the resistivity of the base region is decreased, good junctions are more difficult to make. Here, then, an engineering compromise must be made between low base resistance and good junctions, as evidenced by high alpha and high back-resistance values. The resistance of the "A" region, which is directly between the junctions, is also reduced by the carriers injected by the emitter, i.e., conductivity modulation. Considering the present state of the art and the necessary engineering compromises, a resistivity of 0.6 to 0.8 ohm-centimeter was chosen after some exploratory tests.

Let us examine region "B" to see how this resistance can be reduced. In order to obtain an idea of the magnitude or resistance involved in the region "B" for a thin wafer base, consider the simplified geometry shown in Figure 2. The resistance between concentric cylinders is given by
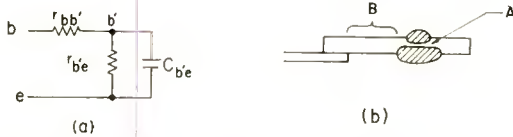
Fig. 1—(a) Equivalent input circuit of the transistor and (b) Transistor cross section showing the physical location of the parts of $r_{bb'}$ on a TA-153 audio-transistor.

$$R = \frac{\rho}{2\pi L} \ln \frac{r_2}{r_1} \text{ ohms}$$

ρ = resistivity of germanium in ohm-centimeters,

r_1, r_2 = radius of the inner and outer cylindrical surfaces,

L = wafer thickness in centimeters.

If r_1 is kept constant at .005 inch (the size of the emitter junction) and r_2 varied from .010 inch, the curves of Figure 2 are obtained.

If such a flat-wafer construction were used for the high-frequency transistor, and $\rho = 3$ ohm-centimeters, we see from Figure 2 that a series resistance of 200 ohms would be introduced to a ring contact .040 inch from the center of the emitter. The curves also show that the contribution of the first few thousandths of an inch around the

[3] W. Shockley, "The Theory of P-N Junctions in Semi-Conductors and P-N Junction Transistors," *Bell Sys. Tech. Jour.*, Vol. 28, pp. 435-489, July, 1949.

junctions is important. From these curves can be seen the disadvantages of high-resistivity germanium and of the flat-wafer construction.

Several methods of reducing the resistance of the region "B" are possible. As a guide, methods other than those finally used are discussed first. One way to reduce the resistance of portion "B" is to solder a ring, a few thousands of an inch larger than the junctions, to the germanium that surrounds the junctions. Great care must then be taken to keep the indium and solder from shorting, and to obtain
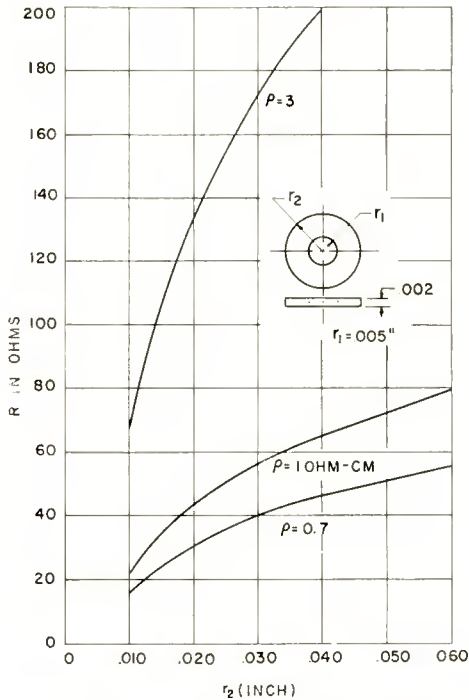
Fig. 2—Resistance between concentric cylinders of germanium.

proper etching after assembly. Another possible procedure is to form junctions, protect the junctions with a suitable lacquer, and then plate a metal on the exposed base wafer. It is necessary to make a plated contact which is ohmic, i.e., does not inject an appreciable number of holes. Such ohmic contact can be made by sand blasting the base and then plating. A word of caution on these methods is in order. As has been shown in another paper,[4] surface recombination is a critical factor in obtaining low-frequency transistor action. An ohmic contact or

---

[4] A. R. Moore and J. I. Pankove, "The Variation of Current Gain with Junction Shape and Surface Recombination in Alloy Transistors," to be published in *Proc. I.R.E.*

plated region of considerable area too near the emitter junction could lead to such a high recombination rate as to make the transistor unsatisfactory. A compromise is necessary which leaves sufficient low-recombination surface around the junctions, and yet not so much as to leave the base resistance high.

After exploration of the above methods, a design was chosen in which only germanium surrounds the junctions. The structure is shown in Figure 3, which is drawn approximately to scale. Here we see that, as soon as we leave the immediate vicinity of the junctions, the thickness of the wafer increases and thus decreases the series base lead resistance; since only germanium surrounds the junctions, low surface recombination can be attained at the same time.
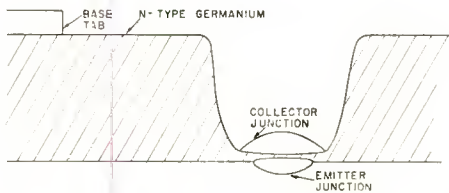
Fig. 3—Cross-sectional view of junction geometry.

The collector-to-base capacitance should be no larger than necessary. The junctions of the alloy type transistor are usually of the abrupt or Shottky type. Formulas for this case are developed by Shockley[3] and, when expressed in convenient units, lead to the following equation for the capacitance of an abrupt junction.

$$C = .071 \, d^2 \frac{1}{\sqrt{\rho_b \, V_c}} \text{ micromicrofarads}$$

where

$d =$ diameter of the junction in mils,

$V_c =$ collector voltage,

$\rho_b =$ resistivity of the base material in ohm-centimeters.

Thus the diameter of the collector has the greatest influence and should be made small. This should preferably be done without decreasing α_{ce}, collector-to-emitter current amplification factor. In order to keep α_{ce} high, the area of the emitter must be kept to two-thirds or less than that of the collector.[4]

As the area of the emitter is reduced, the ratio of emitter circum-

ference to area increases and surface recombination becomes more important. Consequently etching must be carefully done. Also, as the area of the emitter and collector become small, alignment of emitter and collector is more difficult. As an engineering compromise, the emitter was made .010 inch in diameter and the collector .015 inch in diameter.

ELECTRICAL MEASUREMENTS

The electrical engineer likes to reduce an electron device to an equivalent circuit composed of elements with which he is familiar so that he can apply standard circuit theory. Many types of equivalent circuit are possible. The simplest circuit, with the fewest parameters that are all independent of frequency, is best but not always obtainable. Most of the published literature on transistors is in terms of the T-
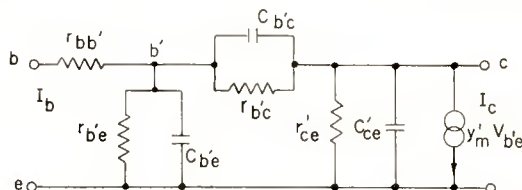
Fig. 4—Single-generator base-input π-equivalent circuit.

equivalent circuit or loop-derived parameters. Many who are familiar with vacuum tube terminology prefer the π-equivalent or nodal-derived parameters. One set of parameters can of course be derived from the other set if the set is complete.[5]

In Figure 4 a single-generator π-equivalent circuit is shown for the common emitter connection. The circuit parameters have been tested and found to be independent of frequency as long as the frequency is not too high. Although not yet completely investigated, the circuit is believed sufficiently close as long as

$$\frac{\omega W^2}{4 D_p} < 0.2$$

where

$\omega =$ angular frequency,

$W =$ spacing between junctions in centimeters,

---

[5] L. J. Giacoletto, "Terminology and Equations for Linear Active Four-Terminal Networks Including Transistors," *RCA Review*, Vol. 14, pp. 28-46, March, 1953.

$D_p =$ diffusion constant for holes.

For the transistors described here the circuit is believed to be a reasonable approximation up to a frequency of the order of 3 megacycles. The elements shown in this circuit were measured in bridges previously described.[2] The values measured on 6 transistors are given in Table I. The value of W, the spacing between junctions, is calculated from $C_{b'c}$ by applying diffusion theory as previously described. The values of the circuit constants in the output were not determined because their effect is negligible in comparison with the other parameters and their measurement is difficult.

Table I—π-equivalent Circuit Parameters
($E_c = -6$ volts, $I_c = -1$ milliampere)

Transistor		A	B	C	D	E	F#	Approx. TA-153 range
$r_{bb'}$	ohms	50	115	60	70	77	100	200-500
$r_{b'e}$	ohms	1250	1500	1400	600	430	500	600-2000
$C_{b'e}$	$\mu\mu$fd	300	700	900	600	800	2100	10,000-25,000
$r_{b'c}$	megohms	1.2	.10	.14	.86	.13	1.9	2
$C_{b'c}$	$\mu\mu$fd	10.4	7.7	16.7	9.5	17.0	11.0	35
W^*	mils	.33	.50	.56	.46	.52	.86	1-3
f_{ca}[†]	mc	20.5	8.8	6.9	10.6	7.7	3.0	.4

[*] Calculated from $C_{b'e}$ as previously described.

[†] Calculated from $f_{ca} = \dfrac{q}{2\pi kT} \dfrac{I_E}{C_{b'e}}$.

This transistor is included to show the deviation to be expected from a higher than normal value of W.

For comparative purposes, a range of values for TA-153 audio p-n-p transistors described in Reference (1) is included. The value of W for the TA-153 transistor was not accurately controlled since the transistor was intended for audio use.

In Table II the low-frequency parameters of the common-base T-equivalent circuit of Figure 5 are shown, again in comparison with those of the TA-153. The parameters r_c and α_{ce} are slightly poorer in the high-frequency transistor because they were compromised to get better high-frequency performance. These low-frequency parameters, of course, give no clues to high-frequency performance, but are included in the data for those who wish to make comparisons.

An important characteristic of a high-frequency transistor is the
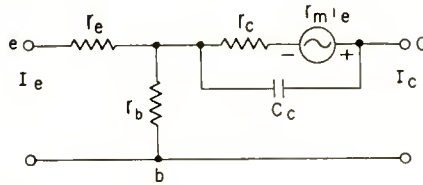
Fig. 5—Low-frequency emitter-input T-equivalent circuit.

single-frequency power gain as a function of frequency. Figure 6 shows a simplified schematic circuit of the test set used to measure power gain. Input matching is made only with the resistive component while the output is conjugate matched by adjusting the capacitance and output impedance. The feedback is not neutralized. In Figure 7 the gain of a transistor with common-emitter and common-base connections is plotted. In Table III the gain of the six transistors is shown for the various conditions described in the footnotes of the table.

Table II—T-equivalent Circuit Parameters
($E_c = -6$ volts, $I_E = 1$ milliampere)

Transistor	A	B	C	D	E	F	Approx. TA-153 range
r_e ohms	4.0	18.0	20.6	14.6	19.4	16.0	5-20
r_b ohms	1000	300	140	270	130	250	400-2000
r_c megohms	.40	.06	.16	.40	.16	.45	.5-3.0
α_{ee}	.977	.982	.976	.955	.952	.963	.95-.99
α_{cb}	41	51	40	21	19	25	20-100
I_{co} μa	20	10	10	14	18	8	2-20

In Table III the noise factor is also given. There is a considerable variation of one-kilocycle noise factor among various units at the present time, but the one-megacycle noise factor does not vary as much. In Figure 8 the noise factor is plotted as a function of frequency up to one megacycle.

Experiments with a simple oscillator circuit show that the high-frequency transistors described will oscillate at frequencies up to 75 megacycles.
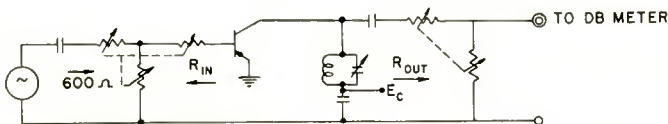
Fig. 6—Simplified diagram of circuit used for measurement of gain versus frequency.

Table III—Gain and Noise Factor Values in Decibels

Transistor	A	B	C	D	E	F	Approx. TA-153 range
4 kc gain*	35.	37.	39.	34.	34.	38.	35 to 48
455 kc gain**	35.	32.	39.	35.	34.	34.	——
1 mc gain†	24.	23.	25.	24.	23.	22.	$<$ 0 to 7.
10 mc gain†	13.	10.	11.	9.	8.	5.	——
1 kc Noise factor‡	14.	23.	33.	24.	16.	20.	15 to 25
1 mc Noise factor#	4.	5.	8.	7.	5.	6.	——

All values of gain measured at $E_c = -6$ volts, $I_B = 1$ milliampere.

* $R_{in} = 500$ ohms, $R_{out} = 30,000$ ohms.

** Input and output conjugate matched and feedback neutralized.

† Input resistive matched and output conjugate matched in circuit of Figure 9.

‡ $E_c = -1$ volt, $I_E = 1$ milliampere, $R_{in} = 560$ ohms.

$E_c = -1$ volt, $I_B = 1$ milliampere, $R_{in} = 100$ ohms.

CONCLUSIONS

A p-n-p triode transistor capable of as much as 39 decibels gain at 455 kilocycles when used in a neutralized, conjugate-matched circuit has been constructed. Without neutralizing, 12 decibels gain can be obtained at 10 megacycles. The noise factor at one megacycle is 4-8 decibels.

A spacing between junctions of .0005 inch and a low base-lead resistance is obtained by using a low-resistivity base section with the collector junction located at the bottom of a well in the germanium. An indium–germanium alloy is used to obtain more planar junctions.

With the continued improvement in the techniques of making and
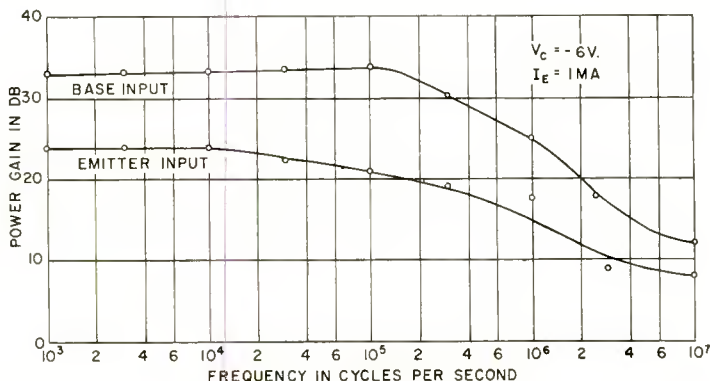
Fig. 7—Single-frequency power gain measured in the circuit of Figure 6.
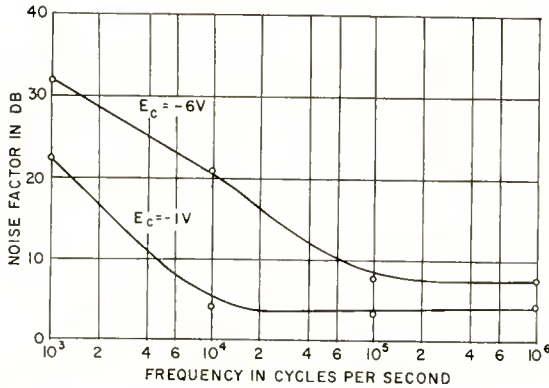
Fig. 8—Noise factor versus frequency; common-emitter connection.

controlling junctions, further improvements by the use of lower re-sistivity germanium and a reduction in all dimensions are possible.

ACKNOWLEDGMENT

Erratum

In the paper entitled "Television Coverage of the Presidential Inauguration," which appeared in the June 1953 issue of RCA REVIEW, the authors inadvertently failed to give due credit to Mr. Lawrence Weiland of the National Broadcasting Company who assembled all of the material for that part of the paper dealing with the mobile Cadillac unit.

RCA TECHNICAL PAPERS†

Third Quarter, 1953

Any request for copies of papers listed herein should be
addressed to the publication to which credited.*

AUTHORS

IRWIN D. BAUMEL received the B.E.E. degree from the College of the City of New York in January 1950. Prior to that, he had served in the U. S. Navy in the Naval electronics program in 1945 and 1946. He was employed by Tele-King Corp., N. Y., and Philco Corp., Philadelphia from 1950 to 1951, at which time he was recalled by the U. S. Navy for a 15 month tour of active duty. Since 1952 Mr. Baumel has been concerned primarily with problems in UHF television tuners at the RCA Industry Service Laboratory, New York, N. Y. He is an Associate Member of the Institute of Radio Engineers.

ROBERT C. DENNISON received the B.S.E.E. degree with honors in 1947 and the M.S. degree in 1948 from Kansas State College. He was a radar officer in the U. S. Navy from 1943 to 1946. From 1948 to 1950, he was instructor in Television and Communication Networks at Kansas State College. Since 1950, he has been working in the Television Studio Equipment Section at RCA Victor Division, Camden, New Jersey. Mr. Dennison is a member of Eta Kappa Nu, Sigma Tau, Pi Mu Epsilon, Phi Kappa Phi, and an Associate Member of the Institute of Radio Engineers.

CARL G. DIETSCH became a shipboard radio operator for the Marconi Wireless Telegraph Company in 1917. He subsequently attended the University of Michigan where he received the B.S. degree in Electrical Engineering. In 1925 he joined RCA as a student engineer, and in 1927 he was placed in charge of the design and construction work for short wave transmitter stations being constructed in Rio de Janeiro and Buenos Aires. In 1931 he transferred to the Engineering staff of the National Broadcasting Company. After World War II, he became Engineer in Charge of the Voice of America stations in Dixon, Cal. In 1947 he transferred to RCA Communications, Inc. where he was engaged in the design and construction of stations at Manila and Tangier. Mr. Dietsch is a Licensed Professional Engineer in New York State and a Senior Member of the Institute of Radio Engineers.

WELLESLEY J. DODDS received the M.S. degree in Physics and Mathematics from the University of Kansas in 1941, where he had been a teaching assistant and the Edwin Emory Slosson Scholar in Science, and had engaged in research on electrets. He then spent a year at the University of Illinois studying biophysics and doing research on activity in nerve. In 1942 he joined the RCA Victor Division as a power tube design engineer, working on transmitting tubes for microwave radar. Since 1945 he has been associated with the RCA Laboratories Division as a research engineer, engaged in the study of beam-deflection tubes, magnetrons, magnetron amplifiers, and traveling-wave tubes. In December 1953 he transferred to the Tube Department of the RCA Victor Division at Harrison, N. J. Mr. Dodds is a Senior Member of the Institute of Radio Engineers, serving in the past as committee member and Chairman of the Annual IRE-AIEE Conference on Electron Tube Research, ad presently as Secretary and Steering Committee Chairman of the IRE Committee on Electron Devices. He is also a member of Sigma Pi Sigma, Pi Mu Epsilon, and Sigma Xi.

L. E. FLORY received the B.S. degree in Electrical Engineering from the University of Kansas in 1930. He was a member of the Research Division of RCA Manufacturing Co., Camden, N. J. from 1930 to 1942. During this time he was engaged in research on television tubes and related electronic problems, particularly in the development of the iconoscope. In 1942 he transferred to the RCA Laboratories Division at Princeton, N. J., where he continued to work on electronic tubes and special circuit problems, including electronic computers, infrared image tubes and sensory devices. Since 1949 he has been in charge of work on storage tubes and industrial television. Mr. Flory is a Member of Sigma XI and a Senior Member of the Institute of Radio Engineers.

EDWIN M. HINSDALE, JR. received the B. S. degree in Electrical Engineering from the University of Tennessee in 1938. From 1938 to 1941 he was employed by Pan American Airways in their communications laboratory. From 1941 to 1942 he was employed by Glenn D. Gillett, Consulting Radio Engineer, in broadcast consulting engineering and the Signal Corps Laboratories at Red Bank, N. J. From 1942 to 1943 he was employed as a field engineer for Pan American Airways Africa Ltd. From 1943 to 1946 he was employed by the Industry Service Laboratory of RCA Laboratories Division. From 1946 to 1951 he was a member of the firm of Glenn D. Gillett and Associates. Since 1951 he has been engaged in television development work at the Industry Service Laboratory, RCA Laboratories Division in New York. He is a member of Tau Beta Pi and is a Senior Member of the Institute of Radio Engineers.

HARVEY O. HOOK received the B.A. degree with Chemistry major from Elon College in 1947, the B.E.E. degree from North Carolina State College in 1949, and the M.S.E.E. degree from North Carolina State College in 1950. Since 1950 he has been with RCA Laboratories Division. Mr. Hook is an Associate Member of the Institute of Radio Engineers and Sigma Xi.

M. KNOLL received the M.S. and Ph.D. degrees in Electrical Engineering in 1922 and 1924 respectively from the Institute of Technology in Munich, Germany. From 1927 to 1945 he was in turn Assistant Professor, Associate and Full Professor for Vacuum Tube design at the Institute of Technology, Berlin-Charlottenburg, Germany, and from 1932 director of its Vacuum Tube Laboratory. After the war this Vacuum Tube Laboratory was affiliated with the University of Munich, where he taught, as a Full Professor, Electron Optics and Vacuum Tube Design until 1947. From 1932 to 1947 he was in charge of the Electron Research Laboratory of the Telefunken Corporation, and was mainly concerned with the development of the television camera, viewing and storage tubes. In December 1948, after serving one year as a consultant to the Evans Signal Laboratories, Belmar, N. J., he joined RCA Laboratories at Princeton, N. J., where he is now engaged in research in electronics. A part of his time is devoted to teaching Electron Optics and Vacuum Tube design at Princeton University as a visiting lecturer with the rank of Full Professor in the Department of Electrical Engineering. Dr. Knoll is a Senior Member of the Institute of Radio Engineers, and a Member of Sigma Xi.

EDMUND A. LAPORT attended Northeastern University, Massachusetts University Extension, and McGill University. In 1924 he joined the Westinghouse Electric and Manufacturing Company of Springfield, Mass., as a radio engineer. From 1933 to 1934 he was with the Paul Godley Company, Montclair, N. J., and from 1934 to 1936 with Wired Radio, Inc., of Ampere, N. J. In 1936 he became associated with the RCA Victor Division, Camden, N. J.; in 1938, Chief Engineer of engineering products in the RCA Victor Company Limited, Montreal; and in 1944, Chief Engineer of the RCA International Division, New York. Mr. Laport is a Senior Member of the Institute of Radio Engineers.

CHARLES W. MUELLER received the B.S. degree in Electrical Engineering from the University of Notre Dame in 1934, the S.M. degree in Electrical Engineering in 1936 from the Massachusetts Institute of Technology, and the degree of Sc.D. in Physics from M.I.T. in 1942. From 1936 to 1938 he was associated with the Raytheon Production Corporation, first in the engineering supervision of factory production of receiving tubes, and then in the development of gas-tube voltage regulators and cold-cathode thyratrons. From 1938 to 1942 he worked at M.I.T. on the development of gas-filled special-purpose tubes for counting operations. Since 1942 he has been a member of the technical staff of RCA Laboratories Division in Princeton, N. J. where he has been engaged in research on high-frequency receiving tubes, secondary electron emission phenomena, and solid-state devises. Dr. Mueller is a member of the American Physical Society and Sigma Xi and a Senior Member of the Institute of Radio Engineers.

JACQUES I. PANKOVE received the B.S. degree in Electrical Engineering in 1944 and the M.S. degree in Electronic Engineering 1948 from the University of California in Berkeley. From 1944 to 1946 he served with the United States Army. Since 1948 he has been engaged in semiconductor research at RCA Laboratories Division in Princeton, N. J. Mr. Pankove is a Member of Sigma Xi and the American Institute of Electronic Engineers and an Associate Member of the Institute of Radio Engineers.

ROLF W. PETER—(See *RCA Review*, Volume XIV, No. 3, September 1953, page 457.)

WINTHROP SEELEY PIKE received the B.A. degree in Physics in 1941 from Williams College. He served with U. S. Army Signal Corps during World War II as radar officer and later as project officer in charge of the Signal Corps Moon Radar project. In 1946 he joined the research staff of RCA Laboratories Division at Princeton, N. J., where he has worked on sensory aids for the blind, storage tube applications, color television and industrial television. Mr. Pike is a Member of the Institute of Radio Engineers, Sigma Xi, and the American Guild of Organists.

JAMES W. RITCEY, JR. received the B.S. degree in Electrical Engineering from the University of Pittsburgh in 1950. Before that time, he served as a radio technician in the United States Marine Corps. Mr. Ritcey entered the RCA Specialized Training Program in 1950 and, upon completion of this program, joined the Testing Engineering Group of the RCA Tube Department at Harrison, N. J. He worked on premium and computer tubes until August of 1953 and has since been working on the design of semiconductor devices. Mr. Ritcey is a member of Phi Eta Sigma, Sigma Tau, and Eta Kappa Nu.

PAUL RUDNICK received the B.S. degree in Physics in 1930 and the Ph.D. degree in Astrophysics in 1936 from the University of Chicago. He was Astronomer at the W. J. McDonald Observatory, Fort Davis, Texas, operated jointly by the University of Chicago and the University of Texas, from 1936 to 1939. From 1939 to 1941 he was Instructor in Physics at the University of Texas. From 1941 to 1952 he was with the RCA Laboratories Division at Princeton, New Jersey working on special electronic tubes and viewing devices. He is at present in the Research Department of the Capehart-Farnsworth Company in Fort Wayne, Indiana. Dr. Rudnick is a Member of Phi Beta Kappa and Sigma Xi, and a Senior Member of the Institute of Radio Engineers.

HENRY E. STUMMAN received the B.S. degree in Electrical Engineering from Syracuse University in 1948. Before that time, he served as an electronic technician in the United States Coast Guard. After graduation, Mr. Stumman entered the RCA Specialized Training Program and, upon completion of this program, joined the Receiving Tube Development Group of the RCA Tube Department at Harrison, N. J. His work is concerned primarily with the development of computer and premium tubes.

RCA REVIEW

a technical journal

RADIO AND ELECTRONICS
RESEARCH • ENGINEERING

INDEX

VOLUME XIV

TABLE OF CONTENTS

September

December

INDEX, VOLUME XIV

Authors, Volume XIV